UNIVERSIDAD NACIONAL AUTÓNOMA DE MÉXICO
PROGRAMA DE POSGRADO EN ASTROFÍSICA

Centro de Radioastronomía y Astrofísica

REFORMULACIÓN DEL CONCEPTO DE EFICIENCIA DE FORMACIÓN ESTELAR EN NUBES MOLECULARES EN EVOLUCIÓN

QUE PARA OPTAR POR EL GRADO DE:
DOCTOR EN CIENCIAS (ASTROFÍSICA)

PRESENTA:
MANUEL ABELARDO ZAMORA AVILES

TUTOR:
DR. ENRIQUE CRISTIAN VÁZQUEZ SEMADENI
CENTRO DE RADIOASTRONOMÍA Y ASTROFÍSICA

MÉXICO, D. F.; MARZO 2015

Resumen

Las estrellas masivas juegan un papel central en la evolución del universo. Su feedback ayuda a moldear y a determinar las propiedades físicas y evolución de las galaxias. Sin embargo, los procesos físicos relevantes en la formación de estas estrellas masivas no están bien establecidos y son objeto de intenso debate en la astrofísica contemporánea.

El objetivo de esta tesis es el de entender el escenario global de formación estelar en nubes moleculares (NMs) en evolución desde dos puntos de vista, uno analítico y otro numérico. Resultados recientes de simulaciones numéricas y de observaciones sugieren que las NMs pueden estar en un estado de contracción gravitacional global, por lo que dirigimos nuestros modelos y simulaciones en este sentido. En este escenario, hemos desarrollado un modelo semianalítico que da cuenta de la evolución completa de NMs en colapso global, siguiéndolas desde su formación hasta su destrucción por la radiación ionizante proveniente de las estrellas masivas. Extendemos este modelo para explorar la dependencia de la tasa y eficiencia de formación estelar en la masa de las NMs. Satisfactoriamente logramos reproducir muchas de las características evolutivas observadas (como la distribución de edades de estrellas en cúmulos y la secuencia temporal de NMs gigantes reportada en la Nube Mayor de Magallanes) dentro de una precisión de medio orden de magnitud.

Posteriormente, presentamos simulaciones numéricas incluyendo campos magnéticos y un modelo detallado del transporte radiativo, para simular el efecto que la radiación ionizannte, proveniente de las estrellas masivas, tiene sobre la dinámica de la nube. Nuestros resultados indican que la radiación ionizante es capaz de erosionar y dispersar las NMs en colapso reduciendo tanto la tasa como la eficiencia de formación estelar a valores consistentes con los observados.

Abstract

Massive stars play a central role in the evolution of the universe. Their feedback helps shape and determine the physical properties and evolution of galaxies. However, the relevant physical processes in the formation of these massive stars are not well established and are subject to intense debate in contemporary astrophysics.

The objective of this thesis is to understand the global scenario of star formation in evolving molecular clouds (MCs) from both an analytical and a numerical standpoint. Recent numerical results and observations suggest that MCs may be in a state of global gravitational contraction, and we cast our model and simulations in this framework. In this scenario, we have developed a semi-analytical model that accounts for the evolution of MCs in global collapse, from the cloud formation to its destruction by ionizing radiation from massive stars. This model is then extended to explore the dependence of the star formation rate and efficiency on the mass of these MCs. We have successfully reproduced many of the observed evolutionary features of MCs (such as the stellar age distribution in clusters and the evolutionary sequence for giant MCs recently reported for the Large Magellanic Cloud) within half an order of magnitude.

Next, we present numerical simulations of the process, including magnetic fields and a detailed model of radiative transfer, to represent the effect of the ionizing radiation from the massive stars on the clouds' dynamics. Our results indicate that ionizing radiation is able to erode and disperse the collapsing MCs and reduce both the star formation rate and efficiency to values consistent with observation.

Agradecimientos

Agradezco de manera muy importante al Dr. Enrique Vázquez por todo su apoyo dentro y fuera del ámbito académico. Sus conocimientos, sus orientaciones, su paciencia, su dedicación y su motivación fueron fundamentales para mi formacin como investigador.

Agradezco mucho a mi familia entera por por estar siempre a mi lado.

Finalmente, agradezco a todo el personal del CRyA, quienes han sido como una segunda familia en esta etapa de mi vida. En especial a mis compaeros y maestros que formaron parte de esta aventura. Gracias a todos ellos.

Dedico esta tesis a mi familia
por su apoyo incondicional
durante todo este tiempo.

A Enrique por empujarme a ser,
en palabras del Ing. Enrique Vázquez,
un paletero de la mitad para arriba.

Contents

List of Figures

List of Tables

List of Symbols and Abbreviations

Abbreviations

AD	ambipolar diffusion	8
AMR	adaptive mesh refinement	88
CNM	cold neutral medium	18
erf	error function, see equation (3.14)	44
GMC	giant molecular cloud	3
IGM	intergalactic medium	1
IMF	initial mass function	39
ISM	interstellar medium	1
MCs	molecular clouds	1
MHD	magnetohydrodynamic	22
OMC	orion molecular cloud	49
ONC	orion nebula cluster	54
PDF	probability density function	32
RMHD	radiation-magnetohydrodynamic	86
SF	star formation	2

SF-MCs star-forming molecular clouds 70

SFE star formation efficiency 1

SFR star formation rate 1

WNM warm neutral medium 6

YSOs young stellar objects 74

ZAMS zero-age main sequence 90

Symbols

$A_{\rm c}$ collisional ionization rate, see equation (2.42) 26

$A_{\mathbf{k}}$ Fourier amplitude, see equation (2.52) 29

$A_{\rm ph}$ photoionization rate, see equation (2.42) 26

α_ν absorption coefficient, see equation (A.15) 113

$\alpha_{\rm R}$ radiative recombination coefficient, see equation (2.42) 26

$\mathbf{B}$ magnetic field, see equation (2.21) 22

c speed of light, see equation (2.30) 23

$c_{\rm s}$ sound speed, see equation (2.19) 21

$c_{\rm s,I}$ sound speed in the ionized gas, see equation (3.5) 39

$\mathbf{E}$ electric field, see equation (2.30) 23

$E_{\rm g}$ gravitational energy, see equation (2.26) 23

$E_{\rm mag}$ magnetic energy, see equation (2.27) 23

E_ν radiant energy, see equation (A.0) 111

$E(k)$ energy spectrum, see equation (2.55) 30

e electron charge, see equation (2.30) 23

$e_{\rm int}$ specific internal energy, see equation (2.4) 16

$e_{\rm tot}$ total specific energy, see equation (2.3) 16

$F_{\rm UV}$	UV flux	90
F_ν	specific radiative flux, see equation (A.2)	111
f	star-forming mass fraction, see equation (3.3)	38
$\mathbf{f}_{\rm L}$	Lorentz force, see equation (2.30)	23
$f_{\rm L}$	Larson parameter	41
Φ	magnetic flux, see equation (2.24)	22
ϕ	scalar potential, see equation (2.13)	20
G	Newton's constant, see equation (2.14)	20
$\mathbf{g}$	gravitational acceleration, see equation (2.13)	20
Γ	heating rate, see equation (2.12)	17
γ	adiabatic index, see equation (2.7)	16
h	Plank's constant, see equation (2.38)	26
h	cloud thickness	39
η	magnetic diffusivity, see equation (2.21)	22
I	total intensity, see equation (A.2)	111
J	mean total intensity, see equation (A.11)	112
J_ν	mean specific intensity, see equation (A.9)	112
$\mathbf{j}$	current density, see equation (2.31)	24
$\mathbf{k}$	vector Fourier mode, see equation (2.52)	29
$k_{\rm B}$	Boltzmann's constat, see equation (2.5)	16
$k_{\mathbf{J}}$	Jeans wave number, see equation (2.17)	21
κ_ν	mass absorption coefficient, see equation (A.15)	113
$L_{\rm inf}$	inflow length	92
l	mean free path	15

1

Introduction

Many aspects of the star formation process remain the subject of intense debate, despite its fundamental importance. One of these aspects, addressed in this work, is the regulation of the rate and efficiency with which stars form in the interstellar medium (ISM) of our Galaxy (the star formation rate [SFR] and efficiency [SFE], respectively). This requires, in turn, to understand the origin and evolution of molecular clouds (MCs), which are the sites where stars form today. This is of vital importance, because the way in which the clouds evolve determines the way in which they form stars and also the way in which the newborn stars impact their environment.

When massive stars die, they return a significant portion of their mass (enriched by nucleosyntesis) into the ISM. In general, it is estimated that about 20% of the mass used up in star formation is fed back into the ISM after the star is born. This return of material, as well as the radiation from newly-formed stars, injects energy and momentum into the ISM (see, e.g., Mac Low and Klessen, 2004). There are also indications that the Galaxy is still accreting some material from the intergalactic medium (IGM), but at the same time is losing some of it into the IGM through diffusion processes or in catastrophic galaxy collisions. Thus, the ISM is highly dynamic and turbulent, with Reynolds numbers $\gtrsim 10^6$ (Elmegreen and Scalo, 2004a). As a result, the structure of the ISM is highly complex and temperature (T), density, and even velocity and magnetic fields vary vastly across the Galaxy, to the point that the ISM has been described as *violent* (McCray and Snow, 1979).

The highly dynamic state of the ISM causes in particular the formation of cold, dense regions which are referred to as *clouds*. These may be composed mainly of Hydrogen atoms (and thus called *atomic clouds*) or, if the column density of this gas is high enough to shield it from the dissociating background UV radiation, they may be composed primarily of Hydrogen molecules, H_2, and

Table 1.1: Phases of the interstellar medium in the Galaxy. Table adapted from Ferrière (2001)

Phase	T (K)	$n\,(\mathrm{cm}^{-3})$	Fraction of Volume	$M\,(10^9 M_\odot)$
Molecular clouds	10-20	$10^2 - 10^6$	0.01	$\sim 1.3 - 2.5$
Cold neutral medium	50-100	20-50	$0.01 - 0.04$	$\gtrsim 6.0$
Warm neutral medium	6000-10 000	0.2-0.5	$0.2 - 0.6$	|
Warm ionized medium	~ 8000	0.2-0.5	$0.15 - 0.4$	$\gtrsim 1.6$
Hot ionized medium	$\sim 10^6$	~ 0.0065	$0.4 - 0.7$	-

in this case the clouds are called *molecular*. It is in these densest, molecular, clouds that star formation (SF) takes place in our Galaxy.

There is no consensus about whether the clouds are in a dynamic state or rather are in a state of equilibrium, although there is growing evidence suggesting that MCs are in a state of hierarchical collapse. This, however, presents a problem, because early studies (Zuckerman and Evans, 1974; Zuckerman and Palmer, 1974) argued that MCs could not be in a state of free-fall, or else the SFR would be much larger than observed, and concluded that MCs should be supported in some way against gravitational collapse. In this frame, the main goal of this thesis, is to demonstrate that the scenario of global cloud collapse, with the star formation rate (SFR) and efficiency (SFE) regulated by massive star-feedback is plausible.

In this chapter we begin by introducing the ISM constituents (section 1.1) and their relation with the formation and evolution of stars (section 1.2). We continue in section 1.3 discussing the dynamic state of MCs, and in section 1.4 we present the corresponding scenarios of star formation. Finally, in section 1.5 we discuss the effects of feedback from massive star on the parental MC.

1.1 The interstellar medium

In our Galaxy, the space between the stars is not completely empty. Instead, it contains an extremely tenuous material known as the ISM, which is mainly composed of ordinary matter (gas and dust), relativistic charged particles (known as cosmic rays) and magnetic fields. The gas and dust are in the form of either individual clouds or in a diffuse background. Interstellar space typically contains about one Hydrogen atom per cubic centimetre and 100 dust particles per cubic kilometre. Cosmic rays are mixed with the gas and dust. There is also a weak (of order a few μG), but still very important, galactic magnetic field.

Each of the components of the ISM plays an important role in the process

Table 1.2: Physical properties of the molecular phase in the Galaxy

	GMCs	Clumps	cores
Mass ($M_\odot$)	$6 \times 10^4 - 2 \times 10^6$	10^2	$1 - 10$
Size (pc)	$20 - 100$	$0.2 - 4$	$0.1 - 0.4$
Density (cm^{-3})	$100 - 300$	$10^3 - 10^4$	$10^4 - 10^5$
Temperature (K)	$15 - 40$	$7 - 15$	10
Magnetic Field (μG)	$1 - 10$	$3 - 30$	$10 - 50$
Line width (km s^{-1})	$6 - 15$	$0.5 - 4$	$0.2 - 0.4$
Dynamical time (Myr)	3	1	0.6

of star formation and the interaction between the different components should be included in a comprehensive theory. However, to describe all components and their interactions an entire book would be needed, so in this section we will concentrate mainly in a short description of the molecular gas phase, the dust, and the magnetic field, which are the initial ingredients for star formation.

1.1.1 Interstellar Gas

The interstellar gas constitutes ∼10-15% of the total mass of our Galaxy, and tends to be concentrated near the galactic plane and through the spiral arms. In these regions, most of the stars are formed, in particular, the most massive ones.

This interstellar gas is composed mostly of hydrogen, with small amounts of carbon, oxygen, iron, and other heavier elements. Specifically, 70.4% of the total gas mass is hydrogen, ∼28.1% is helium, and only ∼1.5% is in heavier elements (see Ferrière, 2001, and references therein). The gas appears in mainly three phases (although as many as 5 or more have been suggested; e.g., Heiles, 2001), a *cold phase* consisting of molecular and atomic hydrogen gas and dust, a *warm phase*, with both atomic and ionized hydrogen gas, and a *hot phase*, containing shocked gas from supernova explosions, as well as what is referred to as coronal gas. The main physical parameters of these phases are listed in Table 1.1.

Of specific interest for star formation is the cold phase of the ISM, and in particular its molecular component, whose sub-components and physical properties are listed in Table 1.2. The molecular gas is mainly concentrated in a ring between 2 and 8 kpc in the Galactic plane and at a height of $\lesssim 0.2\,\mathrm{kpc}$ (Bronfman et al., 1988; Clemens et al., 1988). Also, this molecular gas is contained in hierarchically-organized discrete clouds from giant MCs or complexes (GMCs) with sizes of a few tens of pc, masses above $10^6\,M_\odot$ and number den-

sity, n, of $\sim 100 - 1000\,\mathrm{cm}^{-3}$, to small dense cores with sizes of several tenths of pc, masses $\sim 0.3 - 10^3\,M_\odot$ and number densities $\sim 10^4 - 10^6\mathrm{cm}^{-3}$ (Larson, 1981; Goldsmith, 1987). In general, the MCs are very cold, with temperatures in the range of 10 to 20 K (Goldsmith, 1987, see Table 1.2), corresponding to thermal velocities of $\simeq 0.22$ to $0.31\,\mathrm{km\ s}^{-1}$.

Regarding the dynamical features of MCs, Larson (1981) found what are often referred to as *Larson's relations*. The first relation tells us that MCs are supersonically turbulent with non-thermal velocity dispersion ($\sigma_{\rm rms}$) that increases as a power of the size ($R_{\rm C}$), i.e., $\sigma_{\rm rms} \propto R_{\rm C}^{\beta}$, where the presently-accepted value of β is $\sim 1/2$. Larson's second relation suggests that the density (ρ) decreases as a power of the size as $\rho \propto R_{\rm C}^{-1}$. However, it has been suggested (Kegel, 1989; Scalo, 1990; Vazquez-Semadeni and Gazol, 1995; Heyer et al., 2009; Ballesteros-Paredes et al., 2011a) that these relationships may not be as universal as previously thought, and instead, that the density-size relation is only an artefact of the criterion used to define them (Ballesteros-Paredes et al., 2012), and that the line-width-size relation generalizes to $\sigma_{\rm rms}/R_{\rm C}^{1/2} \propto \Sigma^{1/2}$ (where Σ is the surface density; Ballesteros-Paredes et al., 2011a).

1.1.2 Interstellar Dust

The interstellar dust constitutes about 1% of the gas. Dust grains are microscopic particles (with typical sizes of 0.1 to $1\,\mu$m) composed of dielectric materials and refractors, which are formed in the atmospheres of stars of late spectral type K or M, and expelled to the interstellar space by radiation pressure (Woolf and Ney, 1969; Draine, 1990). Dust particles become apparent by observing the extinction of light along the line of sight to background sources. Because of the small size of the dust particles, more blue light will be scattered than red light and, as a result, the images from the sources appear redder than they were without dust (interstellar reddening).

Gas and dust are well intermixed at all scales, and regions of high gas density are usually also regions of high dust density. A typical interstellar grain consists of a core of rock material (graphite, silicates or possibly iron) surrounded by an ice sheet (water, methane or ammonia), although it has been suggested the presence of ring molecules called polycyclic aromatic hydrocarbons (PAHs; Duley and Williams, 1981; Leger and Puget, 1984). Their thermodynamic properties depend on the environment, the average temperature in interstellar space is ∼10-20 K, but close to hot stars is 100-600 K, and in regions of ionized gas is 70-100 K. Its number density is extremely low, typically ∼100 dust particles per cubic kilometre.

Although dust is a small fraction of the mass of interstellar material, about 1%, and 0.1% of the baryonic mass of our galaxy, is of vital importance, since dust absorbs between 30 and 50% of starlight emitted in the Galaxy and re-emits it in the IR, which means that 0.1% of the baryons are responsible for $\lesssim$50% of the bolometric luminosity of the galaxy. Furthermore, the dust grains are the sites of formation of molecules and are responsible for most of the molecular hydrogen in the ISM (Hollenbach and Salpeter, 1971; Katz et al., 1999).

1.1.3 Magnetic fields

It is well known that magnetic fields permeate the Galaxy and can affect the gas dynamics. Ions tend to follow magnetic field lines, and the field lines can be compressed or expanded by electromagnetic effects (e.g., Shu, 1992).

Troland and Heiles (1986), using the Zeeman effect, reported a magnitude of a few μG with a slight tendency to increase with the increase in the density. This trend is more pronounced in the density range of $10^2 - 10^4\,\mathrm{cm}^{-3}$, where the magnetic field can reach tens of μG (see also Myers et al., 1995; Crutcher, 1999). Rand and Kulkarni (1989) by observing 116 near pulsars concluded that the local magnetic field has an uniform component $\sim 1.6\,\mu$G and an irregular component of $\sim 5\,\mu$G. In the other hand, Rand and Lyne (1994) obtained consistently an uniform field of $\sim 1.4\,\mu$G and they found that the magnetic field increases toward the Galactic center, reaching a magnitude of $\sim 4.2\,\mu$G in a Galactic radius of 4 kpc.

Although it is not clear the origin of the magnetic field, it is thought that it is generated in the interiors of stars and are amplified by the turbulence generated by supernovae explosions.

Magnetic field strength determinations by Zeeman splitting observations in MCs indicate that the magnetic field strength increases with increasing density with a power-law exponent $p \approx 2/3$ at densities $n > 300\,\mathrm{cm}^{-3}$ (Crutcher et al., 2010), which is expected if gravity dominates the magnetic pressure (e.g., Mestel, 1966). Thus, the magnetic pressure is insufficient to balance gravity and prevent contraction (see Section 2.5.2). At lower densities, $\lesssim 300\,\mathrm{cm}^{-3}$, the maximum strength of the interstellar magnetic field seems to be roughly constant $\sim 10\,\mu$G (Crutcher et al., 2010).

1.2 The Interstellar Medium-star cycle

Although the interstellar medium contains only a small fraction of the total mass of galaxies, it plays a vital role in many chemical and physical processes.

In particular, a very important process is the ISM-star cycle, in which stars form from molecular gas and dust in the densest and coldest regions in MCs. During a star's lifetime, depending on its total mass, a significant fraction of that material may be returned to the ISM through the winds of massive stars or mass ejections from young or late evolutionary stages. This ejections enrich the environment and at the same time can induce the formation of new stars from this processed material, thus completing the cycle. Thereby, to understand the evolution of a star, it is important to study the nature and evolution of the ISM, and of MCs in particular.

1.3 The Star Formation Efficiency

It is well known that the ISM and the process of star formation are closely related, since observations towards interstellar clouds reveal that all the current SF in the galaxy is associated with MCs of gas and dust (see, e.g., Blitz, 1993; Williams et al., 2000). On the other hand, regarding the physical processes involved, we know that stars form by gravitational contraction on dense cores in MCs (see, e.g., Shu et al., 1987). However, the complete cycle is not well understood and is a current subject of intense debate.

An important step in understanding the problem is understanding the evolution of giant molecular clouds (GMCs; see, e.g., Vázquez-Semadeni, 2010; Vázquez-Semadeni, 2012), from their birth to their possible destruction by the stars formed. In this context, the concept of star formation efficiency, which is typically defined as the mass fraction of a MC that turns into stars during its lifetime, appears and takes a central role. It is essentially an observable that models of star formation try to explain.

The SFE is an elusive concept of observational origin essentially, but is actually a function of space and time, and depends of what is the final fate of the clouds. Traditionally, it assumes that the cloud is a well-defined gas reservoir and has finite and well defined lifetime and mass. However, recent observational and theoretical studies, suggest that these assumptions are not necessarily verified. In particular, and very importantly, it is highly probable that GMCs are in the process of accreting mass from a reservoir of atomic gas (see, e.g., the review by Molinari et al., 2014). This is supported by observations that invariably suggest that GMCs are immersed in an atomic envelope (see, e.g., Blitz and Thaddeus, 1980; Wannier et al., 1983; Andersson and Wannier, 1993; Ballesteros-Paredes et al., 1999a; Brunt, 2003; Blitz et al., 2007) and increase their mass over time (Kawamura et al., 2009) and by numerical simulations of the formation of MCs from compressions in the warm neutral medium (WNM;

e.g., Ballesteros-Paredes et al., 1999a; Hennebelle and Pérault, 1999; Koyama and Inutsuka, 2000; Koyama and Inutsuka, 2002; Vázquez-Semadeni et al., 2007). For MCs accreting mass from the WNM throughout their lifetimes, converting part of their mass into stars, which inject energy to the cloud destroying or dispersing it, the concept of SFE becomes more elusive.

In this work we attempt to reformulate the concept of SFE in a dynamic environment trying to capture this complex situation.

1.4 Scenarios of Star Formation

An unresolved issue is whether the GMCs are in virial equilibrium or in *global* gravitational contraction. This debate comes from forty years ago. Initially Goldreich and Kwan (1974) proposed that the supersonic line-widths observed in MCs corresponded to movements of global gravitational contraction, but quickly Zuckerman and Palmer (1974) argued that, if this were the case, the SFR in the Galaxy would be much greater than the observed. Zuckerman and Evans (1974) then suggested that the line-widths could correspond to small-scale turbulence, introducing the notion that the clouds are entities in equilibrium, a notion that remained until recently (se e.g., Mac Low and Klessen, 2004). Since then, theoretical models of star formation have been based on the idea that turbulence provides support to the clouds against their self gravity, keeping them in a state of virial quasi-equilibrium (see, e.g., Norman and Silk, 1980; McKee, 1989; Matzner, 2002; Krumholz and McKee, 2005; Li and Nakamura, 2006; Nakamura and Li, 2007; Wang et al., 2010). However, recent observational and theoretical evidence have suggested a return to the possibility that MCs may be in a global state of gravitational contraction (see, e.g., Hartmann et al., 2001; Burkert and Hartmann, 2004; Hartmann and Burkert, 2007; Peretto et al., 2007; Vázquez-Semadeni et al., 2007; Galván-Madrid et al., 2009; Vázquez-Semadeni et al., 2009; Schneider et al., 2010; Csengeri et al., 2011; Peretto et al., 2014). Then, it is necessary to solve the problem of the excessive SFR that this scenario would seem to imply. Of curse, a solution to this problem has existed since the time when the debate first appeared: that the clouds are destroyed early in their evolution by their own stellar products (Field, 1970; Whitworth, 1979; Cox, 1983; Elmegreen, 1983; Franco et al., 1994). In this work we adopt this point of view, and we assume that the radiation of massive stars (ionizing photons, radiation pressure, winds and supernova explosions) can regulate the SFR, maintaining a low SFE, as suggested by the observations (see for example the review of Vázquez-Semadeni, 2010).

These two possible states, clouds in equilibrium and clouds in global gravi-

tational contraction, give rise to two main scenarios that attempt to explain the star formation process: *slow* and *fast* star formation. Both are able to explain the observed SFE. To get a clear picture, we can write the SFE as

$$\mathrm{SFE} = \frac{1}{M_{\mathrm{C}}} \int_{\Delta t} \mathrm{SFR}\, dt, \tag{1.1}$$

where M_{C} is the total cloud mass, and Δt is "the cloud lifetime". Assuming a constant SFR during Δt , we have

$$\mathrm{SFE} = \frac{\mathrm{SFR}}{M_{\mathrm{C}}} \Delta t. \tag{1.2}$$

We intuitively can see from this expression, that a low SFE can be achieved through a low SFR for a long time (a few tens of Myr) consistent with models in which SFR is regulated by turbulence (*slow* star formation), or through a high SFR in a short time (a few Myr) consistent with models of clouds in global gravitational contraction (*fast* star formation).

Other proposals to explain the low SFE in the Galaxy are that global MC collapse is prevented because *i)* strong magnetic fields support the clouds (e.g., Allen and Shu, 2000); or *ii)* GMCs are gravitationally unbound (e.g., Clark and Bonnell, 2004).

1.4.1 Slow Star Formation

For many years, the accepted scenario of star formation (particularly of low-mass) was the *Standard Model*, in which clouds are globally supported by magnetically subcritical magnetic fields, and the cores contract quasi-statically over long times ($\sim$ 10 My) until the magnetic flux has been sufficiently redistributed through the process known as *ambipolar diffusion* (AD), so the magnetic forces are no longer capable of supporting the core, allowing the dynamic gravitational collapse (e.g., Shu et al., 1987; Mouschovias, 1991a). According to this model, the low SFE is explained by the low mass fraction that becomes supercritical by the AD.

However, these ideas of equilibrium or quasi-equilibrium, seem contradictory with the highly turbulent nature of the ISM, so the presence of turbulence within the MCs has recently been considered as a possible mechanism to reduce the SFE, if the *turbulent pressure* is considered as an additional agent of support to the thermal and magnetic pressures against gravity. These ideas give rise to the *Turbulent Model*. The key point in this model is that the turbulence has a dual effect: it supports the cloud as a whole, while locally it induces density

fluctuations (Sasao, 1973; Leorat et al., 1990; Klessen et al., 2000; Vázquez-Semadeni et al., 2003).[1]

In the case of supersonic isothermal turbulence, strong density fluctuations are produced (e.g., von Weizsäcker, 1951; Sasao, 1973; Elmegreen, 1993; Vazquez-Semadeni, 1994; Gammie and Ostriker, 1996; Passot and Vázquez-Semadeni, 1998; Ballesteros-Paredes et al., 1999b; Ostriker et al., 1999; Padoan and Nordlund, 1999; Ostriker et al., 2001), forming dense sheets and filaments (e.g., Vazquez-Semadeni et al., 2000) in which stars form later, even in the presence of supercritical magnetic fields (e.g., Ostriker et al., 1999; Padoan and Nordlund, 1999; Ostriker et al., 2001; Vázquez-Semadeni et al., 2005a). Thus, several numerical studies with (Heitsch et al., 2001; Vázquez-Semadeni et al., 2005a; Vázquez-Semadeni et al., 2005b) and without (Klessen et al., 2000; Vázquez-Semadeni et al., 2003) magnetic field, have shown that increasing the strength (i.e., the Mach number of the turbulence) of the continuously forced turbulence, the effect is to reduce the SFE (see also Mac Low and Klessen, 2004). However, studies in which the turbulence is applied only initially, so that it subsequently decays, showed the opposite effect (Nakamura and Li, 2005), suggesting that the nature and development of turbulence effect is essential in determining the SFE.

In summary, supersonic isothermal turbulence provides global support to the MCs, but produces local collapse, involving small mass fractions, and producing a low SFE (Klessen et al., 2000; Heitsch et al., 2001; Vázquez-Semadeni et al., 2003), as observed in low-mass star forming regions in galactic disks (e.g., Myers et al., 1986; Federrath and Klessen, 2013). In contrast, the lack of turbulent support results in regions collapsing freely. In hydrodynamic simulations (e.g., Wada and Norman, 1999; Klessen and Burkert, 2000), the gas collapses freely form a network of overdensities in which the star formation is highly efficient, as observed in high-mass star forming regions.

In the last decade there have been various analytical models for the SFE based on the notion of turbulent support. The most relevant one for our purposes is the so called *cloud-support* models (Krumholz and McKee, 2005; Hennebelle and Chabrier, 2011; Padoan and Nordlund, 2011; Federrath and Klessen, 2012; Federrath and Klessen, 2013).[2] In these models, the turbulence is the key physical process, since it supports globally the MC against gravity (maintaining the cloud in quasi-equilibrium conditions) and regulates the SFR by inducing local compressions that cause a small fraction of clouds mass to collapse per global free-fall time.

However, this class of models is not fully supported by simulations of MC

[1] See also the review by Vazquez-Semadeni et al. (2000).

[2] These models differ in the way they chose the threshold density.

formation and evolution (Vázquez-Semadeni et al., 2007; Heitsch and Hartmann, 2008; Vázquez-Semadeni et al., 2010; Vázquez-Semadeni et al., 2011). In such simulations, the effect of large-scale turbulence in the warm ISM is to form dense, cold clouds that rapidly engage in global gravitational collapse, the turbulence induced by the formation process being insufficient to support the clouds. Moreover, SF does not begin in those clouds until after several Myr of collapse. Thus, by the time SF starts, the cloud is already collapsing, and so stellar feedback cannot be the driver of the internal cloud turbulence, at least during its early stages.

1.4.2 Rapid Star Formation

The alternative is to return to the scenario of global gravitational contraction. A large number of studies argue in favor of this scenario by noting that several observational properties of clouds and clumps are consistent with models dominated by such contraction (e.g., Hartmann and Burkert, 2007; Peretto et al., 2007; Vázquez-Semadeni et al., 2009; Peretto et al., 2013). Moreover, the notion of random turbulence on a small scale seems contrary to the fact that the main component of the speed differences within the clouds and clumps at all levels seems to occur at the largest scales, consistent with coherent motions in the scale of the clump or cloud (Heyer and Brunt, 2007).

Recent evidence suggests that GMCs start near the magnetically supercritical state (e.g., Crutcher, 1999), which eliminates the long AD time of the standard model (e.g., Ciolek and Basu, 2001; Fatuzzo and Adams, 2002; Heitsch et al., 2004), but perhaps the most compelling evidence in the change of vision is that the MCs seem to form strars synchronously, so that the ages of the stars in the clusters are all very similar, and in fact, very few stars older than the average age of the cluster stars are observed. In particular there is the so called post-T-Tauri problem, which consists of the apparent absence of old T-Tauri stars in the vicinity of star forming regions. Ballesteros-Paredes et al. (1999a) proposed that the solution to this problem is that MCs are formed on short time scales by compression from large scale flows. These authors suggested that, for example, the Taurus MC has formed recently (~ 3 Myr ago) by this mechanism, suggesting that older stars near the region (with ages 5-10 Myr) are field stars.

Numerical studies of formation of clouds by WNM converging flows show that the clouds are born turbulent due to various instabilities, such as Kelvin-Helmholtz, Rayleigh-Taylor, thermal, and the nonlinear thin-shell instability (Koyama and Inutsuka, 2002; Audit and Hennebelle, 2005; Heitsch et al., 2005; Vázquez-Semadeni et al., 2006). The resulting turbulence is subsonic relative to the warm gas, but supersonic with respect to the cold phase (Koyama and Inut-

suka, 2002; Heitsch et al., 2005), involving large density fluctuations (clumps) for which the free-fall time is significantly less than the average of the cloud. Thus, once the global collapse begins, the clumps can complete their collapse faster than the bulk of the cloud, so that these clumps begin to form stars, which then begin to feed energy and momentum back onto their parent clouds, potentially destroying them before they can complete their global collapse (see, e.g., Vázquez-Semadeni et al., 2010; Dale et al., 2012; Colín et al., 2013; Dale et al., 2013).

Specifically, recent numerical studies of cloud formation by converging warm neutral gas streams, which produce an initially atomic dense cloud, show that the cloud grows in mass over time, until it becomes gravitationally unstable and begins to form stars (e.g., Vázquez-Semadeni et al., 2007). Thus, cloud turbulence produced during the process of its formation, is then replaced by large scale motions of gravitational contraction. Vázquez-Semadeni et al. (2008) conducted a systematic study of the topology of the velocity field, finding a clear tendency for denser objects to have more convergent flows. This contradicts the traditional view that the broad lines of the MCs and their substructure correspond to random turbulence. Instead, MCs contain a significant component of large-scale convergence, in accordance with the original proposal of Goldreich and Kwan (1974). In any case, the MCs contain large nonlinear overdensities in which the free-fall time ($t_{\rm ff}$) is significantly shorter than the average MC. Thus, once the global collapse begins, the clumps can complete their collapse faster than the bulk of the cloud if they have masses larger than their Jeans mass. However, if clouds and their substructure are in gravitational contraction, as originally raised by Goldreich and Kwan (1974), is necessary to solve the Zuckerman & Palmer conundrum in this scenario.

1.5 Self-regulated star formation

Many different physical processes contribute to shaping galactic ecosystems. To understand galactic structure, morphology, and evolution, a key question is what regulates the star formation rate. Because stars have an impact on their environment, the rate at which gas can collapse to make new stars is affected by the previous generation of star formation.

Newly born stars appear in or near the MC in which they formed. Generally, when stars are formed, they do so in large numbers and some of them are massive stars. These hot stars immediately begin photoionizing the residual ISM around themselves, giving rise to bright HII regions. Thus, massive stars not only erode the interface between their HII region and the dark MC, they

also *sweep up* material, compressing it and possibly generating new bursts of star formation around of the ionization fronts (Field and Saslaw, 1965).

1.5.1 Feedback from massive stars

As we have mentioned, the stars have a strong effect mainly on their birth environments through their various feedback mechanisms, which could be classified in three main categories (following Krumholz et al., 2014a): *i) momentum feedback*, through protostellar outflows and radiation pressure, which inject momentum into star-forming clouds; *ii) explosive feedback*, through winds from massive stars with $M > 40\,M_{\odot}$, photoionization feedback and supernovae; and *iii) thermal feedback*, through non-ionizing radiation. However, the ionizing feedback from massive stars is generally considered to be the dominant mechanism of stellar energy injection at the scale of GMCs (Matzner, 2002), unless there is a population of stars with masses $\gtrsim 20\,M_{\odot}$, in which case the radiation pressure begins to be the dominant eedback process (Krumholz et al., 2009). Thus, hereinafter we will only consider the ionizing radiation from massive stars in large scale, although a comprehensive study should include all the feedback mechanisms.

Whitworth (1979) analytically estimated the effect of expanding *blister* HII regions (or *champagne flows*) on the parent cloud of massive stars, concluding that once 4% of the mass of a GMC of 10^5 $M_{\odot}$ has been converted to stars, their feedback is sufficient to completely disperse the remaining cloud. Franco et al. (1994) extended this result considering that a fraction of massive stars are embedded in the cloud and do not produce a blister HII region, but rather an embedded one, and estimated the maximum number of massive stars that can be hosted by a GMC before it is destroyed, concluding that the SFE (the mass converted to stars) falls in the range of 2%−16%, with an average of 5%.

However, these authors considered the effects of ionization on smooth clouds of constant mass and density. Also, 2D numerical simulations by Bodenheimer et al. (1979) showed that blister HII regions could be an efficient dispersal mechanism. On the other hand, Mazurek (1980) and Yorke et al. (1989) found that the disruption of clouds by HII regions is strongly impeded if the clouds are in free fall and if the ionizing sources are embedded in the cloud. Dale and Bonnell (2011) in 3D numerical simulations, also found that accretion flows onto an ionizing source strongly limit the effect of ionizing feedback. Thus, the picture from recent numerical simulations of HII regions expanding in highly structured clouds is less clear, because the expanding HII regions can also promote the formation on new stars.

Oort (1954) first suggested the idea of positive feedback, in which expan-

ding ionization fronts might sweep up material forming dense shells which, can fragment and produce cold cloudlets that may eventually collapse. Dale et al. (2005) by numerical simulations of dynamically expanding HII regions, find evidence of both positive and negative feedback, although Mac Low et al. (2007) found that expanding HII regions in a turbulent cloud do not efficiently trigger star formation. Observationally, it is extremely difficult to identify triggered star formation.

1.6 Goal

In this thesis, we will study the effect of ionizing feedback (and magnetic fields) in destroying the clouds and regulating SF in collapsing MCs (within the scenario of *rapid* SF) from an analytical and numerical point of view. Analytical models to date are based on clouds of constant mass and in equilibrium (Whitworth, 1979; McKee, 1989; Franco et al., 1994, see also Section 1.4.1). In Chapters 3 and 4 we present a semi-analytical model extending these previous studies to the case of evolving clouds. For this, we propose a model for the SFR and SFE in MCs formed by the collision of WNM streams (trying to capture the phenomenology observed in numerical simulations as those presented in, e.g., Vázquez-Semadeni et al., 2007). In this scenario, the cloud accretes mass from the diffuse phase and loses mass by SF and ionization from massive stars. Thus, we investigate the competition between destruction and regeneration in the cloud.

On the other hand, in Chapter 5 we perform numerical simulations of MC formation, incorporating magnetic fields, self-gravity, radiative cooling and heating, and stellar feedback. This complements our semi-analytical model and previous numerical studies (Vázquez-Semadeni et al., 2007; Vázquez-Semadeni et al., 2011; Colín et al., 2013).

2

Physics of Star Formation

We now focus on the macro-physics of star formation from a dynamical point of view, addressing different physical processes taking place at different scales of time and space in the star forming clouds. We will use this description mainly in numerical models (Chapter 5).

The chain of events for star formation is as follows. The ISM can be treated as an ideal gas (Section 2.2) obeying the hydrodynamic Equations (Section 2.1), and subject to heating and cooling processes (described in Section 2.3). As is well known, the stars are formed by gravitational collapse in molecular cloud cores, so that gravity (Section 2.4) eventually overcomes the agents that oppose it. Most of these cores are located in the middle plane of our Galaxy, where the magnetic energy density is comparable to the kinetic energy density of the gas, which means that the magnetic field, described in Section 2.5, is important in the energy budget of this gas. Once stars form in a molecular cloud core, the ionizing radiation (Section 2.6), mainly from massive stars, becomes the dominant process in the dynamics of the parental MC, causing its destruction or dispersion. During all evolutionary stages of MCs, the flow regime is turbulent (Section 2.7), with turbulence playing different roles depending on the scale and the physical conditions. Finally, in Section 2.8 we list the final set of equations that we use for the numerical simulations presented in Chapter 5.

2.1 Hydrodynamics

We can treat the ISM as a continuum, since the gas particles undergo many collisions before traversing a significant fraction of the region, sharing their collective physical properties, and therefore their velocity distributions are Maxwellian, implying that we can describe them by a single gas kinetic temperature which

is usually the same for all species of particles present. Thus, the state of the gas can be described in terms of macroscopic properties in addition to temperature (e.g. pressure, density and velocity), which are averages over the properties of many individual particles contained within regions of extent (L) much greater than the mean free path (l). Usually, for most systems in the ISM, the condition $L \gg l$ is satisfied. For example, for the WNM ($L \sim 100\,\mathrm{pc}$, $n \sim 1\,\mathrm{cm}^{-3}$),[1] GMCs ($L \sim 10\,\mathrm{pc}$, $n \sim 100\,\mathrm{cm}^{-3}$), and dense cores($L \sim 0.1\,\mathrm{pc}$, $n \sim 10^4\,\mathrm{cm}^{-3}$), the corresponding mean free path are roughly 10^{-4}, 10^{-6}, and $10^{-8}\,\mathrm{pc}$, respectively.

A more detailed description of the physics described here can be found in, e.g., Dyson and Williams (1980) and Shu (1992).

2.1.1 Euler Equations

The Euler equations for compressible gas dynamics are a set of expressions of the conservation of mass, momentum and energy for isolated systems, neglecting diffusive effects.

In the absence of sources or sinks of mass, the conservation of mass is expressed by the *continuity equation*

$$\frac{\partial \rho}{\partial t} + \nabla \cdot (\rho \mathbf{u}) = 0, \tag{2.1}$$

where ρ is the density and $\mathbf{u}$ the velocity of the fluid.

In the absence of external forces (*body* forces due to gravity or magnetic field), Newton's second law of motion applied to a fluid leads us to the equation of conservation of momentum per unit volume,

$$\frac{\partial (\rho \mathbf{u})}{\partial t} + \nabla \cdot (\rho \mathbf{u}\mathbf{u}) + \nabla P = 0, \tag{2.2}$$

where P is the fluid pressure. As we will show in Section 2.7, viscous effects can be safely neglected. Thus, the interstellar gas can be modeled as an ideal fluid which is governed by the Euler equations.

Next is the first law of thermodynamics. However, to derive the corresponding equation, it is necessary to consider the conservation of total energy, because the exertion of a force onto the system will have an effect on both its internal and its kinetic energy. Thus, we have

$$\frac{\partial (\rho e_{\mathrm{tot}})}{\partial t} + \nabla \cdot [(\rho e_{\mathrm{tot}} + P)\mathbf{u}] = 0, \tag{2.3}$$

[1] See Tables 1.1 and 1.2.

where the total specific energy, $e_{\rm tot}$, is the sum of the specific internal energy, $e_{\rm int}$, and the kinetic specific energy of the gas, i.e.,

$$e_{\rm tot} = e_{\rm int} + \frac{1}{2}u^2, \tag{2.4}$$

Additional source terms must be added to the Euler Equations (2.1)-(2.3) to properly model the star formation process.

Finally, we need another equation to close the system, since the set of partial differential equations given by the Euler equations represent five equations and six variables. This additional equation is the equation of state of an ideal gas, which relates the thermal pressure P to the internal energy of the gas, which we discuss in the next section.

2.2 Thermodynamics of an Ideal Gas

In general, the ISM is assumed to behave as an ideal gas, since its constituent particles (atoms, molecules, and dust) interact only elastically, and also it is in general highly rarified. The thermal equation of state of an ideal gas is

$$P = nk_{\rm B}T, \tag{2.5}$$

where P is the pressure, n the number density, T the gas temperature, and $k_{\rm B}$ the Boltzmann constant. The mass density ρ is given by $\rho = \mu m_{\rm p} n$, μ being the mean molecular weight, and $m_{\rm p}$ the proton mass. Whith this, Equation (2.7.4) can also be written as

$$P = \frac{\rho k_{\rm B} T}{\mu m_{\rm p}}. \tag{2.6}$$

It can be shown that this equation can be rewritten in terms of the adiabatic index, γ, and the specific internal energy, as

$$P = (\gamma - 1)\, \rho\, e_{\rm int}. \tag{2.7}$$

Combining Equations (2.6) and (2.7), we find a relation between specific internal energy and temperature given by

$$T = \frac{\mu m_{\rm p}}{k_{\rm B}}(\gamma - 1) e_{\rm int}. \tag{2.8}$$

In partially ionized plasmas, such as HII regions, it is important to consider the degree of ionization of the gas. Thus, we need to introduce the ionization fraction to Equation (2.8), which becomes

$$T = \frac{\mu m_{\rm p}}{k_{\rm B}} \frac{(\gamma - 1) e_{\rm int}}{1 + x_{\rm HII}}, \tag{2.9}$$

where we have considered a gas containing pure hydrogen with total number density, $n_{\rm H}$, given by

$$n_{\rm H} = n_{\rm HI} + n_{\rm HII}, \tag{2.10}$$

with $n_{\rm HI}$ and $n_{\rm HII}$ respectively being the number density of atomic and ionized hydrogen, so that their respective fractions are

$$x_{\rm HI} = \frac{n_{\rm HI}}{n_{\rm H}}, \qquad x_{\rm HII} = \frac{n_{\rm HII}}{n_{\rm H}}. \tag{2.11}$$

Equation (2.9) completes the set of thermodynamic relations for a partially ionized gas.

2.3 Heating and Cooling

Microscopic and radiative processes govern the heating and cooling in the ISM, which are crucial in MCs for the star formation activity. To form a star, the gas must undergo gravitational collapse. During this collapse, the gas density increases. Collisions between atoms and molecules become more frequent and the gas temperature rises. Since a heated gas tends to expand, the cloud collapse could be halted, unless heat is effectively and continuously removed from the cloud. We account for these processes by adding source terms to the energy Equation (2.3),

$$\frac{\partial(\rho e_{\rm tot})}{\partial t} + \nabla[(\rho e_{\rm tot} + P)\mathbf{u}] \;=\; \Gamma - n\Lambda, \tag{2.12}$$

where we have introduced the heating rate, $\Gamma = \Gamma(n, T)$, and the cooling rate, $n\Lambda = n\Lambda(n, T)$. Several heating and cooling mechanisms are at work within different regions of the ISM. Which mechanism dominates depends on the physical conditions of the ISM, as we will see next.

2.3.1 Heating

In the WNM (where $T \sim 8000\,\mathrm{K}$, and the ionization fraction is $\sim 10^{-3}$), photoelectric heating from grains dominates at densities larger than $0.1\,\mathrm{cm}^{-3}$, but at

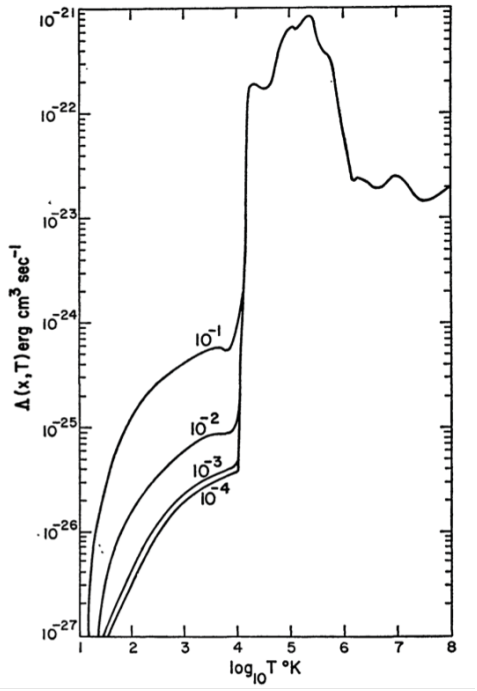

Figure 2.1: Cooling function, Λ, as a function of temperature from Dalgarno and McCray (1972). The labels indicate the ionization fraction.

lower densities the heating becomes dominated by a combination of cosmic ray and X-ray heating, with negligible contributions from carbon photoionization (aided in part by the fact that at 8000 K the carbon ionization fraction is high, making photoionization heating inefficient).

In the cold neutral medium (CNM; where $T \sim 100$ K and the ionization fraction is $\sim 10^{-4}$), photoelectric heating dominates over the entire range of densities, followed by cosmic ray heating down by about a factor of 10-100. Photoionization heating by Carbon and X-ray photoelectric heating are down by many orders of magnitude over the entire range (e.g., Wolfire et al., 1995, see Figure 2.2).

In the cold cores of molecular clouds (where $T \sim 10$ K and the ionization fraction is $\sim 10^{-7}$), UV photons from the interstellar radiation field cannot penetrate and photoelectric heating becomes negligible. Cosmic ray heating dominates over the entire range of densities, and other processes related to gas dynamics become important, but all at least an order of magnitude smaller than cosmic ray heating (e.g., Wolfire et al., 1995; Koyama and Inutsuka, 2000, see Figure 2.2).

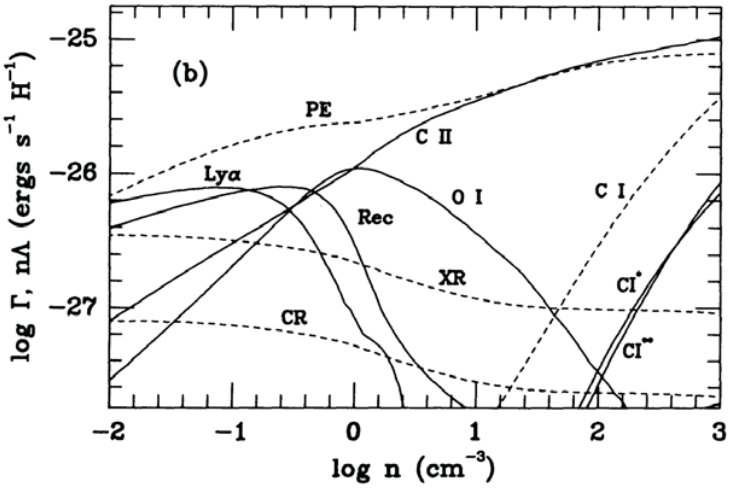

Figure 2.2: Heating and cooling rates per hydrogen nucleus as a function of number density. Solid and dashed lines indicate cooling and heating process, respectively. Labels are as follows. PE: photoelectric heating from small grains and PAHs; XR: X-ray; CR: cosmic ray; CI: photoionization of C; CII: CII fine-structure; OI: OI fine-structure; Rec: recombination onto small grains and PAHs; Lyα: Lyα plus metastable transitions; CI*: fine structure 609 μm; CI**: fine structure 370 μm. Figure from Wolfire et al. (1995).

2.3.2 Cooling

Cooling processes involve the conversion of kinetic energy (thermal motion) to radiant energy (photons) that can escape from the system. This typically occurs through collisional excitation, followed by radiative decay.

The main source of cooling is molecular rotational and vibrational de-excitation, emitting photons from particles previously excited by collisions with H_2, H, dust or electrons. However, if the density is high the de-excitation can also occur through another collision. An important coolant is CO through rotational excitation, as well as trace ions (CII) at low densities, and neutral C and O fine structure excitation at high density. In warm gas ($T \sim 6000\,\mathrm{K}$), the molecules CO, OH and H_2O also make considerable contributions to the cooling, and vibrational H_2 emission cools molecular gas after it has been strongly heated in shock waves to over $\sim$ 1000 K. Rotational excitation of H_2 will also cool gas heated above $\sim$ 200 K. This mechanism of cooling is probably the dominant in MCs (see, e.g., Wolfire et al., 1995; Koyama and Inutsuka, 2000).

A second important cooling mechanism is the dust emission, which occurs when the gas transfers energy to the dust through gas-grain collisions, provided

that the grains are cooler than the gas. The dust grains are efficient radiators in the long wavelength continuum (infrared and submillimetre) and so the radiated energy escapes from the cloud. However, the dust is also a potential heating source through collisions if the dust can be kept warmer than the molecules by background radiation (e.g., Goldsmith, 2001).

Other less relevant cooling processes are bremsstrahlung (important for a fully ionized gas), resonance lines, and recombination (Dalgarno and McCray, 1972).

2.4 Gravity

Gravity is the universal force that causes all matter to attract. In general, when the force of gravity pulling in on a MC is greater than the strength of various forms of internal pressure pushing out, the cloud collapses. Thus, star formation occurs when singularities (in practice, objects much denser than the MC gas) in the density field of an MC begin to appear.

2.4.1 Poisson Equation

The self-gravity of the gas —that is, the mutual gravitational attraction of all particles of the gas— is described as follows. Since the gravitational field is conservative, it can be expressed in terms of a scalar potential ϕ as

$$\mathbf{g} = -\nabla\phi, \tag{2.13}$$

where $\mathbf{g}$ is the gravitational acceleration. The negative sign follows the convention that work is gained from a loss of potential energy. This gravitational potential is related to the gas density through Poisson's equation

$$\nabla^2\phi = 4\pi G\rho, \tag{2.14}$$

where G is the Newton's constant.

The gravitational acceleration enters the momentum Equation (2.2) as a gravitational force per unit volume, $\rho\mathbf{g}$. Thus, the momentum equation in the presence of gravitational forces is

$$\frac{\partial(\rho\mathbf{u})}{\partial t} + \nabla\cdot(\rho\mathbf{u}\mathbf{u}) + \nabla P = \rho\mathbf{g}. \tag{2.15}$$

Finally, we add the corresponding term in the energy Equation (2.3), which then reads

$$\frac{\partial(\rho e_{\rm tot})}{\partial t} + \nabla\cdot[(\rho e_{\rm tot} + P)\mathbf{u}] = \rho\mathbf{u}\cdot\mathbf{g}. \tag{2.16}$$

Therefore the gravitational field can change not only the dynamical properties, but also the thermodynamic properties of the system.

2.4.2 Jeans Gravitational instability

Support against gravity may be provided in particular by thermal pressure. According to the Jeans classic analysis of sound waves propagating through a uniform and isothermal gas of density ρ_0 in the presence of self-gravity, we find that modes with wavelengths larger than the so-called Jeans length, given by

$$\lambda_{\mathbf{J}} = \frac{2\pi}{k_{\mathbf{J}}} = \sqrt{\frac{\pi c_{\rm s}^2}{G\rho_0}}, \tag{2.17}$$

are gravitationally unstable, so that the perturbations grow exponentially. To relate this critical wave number to a critical mass, $M_{\rm J}$, we consider a *sphere* with diameter $\lambda_{\mathbf{J}}$ and density ρ_0. Thus,

$$M_{\rm J} = \frac{4\pi}{3}\rho_0\Big(\frac{\lambda_{\mathbf{J}}}{2}\Big)^3 = \frac{\pi^{5/2}}{6G^{3/2}}\frac{c_{\rm s}^3}{\rho_0^{1/2}}. \tag{2.18}$$

If the mass of a spherical condensation is greater than $M_{\rm J}$, it will collapse. For an isothermal gas, the sound speed is given by

$$c_{\rm s} = \sqrt{\frac{k_{\rm B}T}{\mu m_{\rm p}}}, \tag{2.19}$$

and therefore the Jeans Mass scales as $M_{\rm J} \propto \rho_0^{-1/2}T^{3/2}$. Once the cloud is gravitationally unstable, the free-fall time for spherical homologous collapse,

$$t_{\rm ff} = \Big(\frac{3\pi}{32G\rho}\Big)^{1/2}, \tag{2.20}$$

is a good approximation for the collapse time scale. However, most structures in the ISM are far from spherical, so the Jeans mass must be recalculated, for a planar geometry as we show in Section 3.3.4.

2.5 Magnetic Field

The equation governing the evolution of the magnetic field in a (possibly partially) ionized gas is (see, e.g., Shu, 1992)

$$\frac{\partial \mathbf{B}}{\partial t} = \nabla \times (\mathbf{u} \times \mathbf{B}) - \nabla \times \Big(\eta \nabla \times \mathbf{B}\Big), \tag{2.21}$$

where η is the magnetic diffusivity. The second term in the right hand side of Equation (2.21) represents the effect of Ohmic dissipation, which we can neglect, not because the conductivity of astrophysical gases has much larger values in comparison with normal terrestrial materials, but because typical systems have enormous dimensions, L, and the characteristic diffusion time, defined as $t_{\rm D} \sim L^2/\eta$, is much longer than the dynamic time ($\sim L/c_{\rm s}$) of these systems. This case is referred to as *ideal* magnetohydrodynamic (MHD). Thus, we have that Equation (2.21) simplifies to

$$\frac{\partial \mathbf{B}}{\partial t} = \nabla \times (\mathbf{u} \times \mathbf{B}). \tag{2.22}$$

This equation is known as the induction equation. Also, we need to consider that magnetic monopoles do not exist in Nature. This condition is expressed by the condition

$$\nabla \cdot \mathbf{B} = 0, \tag{2.23}$$

which must be satisfied at all times.

2.5.1 Magnetic flux freezing

We define the magnetic flux across a cross-sectional area A of the fluid as

$$\Phi \equiv \int_A \mathbf{B} \cdot \mathbf{n} dA. \tag{2.24}$$

Using Stokes' theorem, the Lagrangian derivative of the magnetic flux is

$$\frac{d\Phi}{dt} = \int_A \frac{\partial \mathbf{B}}{\partial t} \cdot \mathbf{n} dA + \int_A \nabla \times (\mathbf{B} \times \mathbf{u}) \cdot \mathbf{n} dA = 0, \tag{2.25}$$

which we have equated to zero using Equation (2.22) ignoring the dissipative term. This implies that the magnetic flux does not change as a fluid parcel evolves, changing its cross-section area in the *ideal* MHD regime, i.e., in the absence of resistive effects. This effect is commonly referred to as *flux freezing*. For collapsing dense cores, thus implies that the field is carried with gas during the collapse.

In the ISM in general, the resistivity is extremely low and so flux freezing is applicable at all but the highest densities.

2.5.2 Mass-to-flux ratio and magnetic support

To get an idea about the support provided by a magnetic field to a cloud against its self-gravity, we consider a spherical cloud of radius R, uniform density ρ, constant temperature T, and permeated by uniform magnetic field of magnitude B. The gravitational energy is

$$E_{\rm g} = -G \int \frac{M'(r)}{r} dr \approx -\frac{3}{5}\frac{GM^2}{R}, \tag{2.26}$$

whereas that the magnetic energy is

$$E_{\rm mag} = \int \frac{B^2}{8\pi} dV \approx \frac{B^2 R^3}{6}. \tag{2.27}$$

Then, the ratio of the gravitational to the magnetic energy is

$$\frac{|E_{\rm g}|}{E_{\rm mag}} \approx \frac{18\pi^2 G}{5}\Big(\frac{M}{\Phi}\Big)^2, \tag{2.28}$$

where $\Phi \approx \pi R^2 B$ is approximately the magnetic flux (Equation (2.24)) in this geometry. The term (M/Φ) is known as *mass-to-flux ratio*. The condition for collapse, $|E_{\rm g}| > E_{\rm mag}$, implies

$$\frac{M}{\Phi} > \Big(\frac{M}{\Phi}\Big)_{\rm crit} \equiv \sqrt{\frac{5}{18\pi^2 G}} = \text{cst.}, \tag{2.29}$$

although the exact value of the numerical factor depends on the geometry. A cloud with $M/\Phi > (M/\Phi)_{\rm crit}$ is referred to as *magnetically supercritical*; otherwise it is referred to as *magnetically subcritical*.

2.5.3 Coupling to Hydrodynamics

The magnetic field can affect the dynamics and thermodynamics of the gas through the Lorentz force, $\mathbf{f}_{\rm L}$, exerted on a charged particle of velocity $\mathbf{u}$ moving in an electric field $\mathbf{E}$ and a magnetic field $\mathbf{B}$. The force due to the magnetic field is perpendicular to both the direction of the velocity vector and the magnetic field, and is given by

$$\mathbf{f}_{\rm L} = e n_e \Big(\mathbf{E} + \frac{\mathbf{u}}{c} \times \mathbf{B}\Big), \tag{2.30}$$

where e is the electron charge, n_e is the electron number density, and c is the speed of light. We have assumed that the fluid is electrically neutral. Providing

that electric fields are negligible, charged particles are forced to spiral around magnetic field lines and cannot actually cross them except by collisions. Thus, Equation (2.30) becomes

$$\mathbf{f}_{\mathrm{L}} = -\frac{2en_e}{c}(\mathbf{u}_i \times \mathbf{B}) = \frac{\mathbf{j}}{c} \times \mathbf{B} = \frac{1}{4\pi}(\nabla \times \mathbf{B}) \times \mathbf{B} = \frac{1}{4\pi}(\mathbf{B} \cdot \nabla)\mathbf{B} - \frac{1}{8\pi}\nabla B^2, \tag{2.31}$$

where we have used some standard vector identities ($\mathbf{j}$ is the current density and $\mathbf{u}_i$ is the ion velocity). Including this force, we can rewrite the equation of momentum (2.2) as

$$\frac{\partial(\rho\mathbf{u})}{\partial t} + \nabla \cdot (\rho\mathbf{u}\mathbf{u}) = -\nabla\Big(P + P_B\Big) + \frac{1}{4\pi}(\mathbf{B} \cdot \nabla)\mathbf{B}, \tag{2.32}$$

where we have defined the magnetic pressure as $P_B \equiv B^2/8\pi$, whose effect is to oppose to the gathering together of the magnetic field lines.

Finally, the equation of energy (2.3) reads

$$\frac{\partial}{\partial t}\Big(\rho e_{\mathrm{tot}}\Big) + \nabla \cdot \left[\Big(\rho e_{\mathrm{tot}} + P + P_B\Big)\mathbf{u} - \frac{1}{4\pi}(\mathbf{u} \cdot \mathbf{B})\mathbf{B}\right] = 0. \tag{2.33}$$

2.5.4 Magnetohydrodynamic waves

Small-amplitude perturbations in a magnetised fluid can produce three different types of the so-called MHD waves, which transmit disturbances over appreciable lengths. The first one is the so-called Alfvén wave, which propagates at the *Alfvén speed*

$$v_{\mathrm{A}} = \frac{B}{\sqrt{4\pi\rho}} \tag{2.34}$$

in the same direction as the magnetic field. The Alfvén wave is a transverse wave and does not produce pressure or density fluctuations. However, the magnetic field tension provides a restoring force. The other two waves are referred as *fast* and *slow magneto-sonic waves*, and propagate at different phase velocities. The Alfvén velocity lies between these two speeds. For a detailed derivation and discussion see, e.g., Shu (1992).

2.6 Radiation

Radiation from stars has a strong impact on MCs, so that any model without this ingredient is incomplete. Moreover, and regardless of the scenario of SF, ionizing radiation from massive stars is proposed as the main mechanism for energy injection into MCs (Matzner, 2002, see also Sections 1.4.1 and 1.4.2). Therefore, we include effects of ionizing feedback (such as HII regions), first in a semi-analytical model (Chapters 3 and 4) and then in numerical simulations (Chapter 5).

In Appendix A we introduce the basic definitions required to characterize the radiation field, which can be treated from two points of view, using macroscopic and quantum descriptions. Each of these approaches yields useful information and, taken together, they provide a full picture of the nature of the field. However, we will concentrate mainly on the macroscopic description, which can be directly connected to the thermodynamics. Thus, in this section we describe the physics of radiative transfer and its coupling to the hydrodynamic equations described in Section 2.1. The discussion in this section follows that in Rijkhorst et al. (2006) and Peters et al. (2010).[1] See also, e.g., Rybicki and Lightman (1979), Osterbrock (1989), Shu (1991), Frank and Mellema (1994), Rijkhorst et al. (2006), and Peters et al. (2010)

2.6.1 Point sources

For the purpose of the simulations to be presented in Chapter 5, we can safely model the *stars* as point sources (see Section 5.3). Then, the specific flux at distance r from a star of radius $r_{\rm star}$ and emitting a uniform specific intensity at its surface, $I_\nu(0)$, is

$$F_\nu = \pi I_\nu(r)\left(\frac{r_{\rm star}}{r}\right)^2. \tag{2.35}$$

Because of the symmetry of the problem, there is only a flux in radial direction. Thus, the integrals in Equations (A.3) and (A.9) are equal ($\cos\theta = 1$), and we have

$$F_\nu(r) = 4\pi J_\nu(r). \tag{2.36}$$

We can use Equation (A.16) as a solution of the radiative transfer equation along rays, and modeling the specific intensity of the protostar with a blackbody spectrum of temperature $T_{\rm star}$, i.e. $I_\nu(0) = B_\nu(T_{\rm star})$, we can analytically

[1] See also the PhD thesis by Thomas Peters (available in http://www.mpia-hd.mpg.de/imprs-hd/theses/thesis_peters.pdf), on which the simulations presented in Chapter 5 and some sections of this chapter are based.

express the mean specific intensity as

$$J_\nu(r) = \left(\frac{r_{\rm star}}{r}\right)^2 \frac{1}{2c^2} \frac{h\nu^3}{\exp(h\nu/k_{\rm B}T_{\rm star}) - 1} \exp(-\tau_\nu(r)), \tag{2.37}$$

where we have used

$$B_\nu(T) = \frac{2h}{c^2} \frac{\nu^3}{\exp(h\nu/k_{\rm B}T) - 1}, \tag{2.38}$$

h being the Plank constant and $k_{\rm B}$ the Boltzmann constant. Finally, to find the radius of the star, $r_{\rm star}$, we invoke the Stefan-Boltzmann law

$$L = 4\pi\sigma r_{\rm star}^2 T_{\rm star}^4, \tag{2.39}$$

where L and $T_{\rm star}$ can be determined directly from stellar evolution models.

2.6.2 Coupling to Hydrodynamics

We couple the radiation field to the energy equation through the ionization heating term. The photoionization heating rate is given by (Osterbrock, 1989)

$$\Gamma_{\rm ph} = n_{\rm HI} \int_{\nu_{\rm T}}^{\infty} \frac{4\pi J_\nu}{h\nu} \sigma_\nu h(\nu - \nu_{\rm T}) d\nu. \tag{2.40}$$

Using the equation for the specific mean intensity (2.37), this equation becomes

$$\Gamma_{\rm ph} = n_{\rm HI} \left(\frac{r_{\rm star}}{r}\right)^2 \frac{2\pi h}{c^2} \int_{\nu_{\rm T}}^{\infty} \frac{\sigma_\nu \nu^2 (\nu - \nu_{\rm T}) \exp(-\tau_\nu(r))}{\exp(h\nu/k_{\rm B}T_{\rm star}) - 1} d\nu, \tag{2.41}$$

where the optical depth $\tau_\nu(r)$ is given by Equation (A.18). Since this heating mechanism dominates in HII regions, we neglect other heating sources such as dust and accretion heating.

2.6.3 Ionization

The evolution of the ionization fraction $x_{\rm HII}$ (Equation 2.11), is governed by the equation

$$\frac{dx_{\rm HII}}{dt} = x_{\rm HI}(A_{\rm ph} + A_{\rm c}) - x_{\rm HII} n_{\rm e} \alpha_{\rm R}, \tag{2.42}$$

where $A_{\rm ph}$ and $A_{\rm c}$ are defined below, and $\alpha_{\rm R}$ is the radiative recombination rate (Rijkhorst et al., 2006). This equation accounts for neutral hydrogen atoms that can be ionized, and for hydrogen ions that can recombine.

The first contribution to the ionization term is the photoionization rate (Osterbrock, 1989), where

$$A_{\rm ph} = \int_{\nu_{\rm T}}^{\infty} \frac{4\pi J_\nu}{h\nu} \sigma_\nu d\nu \tag{2.43}$$

represents the number of ionizations per hydrogen atom per second. With the specific mean intensity given by Equation (2.37), $A_{\rm ph}$ becomes

$$A_{\rm ph} = \left(\frac{r_{\rm star}}{r}\right)^2 \left(\frac{2\pi}{c^2}\right) \int_{\nu_{\rm T}}^{\infty} \frac{\sigma_\nu \nu^2 \exp(-\tau_\nu(r))}{\exp(h\nu/k_{\rm B}T_{\rm star}) - 1} d\nu. \tag{2.44}$$

The second contribution to the ionization rate is the collisional ionization rate (Cox and Tucker, 1969), where

$$A_{\rm c} = A_{\rm HI} n_{\rm e} \sqrt{T} \exp -I_{\rm HI}/k_{\rm B}T, \tag{2.45}$$

with $A_{\rm HI} = 5.84 \times 10^{-11}$ cm^{3}K$^{-1/2}$s^{-1} and $I_{\rm HI} = 3.6\,$eV being the hydrogen ionization energy.

For the recombination term, we use the on-the-spot approximation (see, e.g., Osterbrock, 1989), which allows us to use the recombination coefficient given by

$$\alpha_{\rm R} = \alpha_{\rm R}(10^4\,{\rm K}) \left(\frac{T}{10^4\,{\rm K}}\right), \tag{2.46}$$

where $\alpha_{\rm R}(10^4\,{\rm K}) = 2.59 \times 10^{-13}$ cm^{3}s^{-1}.

Since the ionization affects the thermodynamics of the gas, we use the form of the equation of state relevant for a partially ionized gas, given by Equation (2.9). Also, the ionization affects the optical depth, and thus we use the photoionization heating rate, described by Equation (2.41).

2.6.4 HII Regions: ionization balance and expansion

When a massive star appears, almost immediately it begins to radiate energy within the MC in which it was born. This energy is mainly in the form of ionizing photons, with energies above 13.6 eV, which first dissociate the H_2 and then ionize the resulting HI, producing a so-called HII region. At the same time electrons and protons recombine, creating new atomic hydrogen. Since each ionization event removes a photon from the beam, only a limited region of the surrounding cloud can be ionized.

We assume that the star emits photons at a constant rate, S_*, and that the number density of electrons, n_e, and the temperature of the plasma are

spatially constant, so that the balance between ionizations and recombinations is described by

$$S_* = \frac{4\pi}{3} n_e^2 \alpha(T) R_{\rm s}^3 \tag{2.47}$$

where $R_{\rm s}$ is the *Strömgren radius*. We then solve for $R_{\rm s}$, assuming that the ionization spreads so quickly that the original cloud density, $n_{\rm H}$, does not change appreciably, so that $n_e \simeq n_{\rm H}$, and

$$R_{\rm s} = \Big(\frac{3S_*}{4\pi\alpha n_{\rm H}^2}\Big). \tag{2.48}$$

After the Strömgren radius is reached, all ionizing photons are consmed, but the ionized gas has a pressure two orders of magnitude higher than the neutral gas because the electrons removed from the atoms are typically expelled at velocities of several kms. The overpressure in the bubble causes it to expand at velocities of order the sound speed. In a uniform medium, this leads to the so-called Spitzer solution (Spitzer 1978)

$$R(t) = R_{\rm s}\Big(1 + \frac{7}{4}\frac{c_{\rm s}t}{R_{\rm s}}\Big)^{4/7}. \tag{2.49}$$

The final equilibrium state can never be reached, since the expansion time scale is typically an order of magnitude larger than the lifetime of a massive star. Nevertheless, the expanding period is important because it imparts momentum to the surrounding gas, and larger masses of gas can be ionized as the density decreases (see Equation 2.47). Furthermore, the analytical result is important because it allows testing numerical simulations containing expanding HII regions.

2.7 Turbulence

Turbulence is a highly chaotic regime of flow that tends to *stir* the fluids and occurs when molecular viscosity in the fluid is negligible compared to the momentum advection term (see Equation (2.50) below). However, a certain degree of order persists as scale-dependent spatial correlations among the flow variables. Generally it is agreed that a turbulent flow is characterized by the following features, *i)* it contains an extremely large number of excited degrees of freedom (or *modes*); *ii)* the modes are able to nonlinearly exchange energy; *iii)* the system is unpredictable; i.e., it is "sensitive to initial conditions"; and *iv)* the system has a highly mixing nature. For a more detailed discussion

of the complex statistical characteristics of turbulence, see e.g., Scalo (1987), Frisch (1995), Vázquez-Semadeni (1999), Biskamp (2003), Elmegreen and Scalo (2004a), Mac Low and Klessen (2004), and Lesieur (2008).

2.7.1 The Navier-Stokes equation

To characterize the turbulence, we first define the *Reynolds number*, Re. The momentum equation, (2.2), including the viscous terms is known as the Navier-Stokes equation, and reads

$$\frac{\partial \mathbf{u}}{\partial t} + \mathbf{u} \cdot \nabla \mathbf{u} = -\frac{1}{\rho} \nabla P + \nu_{\mathbf{K}} (\nabla^2 \mathbf{u} + \nabla \nabla \cdot \mathbf{u}), \tag{2.50}$$

where $\nu_{\mathbf{K}}$ is the kinematic viscosity and we have neglected the so-called second-viscosity. From this equation, we can distinguish the two relevant terms for the turbulence. The first is the *advection* term ($\mathbf{u} \cdot \nabla \mathbf{u}$), which tends to mix the fluid, and the second is the viscous term, which has the opposite effect, of tending to homogenize the velocity field. In general, this term involves second spatial derivatives of the velocity. The ratio of these defines the Reynolds number, which, to order of magnitude, is

$$Re \sim \frac{U^2 L^{-1}}{\nu_{\mathbf{K}} U L^{-2}} \sim \frac{UL}{\nu_{\mathbf{K}}}, \tag{2.51}$$

where U and L are the characteristic velocity and scale lengths, respectively. Experimentally, it is found that a flow becomes fully turbulent when $Re \gtrsim$ a few $\times\, 10^3$. Thus, we can consider that the ISM is highly turbulent, since typical parameters imply $Re \gtrsim 10^6$ (e.g., Elmegreen and Scalo, 2004a).

Much of the turbulent theory is developed in Fourier space, writing the fields (density, velocity) as a superposition of Fourier modes, allowing a description of the flow in terms of length scales, characterized by their wavelength, λ. The Fourier decomposition for an arbitrary physical field, $A(\mathbf{x}, t)$, takes the form

$$A(\mathbf{x}, t) = \int A_{\mathbf{k}}(t) e^{i\mathbf{k}\cdot\mathbf{x}} d^3k, \tag{2.52}$$

where $\mathbf{k}$ is the vector Fourier mode, with associated wavenumber $k = |\mathbf{k}| = 2\pi/\lambda$, and $A_{\mathbf{k}}$ is the corresponding Fourier amplitude, a complex number which we assume depends only on time. Thus, the decomposition of the velocity field is

$$\mathbf{u}(\mathbf{x}, t) = \int \mathbf{u}_{\mathbf{k}}(t) e^{i\mathbf{k}\cdot\mathbf{x}} d^3k, \tag{2.53}$$

with an analogous one for the density and magnetic fields. We use the property that the differentiation operation in real physical space becomes a multiplication in Fourier space; that is, $\nabla[A_{\mathbf{k}}(t)e^{i\mathbf{k}\cdot\mathbf{x}}] = i\mathbf{k}A_{\mathrm{k}}(t)$. With this, the Navier-Stoques equation (2.50) in Fourier space for an incompressible flow ($\nabla\mathbf{u} = \mathbf{k}\cdot\mathbf{u}_{\mathbf{k}}$) becomes

$$\frac{d\mathbf{u}_{\mathbf{k}}}{dt} + \frac{i}{2}\sum_{\mathbf{p}+\mathbf{q}=\mathbf{k}}\left[(\mathbf{q}\cdot\mathbf{u}_{\mathbf{p}})\mathbf{u}_{\mathbf{q}} + (\mathbf{p}\cdot\mathbf{u}_{\mathbf{q}})\mathbf{u}_{\mathbf{p}}\right] = -\frac{i}{\rho}\mathbf{k}P_{\mathbf{k}} - \nu_{\mathbf{K}}k^2\mathbf{u}_{\mathbf{k}}, \tag{2.54}$$

with the set of wavevectors $\mathbf{p}$, $\mathbf{q}$ and $\mathbf{k}$, which are known as *triads* and satisfy the condition $\mathbf{p}+\mathbf{q}=\mathbf{k}$.

2.7.2 The energy spectrum

The Fourier representation of the flow leads to the definition of an important concept in the theory of turbulence —the turbulent energy spectrum $E(k)$, which is defined as the specific kinetic energy contained in wavenumber modes in the interval k and $k+dk$:

$$E(t) = \frac{1}{2}\int_{V_x}|\mathbf{u}(x)|^2 d^3x = \frac{1}{2}\int_{V_k}|\mathbf{u}_{\mathbf{k}}|^2 d^3k \equiv \frac{1}{2}\int_0^\infty E(k)dk, \tag{2.55}$$

where the second equality comes from Parseval's theorem for complex variables, and the identity defines $E(k)$. Thus,

$$E(k) \equiv \frac{1}{2}\int_{\theta_k}\int_{\phi_k}|\mathbf{u}_{\mathbf{k}}|^2 k^2 \sin\theta_k d\theta_k d\phi_k, \tag{2.56}$$

where the quantity $|\mathbf{u}_{\mathbf{k}}|^2$ is sometimes referred to as the *velocity power spectrum*. In the incompressible regime, with ρ =cst., the kinetic energy is simply proportional to the specific kinetic energy. However, in the compressible case this result is no longer valid since the total kinetic energy needs to be calculated taking into account the density variations, as

$$\mathcal{E}(k) \equiv \frac{1}{2}\int_V \rho u^2 d^3x. \tag{2.57}$$

2.7.3 The Kolmogorov-Obukhov theory

Kolmogorov (1941) and Obukhov (1941) independently derived the expected functional form of the energy spectrum for *homogeneous*[1] incompressible turbulence. This result is often referred to as the K41 theory, which is based on the

[1] In the sense that average properties are independent of position in the fluid.

following assumptions: *i)* A very large range of scales are present in the flow; *ii)* energy is injected primarily at the largest scale in the flow, L, and dissipated at some small scale, $l_{\rm visc}$; *iii)* the energy is transferred among the modes (or scales), and the transfer is local in Fourier space (in triads with $p \sim q \sim k$); and *iv)* the system is in a stationary state, so that the energy transfer rate in the *inertial range* (i.e. scales between L and $l_{\rm visc}$) is independent of wavenumber k, and equals the energy injection and dissipation rates.

With these assumptions, the form of the spectrum in the inertial range can be estimated from dimensional analysis as follows. The energy transfer rate for eddies of scale size l can be written as $\epsilon \sim u_l^2/\tau_l$, where u_l is the characteristic velocity difference across the eddy, and $\tau_l = l/u_l$ is the circulation time at scale l. Thus, using assumption *iv)* we have

$$u_l = (\epsilon l)^{1/3}. \tag{2.58}$$

Now, the characteristic velocity difference at scale l can be identified with the rms specific kinetic energy contained in scales $l' < l$, which is given by the energy spectrum as

$$u_l^2 = 2\int_{2\pi/l}^{\infty} E(k)dk. \tag{2.59}$$

Assuming that the spectrum has a power-law dependence on wavenumber, $E(k) \propto k^n$, and substituting the scaling relation (2.58), we find $n = -5/3$. This is the famous *Kolmogorov* $-5/3$ *law*. Although there is no fully deductive theory that starts from the Navier-Stokes equations to derive it, Kolmogorov's law has been verified experimentally in terrestrial flows (e.g., Grant et al., 1962) and in astrophysical flows that are expected to behave nearly incompressible (Armstrong et al., 1995).

2.7.4 Compressible turbulence

Gas flows in the ISM, however, are highly compressible, and the driving of the turbulence is not uniform, so the Kolmogorov-Obukhov theory is no longer applicable and numerical simulations are required to study these systems.

An immediate consequence of non-incompressibility is that we need to consider the continuity equation in its full extent, rather than in the incompressible form, $\nabla \cdot \mathbf{u} = 0$. In principle, the internal energy equation, Equation (2.3) must also be considered, although, in this case, an intermediate step is possible, which is the assumption of a barotropic flow, in which the thermal pressure depends only on the density, $P = P(\rho)$, so that the energy equation may still be bypassed. A frequently used approximation is that of polytropic flows, where the

dependence is assumed to be a power law,

$$P \propto \rho^{\gamma_{\rm eff}}, \tag{2.60}$$

where $\gamma_{\rm eff}$ is the effective polytropic exponent, and is a free parameter, that represents any net heating and cooling acting on the gas. This case includes the extremely common assumption of isothermal flows, for which $\gamma_{\rm eff} = 1$.

To know the magnitude of the density fluctuation, we consider the ratio of the advection and the pressure gradient term two terms, and assume it is of order unity, so that both terms contribute equally to the momentum equation. That is,

$$\frac{|\mathbf{u}\cdot\nabla\mathbf{u}|}{|\frac{\nabla P}{\rho}|} \sim 1, \tag{2.61}$$

which can be rewritten as

$$|\mathbf{u}\cdot\nabla\mathbf{u}| \sim |\frac{c_{\rm s}^2\nabla\rho}{\rho}| \tag{2.62}$$

where we have used the equation of state () with the pressure given by Equation (2.60, with $\gamma_{\rm eff} = 1$), which implies $\nabla P \approx c_{\rm s}^2\nabla\rho$. To order of magnitude, this gives

$$\frac{U^2}{L} \sim \frac{c_{\rm s}^2}{\rho}\frac{\delta\rho}{L} \tag{2.63}$$

or, equivalently,

$$\frac{\delta\rho}{\rho} \sim \frac{U^2}{c_{\rm s}^2} \equiv \mathcal{M}_{\rm s}^2 \tag{2.64}$$

where $\mathcal{M}_{\rm s}$ is the sonic Mach number. We see then that the typical relative density fluctuation is of the order of the Mach number squared. In Section 3.3.5 we will discuss the probability density distribution (PDF) of these density fluctuations.

In the compressible case, in order to study the energy spectrum, it is convenient to decompose the velocity field in a rotational (or solenoidal), $\mathbf{u}_{\mathbf{k},\rm s}$, and a compressible (or potential) component, $\mathbf{u}_{\mathbf{k},\rm c}$, such that

$$\mathbf{k}\cdot\mathbf{u}_{\mathbf{k},\rm s} = 0 \quad \mathbf{k}\times\mathbf{u}_{\mathbf{k},\rm c} = 0 \tag{2.65}$$

Note that these two components are orthogonal to each other in Fourier space. These components of the velocity field can have different dynamic properties and energy transfer between these two modes affects the dynamics of compressible flows. The transfer is predominantly from rotational modes to the compressible ones (Vazquez-Semadeni et al., 1996), so that the rotational

energy tends to decay if there are no sources of vorticity. This is particularly interesting because turbulence is typically manifested by rotational phenomena.

Thus, contrary to the incompressible case, for which the Kolmogorov spectrum seems to be universal, in the compressible case the spectral slope depends on the degree of compressibility of the flow. Numerical simulations of isothermal supersonic turbulence suggest that, as the Mach number is increased, the slope of the (specific) energy spectrum shifts from the kolmogorov value of $-5/3$ (in the weakly compressible regime) to -2 (at a very high compressibility) for both compressive and solenoidal components (Kritsuk et al., 2007). The latter case is likely to occur in the ISM, and particularly in MCs where the Mach number is high.

Indeed, in the limit of zero pressure, the system described by Equation (2.50; in one dimension) produces a network of overlapping shocks with a spectral slope of -2 (Frisch & Bec 2001), in agreement with the numerical simulations. This state is known as *Burgers Turbulence*. Kritsuk et al. (2007) have suggested, additionally, that the quantity $\rho^{1/3}u$ exhibits Kolmogorov scaling even in the compressible case, and supported this suggestion with numerical simulations.

2.8 The final set of equations

Considering the Euler equations (Section 2.1.1) with all the astrophysically relevant source terms, namely self-gravity (Section 2.4), magnetic fields (Section 2.5.3), and heating and cooling (Sections 2.3 and 2.6.2), we arrive to the set of the ideal magnetohydrodynamic equations

$$\begin{aligned}
\frac{\partial \rho}{\partial t} + \nabla \cdot (\rho \mathbf{u}) &= 0, \\
\frac{\partial (\rho \mathbf{u})}{\partial t} + \nabla \cdot (\rho \mathbf{u}\mathbf{u}) &= \rho \mathbf{g} - \nabla\Big(P + P_B\Big) + \frac{1}{4\pi}(\mathbf{B} \cdot \nabla)\mathbf{B}, \\
\frac{\partial}{\partial t}\Big(\rho e_{\rm tot}\Big) + \nabla \cdot \Big[\Big(\rho e_{\rm tot} + P + P_B\Big)\mathbf{u} - \frac{1}{4\pi}(\mathbf{u} \cdot \mathbf{B})\mathbf{B}\Big] &= \\
&= \Gamma - \Lambda + \rho \mathbf{u} \cdot \mathbf{g}, \\
\frac{\partial \mathbf{B}}{\partial t} &= \nabla \times (\mathbf{u} \times \mathbf{B}), \\
\nabla \cdot \mathbf{B} &= 0, \\
\nabla^2 \phi &= 4\pi G \rho,
\end{aligned} \tag{2.66}$$

which, together with the equation of state (2.6), form a closed coupled set of equations that can be solved numerically (see Chapter 5).

3

An evolutionary model for collapsing Molecular Clouds and their Star Formation activity

3.1 Abstract

We present an idealized, semi-empirical model for the evolution of gravitationally contracting molecular clouds (MCs) and their star formation rate (SFR) and efficiency (SFE). The model assumes that the instantaneous SFR is given by the mass above a certain density threshold divided by its free-fall time. The instantaneous number of massive stars is computed assuming a Kroupa initial mass function. These stars feed back on the cloud through ionizing radiation, eroding it. The main controlling parameter of the evolution turns out to be the maximum cloud mass, $M_{\rm max}$. This allows us to compare various properties of the model clouds against their observational counterparts. A giant molecular cloud (GMC) model ($M_{\rm max} \sim 10^5\ M_\odot$) adheres very well to the evolutionary scenario recently inferred by Kawamura et al. for GMCs in the Large Magellanic Cloud. A model cloud with $M_{\rm max} \approx 2000\ M_\odot$ evolves in the Kennicutt–Schmidt diagram first passing through the locus of typical low- to intermediate-mass star-forming clouds, and then moving toward the locus of high-mass star-forming ones over the course of $\sim$ 10 Myr. Also, the stellar age histograms for this cloud a few Myr before its destruction agree very well with those observed in the ρ-Oph stellar association, whose parent cloud has a similar mass, and imply that the SFR of the clouds increases with time. Our model thus agrees well with various observed properties of star-forming MCs, suggesting that the scenario of gravitationally collapsing MCs, with their SFR regulated by stellar feedback, is entirely feasible and in agreement with key

observed properties of MCs.

3.2 Introduction

A crucial ingredient in understanding the star formation efficiency (SFE) of giant molecular clouds (GMC) is the study of their evolution, from their formation to their destruction by the massive stars they form. A still unsolved problem is whether the GMCs are in approximate virial equilibrium, or rather they are in gravitational contraction. Initially, Goldreich & Kwan (1974) proposed that the supersonic linewidths observed in GMCs correspond to global gravitational contraction, but Zuckerman & Palmer (1974) readily argued that if all the molecular gas in the Galaxy were in free fall, then the total star formation rate (SFR) in the Galaxy would be about two orders of magnitude higher than observed (we will refer to this as the "SFR conundrum"). Zuckerman & Evans (1974) subsequently suggested that the linewidths could correspond to small-scale turbulent motions, giving rise to the notion that clouds are quasi-equilibrium entities, a notion that has survived until today (see, e.g., the reviews by Mac Low and Klessen, 2004; McKee and Ostriker, 2007).

Since then, most theoretical models of star formation (SF) have been based on the assumption that turbulence provides support against the clouds' self-gravity, and allows them to maintain a quasi-virial equilibrium state, thus preventing global collapse and maintaining a low global SFR (e.g., Norman and Silk, 1980; McKee, 1989; Matzner, 2002; Krumholz and McKee, 2005; Li and Nakamura, 2006; Nakamura and Li, 2007; Wang et al., 2010). In these models, the turbulence is maintained by the energy feedback into the cloud from the stars it forms. One interesting model where strict equilibrium was not assumed, was that by Krumholz et al. (2006), where the fully time-dependent virial theorem was solved numerically for a cloud under the influence of its self-gravity and the pressure produced by feedback from H II regions, although the cloud was restricted to have a spherical geometry, and mass loss by the cloud due to ionizing radiation by massive stars was not considered. Those authors found that clouds undergo a few expansion–contraction oscillations, until they are finally dispersed, and the SFEs over the clouds' lifetimes were found to be $\sim 5\%$ – 10%. More recently, a similar model, with the same restrictions but including mass accretion from the environment, was considered by Goldbaum et al. (2011). In this model, the clouds again reach virial equilibrium, and maintain roughly constant column densities.

However, recent theoretical and observational evidence has suggested a return to the global gravitational contraction scenario of Goldreich & Kwan (1974)

(e.g., Hartmann et al., 2001; Burkert and Hartmann, 2004; Hartmann and Burkert, 2007; Peretto et al., 2007; Vázquez-Semadeni et al., 2007; Galván-Madrid et al., 2009; Vázquez-Semadeni et al., 2009; Schneider et al., 2010; Csengeri et al., 2011). Additionally, Clark and Bonnell (2005) have suggested that molecular cloud (MC) turbulence, rather than directly producing Jeans-unstable clumps, only produces the seed nonlinear density fluctuations for subsequent gravitational fragmentation, which proceeds on different timescales due to the spatial variations on the local free-fall time induced by the turbulence (Heitsch and Hartmann, 2008). But then, if we again allow for clouds and their substructures to be in gravitational contraction, it is necessary to find a solution for the SFR conundrum in this scenario. The semi-empirical model presented here investigates whether stellar feedback can accomplish this.

Our model is motivated by the numerical simulations of Vázquez-Semadeni et al. (2010), who have investigated the evolution of clouds formed by the collision of warm neutral medium (WNM) cylindrical streams, including stellar feedback from ionization heating from massive stars. Those authors found that the clouds are in general not stabilized by the feedback, but rather are either dispersed or continue to contract globally, depending on their mass. Here, we construct a model that attempts to capture the phenomenology observed in those simulations, scanning the space of the parameters that determine the physical properties of the cloud. Rosas-Guevara et al. (2010) have also presented a parameter-space study, but using numerical simulations, and without feedback, while Dib et al. (2011) have produced an analytical model similar to ours, but aimed at investigating the effect of varying metallicity on the SFE.

The plan of the paper is as follows. In Section 3.3, we describe the general model, which we then calibrate against a fiducial numerical simulation from Vázquez-Semadeni et al. (2010) in Section 3.4. In Section 3.6, we compare the calibrated model against various observational properties of both large and small MCs, parameterized only by their mass. In Section 3.7 we present a discussion, and finally a summary and our conclusions in Section 3.8.

3.3 The Model

We construct a model for studying the SFE in a thin cylindrical cloud undergoing gravitational contraction, as observed in various simulations (Vázquez-Semadeni et al., 2007; Heitsch and Hartmann, 2008; Vázquez-Semadeni et al., 2010; Vázquez-Semadeni et al., 2011). The system is schematically illustrated in Figure 3.1. In the simulations, the collision of WNM streams nonlinearly triggers thermal instability, forming a thin cloud of cold atomic gas (e.g., Hen-

nebelle and Pérault, 1999; Koyama and Inutsuka, 2000; Walder and Folini, 2000; Koyama and Inutsuka, 2002), which becomes turbulent by the combined action of various dynamical instabilities (Hunter et al., 1986; Vishniac, 1994; Koyama and Inutsuka, 2002; Heitsch et al., 2005; Vázquez-Semadeni et al., 2006). The cloud soon begins to contract gravitationally as a whole. However, before this global collapse is completed, some local, nonlinear (i.e., large-amplitude) density enhancements produced by the initial turbulence manage to collapse on their own, since their local free-fall time is shorter than the average one for the entire cloud (Heitsch and Hartmann, 2008; Pon et al., 2011). These local collapses thus involve only a fraction of the cloud's total mass. Also, we assume that the newly-formed stars feed energy back into the cloud. We only consider the ionizing radiation from massive stars, since this radiation is probably the dominant mechanism of stellar energy injection at the scale of GMCs (Matzner, 2002).

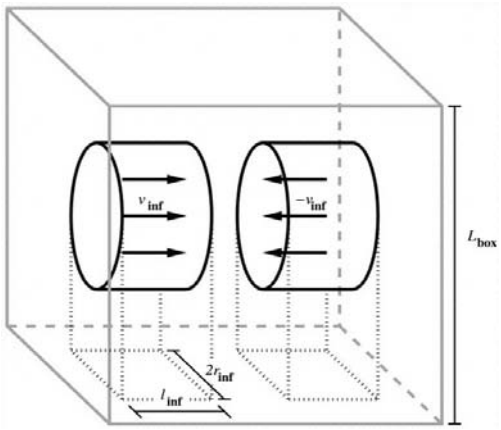

Figure 3.1: Model setup. Cylindrical streams of WNM are assumed to collide head-on to form first a flattened CNM cloud, which proceeds to collapse, becoming molecular and star forming in the process. The main parameters of the model are the radius of the cylinders $R_{\rm inf}$, and the density and velocity of the inflowing warm gas.

In what follows, we investigate the competition between the cloud's gravitational contraction and its destruction by the mass consumption by star formation (SF) as well as by the ionization produced by the newly formed massive stars. Below we describe how we calculate the contributions from these processes. It is important to note that we do not follow the chemistry, but rather consider that all the cold gas, either atomic or molecular, is involved in the gravitational contraction and, eventually, star formation.

3.3.1 Mass accretion

In our scenario, the cloud's mass ($M_{\rm C}$) at time t is given by

$$M_{\rm C}(t) = \int_0^t \dot{M}_{\rm inf}(t')\ dt' - M_{\rm S}(t) - M_{\rm I}(t), \tag{3.1}$$

where $\dot{M}_{\rm inf}(t)$ is the mass accretion rate onto the cloud from the WNM inflows, $M_{\rm S}(t)$ is the total mass in stars, and $M_{\rm I}(t)$ is the mass ionized by stellar feedback. Note that all these masses are considered to be functions of time. We assume that

$$\dot{M}_{\rm inf}(t) = 2\,\rho_{\rm inf}\,v_{\rm inf}\,(\pi\,R_{\rm C}^2), \tag{3.2}$$

where $v_{\rm inf}$ is the inflow speed, $\rho_{\rm inf} = n_{\rm inf}\,\mu_{\rm H}\,{\rm m_H}$ is the inflow mass density (with $n_{\rm inf}$ being the number density of the inflows, $\mu_{\rm H}$ the mean atomic weight of the diffuse gas, and $m_{\rm H}$ the atomic hydrogen mass). Note that $\pi\,R_{\rm C}^2$ is also the cross-sectional area of the thin, cylindrical, cold and dense cloud that forms by thermal instability at the layer compressed by the inflows. We take the cloud's radius $R_{\rm C}(t)$ as being initially equal to the inflow radius $R_{\rm inf}$ and to later decrease as the cloud contracts gravitationally. The factor of two in Equation (3.2) represents the fact that there are two inflows, one on each side of the forming cloud.

3.3.2 Mass in Stars

We assume that the SFR is given by the ratio of the gas mass in the high-density tail ($n > n_{\rm SF}$) of the density distribution produced by the turbulence in the cloud, to its local free-fall time, $t_{\rm ff}(n_{\rm SF}) = \sqrt{3\pi/32G\mu m_{\rm H} n_{\rm SF}}$. We refer to $n_{\rm SF}$ as the threshold density for star formation, and denote by $f(t)$ the fraction of the cloud's mass that is at densities above $n_{\rm SF}$ (discussed in Section 3.3.6). We then have

$${\rm SFR}(t) = \frac{M_{\rm C}(t)}{t_{\rm ff}(n_{\rm SF})}\,f(t), \tag{3.3}$$

so that the mass in stars at time t is

$$M_{\rm S}(t) = \int_0^t {\rm SFR}(t')dt' = \int_0^t \frac{M_{\rm C}(t')}{t_{\rm ff}(n_{\rm SF})}\,f(t')\ dt'. \tag{3.4}$$

We assume that the initial density of the cloud is that of the cold neutral medium (CNM), in balance with the sum of the thermal and ram pressures of the inflows, as described in Vázquez-Semadeni et al. (2006). Typically, $n_{\rm CNM} \approx 100\,{\rm cm^{-3}}$, and we use a mean molecular weight of $\mu = 2.35$, adequate

for molecular gas. As the cloud evolves by contraction, the mean density evolves as determined by its mass and size, so that $\bar{\rho} = M_{\rm C}/\pi R_{\rm C}^2 h$, where h is the cloud thickness (cf. Section 3.3.4).

3.3.3 Ionized Mass

To model the cloud evaporation by massive stars, we use the results from Franco et al. (1994). These authors found that the cloud evaporation rate by a massive star near the cloud surface is

$$\dot{M}_{\rm I,sur}(t) \approx 2\pi R_{\rm S,0}^2 m_{\rm H} \bar{n} c_{\rm s,I} \left(1 + \frac{5 c_{\rm s,I}\, t}{2 R_{\rm S,0}}\right)^{1/5}, \tag{3.5}$$

where t is the age of the massive star, $c_{\rm s,I}$ is the sound speed in the ionized gas, $\bar{n} = \bar{\rho}/\mu m_{\rm H}$ is the mean number density of the MC, and $R_{\rm S,0}$ is the initial Strömgren radius of the massive star in the cloud ($R_{\rm S,0} = [3S_*/4\pi\alpha_{\rm B}(2\bar{n})^2]^{1/3}$, with S_* being a representative value of the UV Lyman-continuum photon flux (Franco et al., 1994) and $\alpha_{\rm B}$ the recombination coefficient for the ionized gas). We assume that $R_{\rm S,0}$ is reached immediately at the instantaneous mean density of the cloud, which, in our model, is continually increasing as the cloud contracts. Therefore, over a short time interval Δt (between t and $t + \Delta t$), over which the cloud's density can be assumed constant, a massive star near the cloud's surface can ionize a mass $\Delta M_{\rm I,sur} = \dot{M}_{\rm I,sur}(t)\Delta t$.

In addition, we consider that, during the time interval Δt, the cloud forms $\Delta N_{\rm OB}(t) = x_{\rm OB}{\rm SFR}(t)\Delta t/\langle M_{\rm OB}\rangle$ new massive stars of average mass $\langle M_{\rm OB}\rangle$, where $x_{\rm OB}$ is the mass fraction of massive stars, which we calculate assuming an initial mass function (IMF) from Kroupa (2001), with lower and upper mass limits of 0.01 and 60 $M_\odot$ respectively. Defining a star as "massive" if it has a mass $M \geq 8M_\odot$, we obtain $x_{\rm OB} = 0.12$ and a mean massive-star mass $\langle M_{\rm OB}\rangle = 17\ M_\odot$. Furthermore, in Equation (3.5) we take $S_* = 2 \times 10^{48}\,{\rm s}^{-1}$, $c_{\rm s,I} = 12.8\,{\rm km\,s}^{-1}$, and $\alpha_{\rm B} = 2.6 \times 10^{-13}\,{\rm cm}^{-3}\,{\rm s}^{-1}$ where we have assumed that the temperature of ionized gas in the HII region is 10^4 K.

With the above considerations, and discretizing the time variable, the ionized mass at time t_i is given by

$$M_{\rm I}(t_i) = M_{\rm I}(t_{i-1}) + \sum_{j=k}^{i} \Delta N_{\rm OB}(t_j)\Delta M_{\rm I,sur}(t_j), \tag{3.6}$$

where t_k is the time at which the oldest remaining OB stars were formed, $k = i - {\rm int}\,(t_{\rm OB}/\Delta t)$, 'int' is the integer function, and $t_{\rm OB} = 5$ Myr is the main-sequence lifetime of our representative OB star. The second term in the

right-hand side of Equation (3.6) thus gives the mass ionized over the time interval $\Delta t = t_i - t_{i-1}$ by the stars formed between t_k and the present time, t_i. Note that we have neglected the possibility that part of the ionized gas can recombine and return to the cloud, as we expect the ionized gas to escape to the diffuse medium.

Finally, to account for the fact that the massive stars are born in dense environments, in Equation (3.5) we take the density as the maximum between the instantaneous cloud density $n(t)$ and 10^3 cm^{-3} (typical of clumps), in order to avoid an over ionization when the cloud density is low.

3.3.4 Global gravitational collapse

Following the trend seen in the numerical simulations, we assume that our clouds evolve in two stages. First, a mass-growth stage occurs, during which the cloud (initially of zero mass) increases its mass by accretion from the WNM at constant radius and density, so that only its thickness increases (see, e.g., Folini and Walder, 2006; Vázquez-Semadeni et al., 2006; Vázquez-Semadeni et al., 2007), until it reaches its thermal Jeans mass. At that point, the second stage begins, during which the cloud undergoes global gravitational contraction. For circular modes in a self-gravitating isothermal sheet of finite thickness, the Jeans mass is given by (Larson, 1985):

$$M_{\rm J} = 4.67 \frac{c_{\rm s}^4}{G^2 \Sigma}, \tag{3.7}$$

where $c_{\rm s}$ is the cloud sound speed, and $\Sigma = M(t)/\pi R^2(t)$ is the surface density, with $M(t)$ and $R(t)$ being the instantaneous mass and radius of the cloud, respectively. In order to calculate the sound speed we first compute the cloud's temperature. To do this, we use the fit by Koyama & Inutsuka (2002; see also the note in Vázquez-Semadeni et al. 2007) to the heating and cooling processes considered by Koyama and Inutsuka (2000). This allows us to solve for the temperature of thermal equilibrium (heating = cooling) as a function of the density. In this way, we get temperatures of $T \approx 42$ K for a density of $n = 10^2$ cm^{-3} and $T \approx 7$ K for $n \sim 10^7$ cm^{-3}.

During the mass-growth stage, over which the cloud's radius remains constant ($R = R_{\rm inf}$), the cloud's thickness h is given by the condition of constant number density:

$$h(t) = \frac{M_{\rm C}(t)}{n_{\rm CNM}\, \mu\, m_{\rm H} (\pi\, R_{\rm inf}^2)}. \tag{3.8}$$

where $n_{\rm CNM} = 100$ cm^{-3} is the assumed CNM density. Once the collapse begins, we assume that the thickness remains constant at the final value achieved during

the growth stage, and that its volume density increases only due to the radial contraction, as suggested by simulations including self-gravity (e.g., Vázquez-Semadeni et al., 2007; Heitsch and Hartmann, 2008; Vázquez-Semadeni et al., 2010; Vázquez-Semadeni et al., 2011). This assumption is equivalent to assuming that the average thickness of the cloud is much smaller than its Jeans length throughout its evolution. In general, this is a good approximation until when the cloud has contracted to radii of a few pc.

To determine the radial evolution during the contraction stage, we first calculate the acceleration at the cloud's edge. We take a reference frame with its origin at the cloud's center and with its x-axis along the inflow direction (i.e., perpendicular to the plane of our flattened cloud). We integrate over mass elements $\bar{\rho}\, dzdydx$ located at a distance $[(R-z)^2+y^2+x^2]^{1/2}$ from the edge. At a certain time t_i, the acceleration at the cloud edge is

$$a(t_i) = 2\,G\,\bar{\rho}_i \int_{-R_i}^{R_i} dz \int_0^{\sqrt{R_i^2-z^2}} dy \int_{-h/2}^{h/2} \frac{R_i - z}{[(R_i-z)^2+y^2+x^2]^{3/2}}\, dx, \quad (3.9)$$

where $\bar{\rho}_i = \bar{\rho}(t_i)$ and $R_i = R_{\rm C}(t_i)$. We solve the first integral analytically, while the second and third ones are solved numerically by the composite Simpson rule. After a small time increment $\Delta t = t_i - t_{i-1}$, the change in the cloud radius is

$$R_{i+1} = R_i - v_{0,i}\,\Delta t - \frac{1}{2} a(R_i)\Delta t^2, \quad (3.10)$$

where the instantaneous velocity at time t_i is $v_{0,i} = \sum_{j=0}^{i} a(R_j)\Delta t$ for constant Δt.

Finally, we introduce a correction factor, representative of the fact that true gravitational collapse of a gaseous mass does not occur in strict free fall, since thermal pressure is never completely negligible, as pointed out in the pioneering work by Larson (1969, Appendix C). There, he reported that the collapse of his simulations occurred in a time longer than the free-fall time by a factor of 1.58. Thus, at each time step, we divide the radius given by Equation (3.10) by a factor $f_{\rm L}$, which we refer to as the "Larson parameter", and calibrate in Section 3.4.

3.3.5 Density distribution

A key ingredient in our evolutionary model is the fraction of dense gas that is participating in the SF process, and therefore so is the evolution of the probability density function (PDF) of the cloud's density field.

In our model, we consider that our clouds are born transonically turbulent, as a consequence of the various instabilities at play in the compressed layer

between the streams (Vishniac, 1994; Walder and Folini, 2000; Heitsch et al., 2005; Heitsch et al., 2006; Vázquez-Semadeni et al., 2006). Also, in the absence of direct stellar irradiation, the temperature in the cold gas varies at most by factors of a few for densities $100 < n < 10^7$ cm^{-3}, and thus, as a first approximation, we consider it to be isothermal. Therefore, we assume that the density field within the cloud is initially characterized by a log-normal PDF, appropriate for supersonically turbulent, isothermal gas (Passot and Vázquez-Semadeni, 1998). The PDF is then given by

$$P(s) = \frac{1}{\sqrt{2\pi\sigma_s^2}} \exp\left[-\frac{(s-s_{\rm p})^2}{2\sigma_s^2}\right], \tag{3.11}$$

where

$$s \equiv \ln(\rho/\bar{\rho}), \quad s_{\rm p} = \ln(\rho_{\rm p}/\bar{\rho}) = -\sigma_s^2/2, \tag{3.12}$$

with $\rho_{\rm p}$ being the peak density, and

$$\sigma_s^2 = \ln(1 + b^2\mathcal{M}_{\rm rms}^2), \tag{3.13}$$

where b is a proportionality constant related with the compressibility induced by the turbulent forcing, which for simplicity we take equal to unity (see, e.g., Vazquez-Semadeni, 1994; Padoan et al., 1997; Passot and Vázquez-Semadeni, 1998; Federrath et al., 2008).

However, more recent numerical and observational studies suggest that the density PDF in gravitationally contracting systems does not preserve its log-normal shape during the collapse, but rather develops a power-law tail at high densities (Klessen, 2000; Dib and Burkert, 2005; Vázquez-Semadeni et al., 2008; Kainulainen et al., 2009; Ballesteros-Paredes et al., 2011b; Kritsuk et al., 2011). In particular, Kritsuk et al. (2011) have suggested that the final slope should be in the range [3/2,7/4], but at the present time we know of no theoretical prediction as to how the slope nor the transition point between the log-normal and the power law should evolve in time. We experimented with various options for modeling the evolution of the PDF's power-law tail, but found the behavior to be very sensitive to the parameters used, while we had no physical ways of constraining them. Finally, Kritsuk et al. (2011) proposed that the origin of the power-law tail is the development of local collapsing flows, that may have either Larson–Penston (Larson, 1969; Penston, 1969) or Shu (1977) density profiles. In this case, the power-law tail is an *effect* of the gravitational collapse rather than its *cause*, and thus it should not be counted as providing turbulent seeds for future collapses. For all of these reasons, we do not consider the power-law form of the PDF and stick to the log-normal.

It is worth noting that the density PDF we consider here refers only to the cold (approximately isothermal) gas that makes up the cloud and not to the entire gas contents of the system. This means that this PDF is not directly comparable to that observed in the numerical simulations of the same process, which corresponds to thermally bistable gas. Thus, we did not consider the possibility of using a PDF extracted from numerical simulations, either.

We model the evolution of the lognormal density PDF as follows. First, as indicated by Equation (3.12), the mean of the PDF is given by the cloud's mean density, given by $\bar{\rho} = M_{\rm C}/\pi R_{\rm C}^2 h$. In turn, we prescribe that $\bar{\rho}$ varies as follows. During the mass-growth stage, it remains constant, at 100 cm^{-3}. Once the contraction stage begins, it increases, causing the density PDF to shift to higher values. Eventually, however, the SFR becomes large enough that the ionization by newly born massive stars reduces the cloud's mass rapidly enough as to cause the PDF to shift back toward lower densities again.

Second, the standard deviation of the PDF is determined by the turbulent rms Mach number, as indicated by Equation (3.13). Unfortunately, the evolution of the *turbulent* component of the Mach number remains rather uncertain. Standard relations, such as Larson's (1981) velocity dispersion size cannot be assumed here. Indeed, in our collapsing-cloud scenario, the majority of the velocity dispersion is due to the contracting motions (Ballesteros-Paredes et al., 2011a) rather than to random turbulent motions, and should not be counted as turbulence capable of producing new density fluctuations susceptible of subsequent collapse.

Of course, it is natural to assume that a fraction of the kinetic energy in the collapsing motions will be transferred to random motions, but this problem remains largely unexplored in the case of gaseous media. Vázquez-Semadeni et al. (1998) numerically investigated the scaling of the non-collapsing component of the velocity dispersion in collapsing spherical clouds. Those authors found that the turbulent velocity dispersion scaled as ρ^x, with $x \in [1/4, 1/2]$, depending on the particular setup of the collapse and on the presence of magnetic fields. However, that study was performed at low resolution and was restricted to spherical geometry, so it cannot be taken as definitive. More recently, Klessen and Hennebelle (2010) suggested that the rate of kinetic energy injection by the warm neutral streams feeding an MC is at least one order of magnitude larger than the rate of turbulent energy dissipation within the clouds. However, these estimates are not enough to properly constrain the evolution of the turbulent kinetic energy in our model clouds. Thus, we simply take a *constant* value of the turbulent Mach number, which represents a compromise between turbulent decay by dissipation and feeding of the turbulence by transfer from the collapsing motions. This thus implies that the width of the PDF in our model remains

constant through the cloud's evolution as well. We take this constant value of the turbulent Mach number as $\mathcal{M}_{\rm rms} = 3$, the canonical value for the cold neutral medium (Heiles and Troland, 2003).

3.3.6 Star-forming mass fraction

Finally, as mentioned in Section 3.3.2, we assume that only gas with number density higher than a threshold value $n_{\rm SF}$ participates in the *instantaneous* SF process. This amounts to assuming that $n_{\rm SF}$ is sufficiently larger than the cloud's mean density $\bar{n}$ as to guarantee that $t_{\rm ff}(n_{\rm SF}) \ll t_{\rm ff}(\bar{n})$, where $t_{\rm ff}(n)$ is the free-fall time corresponding to density n. In a sense, this prescription may be thought of as the model's analogue of sink particles in a numerical simulation (Bate et al., 1995; Federrath et al., 2010a), in which gas at sufficiently high densities is replaced by point mass particles representing collapsed objects.

Thus, for the assumed log-normal PDF the fraction of dense gas that forms stars is given by

$$f(t) = \frac{1}{2}\left[1 - \mathrm{erf}\left(\frac{2\,s_{\rm SF}(t) - \sigma_s^2}{\sqrt{2}\sigma_s}\right)\right], \tag{3.14}$$

where $s_{\rm SF} = \ln(\rho_{\rm SF}/\bar{\rho})$, and $\rho_{\rm SF}$ is the volume density corresponding to $n_{\rm SF}$ (see also Elmegreen, 2002; Krumholz and McKee, 2005; Dib et al., 2011). The value of $n_{\rm SF}$ is calibrated against a numerical simulation by Vázquez-Semadeni et al. (2010) in Section 3.4.

3.3.7 Temporal evolution

With all the above ingredients, we discretize Equation (3.1) as

$$M_{\rm C}(t_i) = \sum_{j=0}^{i} \dot{M}_{\rm inf}(t_j)\Delta t - \sum_{j=0}^{i} \frac{M_{\rm C}(t_j)\,\Delta t}{t_{\rm ff}(t_j)}\, f(t_j) - \left[M_{\rm I}(t_{i-1}) + \sum_{j=k}^{i} \Delta N_{\rm OB}(t_j)\Delta M_{\rm I,sur}(t_j)\right] \tag{3.15}$$

We integrate this equation numerically over time, taking $\Delta t = 4 \times 10^{-4}\,$Myr. We choose this value as a reasonable compromise between speed and accuracy, after experimenting with timesteps down to 0.01 times this value, from which we found (with arbitrary free parameters) that the chosen value gives already well-converged values of the final cloud masses, the variable that turned out to be most sensitive to the size of the timesteps.

We consider that the cloud's evolution ends either because the cloud gets completely evaporated by the massive-star ionization or because its average density reaches $n_{\rm SF}$, a point at which the remaining mass is fully converted into stars and the cloud disappears.

3.4 Calibration of the model

With all the model ingredients defined, we now proceed to calibrate it by matching it to one of the numerical simulations by Vázquez-Semadeni et al. (2010). We consider the simulation labeled SAF1 in that paper, which most resembles the physical conditions built into our model. The label SAF indicated that it contained small-amplitude initial velocity fluctuations ($\sim 2\%$ of $v_{\rm inf}$), which were sufficient to trigger the instabilities responsible for turbulence production in the forming cloud, but not large enough to significantly distort its sheet-like geometry.

The simulation considered the collision of two cylindrical WNM streams with $n_{\rm inf} = 1\,{\rm cm}^{-3}$, $T_{\rm inf} = 5000\,{\rm K}$, inflow radius of $R_{\rm inf} = 64\,{\rm pc}$, and an initial inflow speed $v_{\rm inf} = 7.5{\rm km\ s}^{-1}$.[1] Thus, for our calibration purposes, we use these same values for our model, except for $v_{\rm inf}$. We do this because, in the simulation, the inflow speed decreases over time, because the rear end of the inflowing cylinder leaves a vacuum behind it. As a consequence, in the reference frame of the inflow, the inflow's rear end tends to re-expand into this vacuum, producing a velocity gradient along the cylinder. Instead, in the model we use a constant inflow speed, and thus we take a smaller value, representative of the time-averaged speed in the simulation. We find that a value of $v_{\rm inf} = 4.5{\rm km\ s}^{-1}$ provides the best match for the evolution of the simulation cloud's mass. Also, we find that the temporal evolution of the cloud's radius is best matched with a value of the Larson parameter of $f_{\rm L} = 1.7$, very close to the original value of 1.58 originally proposed by Larson (1969). We show the evolution of these quantities for both the simulation and the model in Figure 3.2. Note that the evolution for the model with the ionizing stellar feedback turned both on and off is shown. We refer to the model with feedback off as the LN-F0 case, and to the one with the feedback on, as the LN-F1 case.

Next, keeping the above parameters fixed, we vary the $n_{\rm SF}$ parameter, the density threshold for star formation, to match the SFR and SFE of the simulation, with the SFE being defined as

$$\mathrm{SFE(t)} = \frac{M_{\rm S}(t)}{M_{\rm C}(t) + M_{\rm S}(t) + M_{\rm I}(t)}, \tag{3.16}$$

where $M_{\rm C}$ is the dense gas mass, $M_{\rm S}$ is the total mass in stars, $M_{\rm I}$ is the total mass ionized by stars, all quantities being time dependent. Figure 3.3 shows the evolution of the SFR and SFE of the model for $n_{\rm SF} = 10^5$, 10^6, and $10^7\ {\rm cm}^{-3}$, and compares them with the evolution of the corresponding

[1] Note that there are typographical errors in the numbers reported by Vázquez-Semadeni et al. (2010). The values given here are the correct ones.

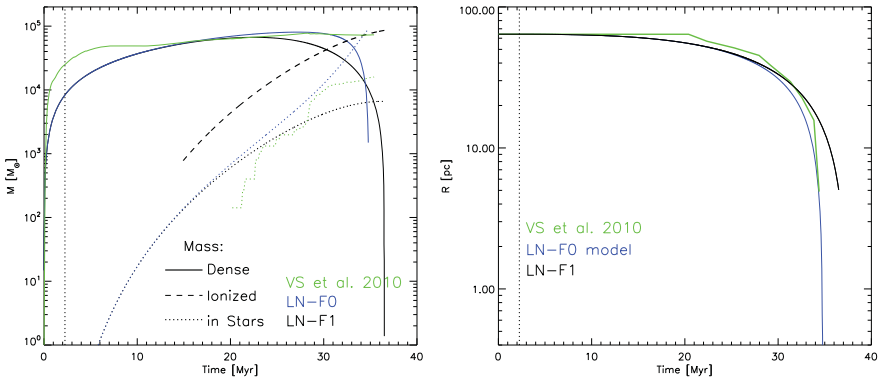

Figure 3.2: Left: evolution of the dense gas mass, ionized gas mass, and mass in stars for the model cloud with parameters that best match the corresponding quantities (except for the ionized mass, which is not measured) in the SAF1 simulation of Vázquez-Semadeni et al. (2010). The green lines represent the simulation, the blue lines represent the model cloud with stellar feedback turned off, and the black lines represent the model cloud with the stellar feedback turned on, with $n_{\rm SF} = 10^6$ cm^{-3}. The vertical line represents the beginning of global collapse. Right: evolution of the cloud radius in the model and in the simulation, with the same color coding as in the left panel.

quantities in the simulation, showing that the best match is obtained with a value $n_{\rm SF} = 10^6$ cm^{-3}, which we use in the rest of the paper. This value is reassuring since, on the one hand, it is comparable to the sink-formation density threshold used in the numerical simulations (Vázquez-Semadeni et al., 2007; Vázquez-Semadeni et al., 2010), and on the other, it is high enough that the material above those densities can be safely assumed to be locally gravitationally bound (Galván-Madrid et al., 2007; Heitsch and Hartmann, 2008).

3.5 Discussion of the calibrated model's evolution

Once the model parameters have been calibrated with the SAF1 simulation, it is illustrative to discuss the general features of the model cloud's evolution, which hold qualitatively for the other cases we explore in Section 3.6, where varying only the inflow radius $R_{\rm inf}$ we are able to match and explain several observed features of MCs and their star-forming activity.

First, we note from the right panel of Figure 3.2 that the radius of the model

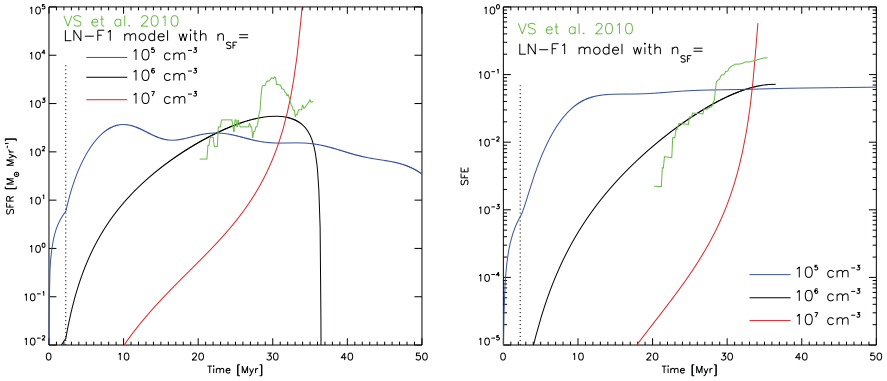

Figure 3.3: Left: evolution of the star formation rate (SFR) for the model cloud for the cases $n_{\rm SF} = 10^5$, 10^6, and 10^7 cm^{-3}, compared to the evolution of the SFR in the SAF1 simulation of Vázquez-Semadeni et al. (2010). Right: same as the left panel, but for the star formation efficiency (SFE). The green lines represent the numerical simulation.

with feedback (LN-F1) evolves slightly more slowly than that of the case without feedback (LN-F0). This is because the stellar feedback erodes the cloud through ionization, thus reducing its mass, which in turns causes a lower gravitational acceleration, thus slowing the collapse. We also note that the radius of the LN-F0 case approaches zero at late times, while that of the LN-F1 ends at a finite radius, implying that the evolution is terminated because the cloud is completely evaporated before it reaches zero radius (see below).

Second, from the left panel of Figure 3.2, we note that the dense gas mass of *both* the LN-F0 and LN-F1 models decreases at late times. This is because even in the non-feedback LN-F0 model, gas is consumed due to the conversion of gas to stars. However, we see that the mass consumption is much more abrupt in the LN-F0 model, while in the LN-F1 model it proceeds more slowly. This indicates that the feedback inhibits star formation to the level that the mass consumed by ionization from the feedback is *less* than the mass that would be consumed by star formation were there no feedback. Nevertheless, note that the dense gas mass in the LN-F1 model approaches zero at the end of the evolution, indicating that all of the cloud's mass is used up by the combined action of ionization and star formation. This corresponds to the well-known fact that clusters eventually destroy their natal cloud and are left with no gas around them after several million years (Leisawitz et al., 1989).

Finally, note from Figure 3.4 that both the SFR and the SFE increase at an ever faster pace until the end of the simulation in the non-feedback case

LN-F0, while their growth slows down in the case of LN-F1. In this case, the SFR eventually begins to decrease and goes to zero at the end of the evolution, as the dense gas mass is completely consumed by the ionization, leaving no further fuel for star formation. Instead, the SFR in the LN-F0 case would reach a singularity at a finite time were it not for the time discretization of our model.

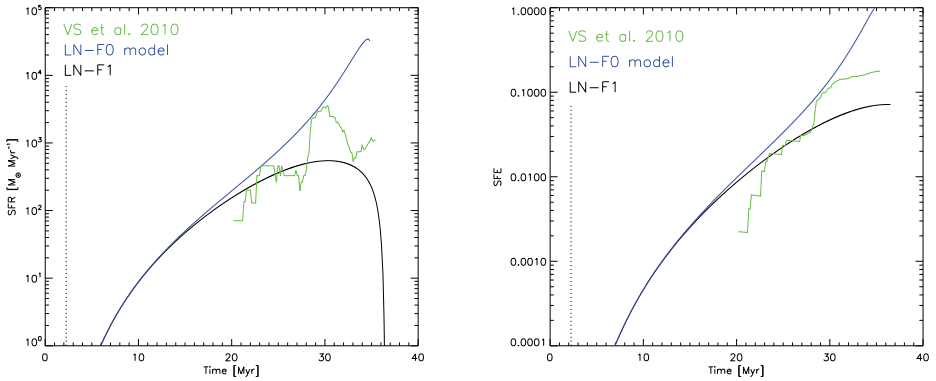

Figure 3.4: Evolution of the SFR (left) and the SFE (right) of the calibrated model with $n_{\rm SF} = 10^6$ cm^{-3} for a case with feedback turned off (LN-F0, blue line) and a case with feedback on (LN-F1, black line). The green lines represent the numerical simulation. The LN-F0 model has accelerating SFR and SFE, while they decelerate for model LN-F1. See also discussion in Section 3.7.3

3.6 Comparison with observations and previous work

We now proceed to compare the results of our model with related observational results. For the various comparisons, we vary only the inflow radius parameter, $R_{\rm inf}$, which determines the maximum dense gas mass attained by the model.

3.6.1 Evolutionary stages

As a first case in point, we consider the evolutionary stages of the clouds. Recently, Kawamura et al. (2009) have suggested that GMCs in the Large Magellanic Cloud undergo four evolutionary stages. In the first stage (Type I, with a duration of ~ 7 Myr and a median mass $M_{\rm tI} \sim 10^{4.8}\ M_\odot$), the GMCs show no sign of massive star formation. In the second stage (Type II; 14 Myr; $M_{\rm tII} \sim 10^{5.2}\ M_\odot$), the GMCs have only HII regions, while in the third (Type

III; 6 Myr; $M_{\rm tIII} \sim 10^{5.4}\ M_\odot$), the GMCs contain both HII regions and clusters. Finally, the last stage (IV) corresponds to the time when the GMCs have been completely dispersed, and only young clusters and/or supernova remnants are found.

Because the masses of the clouds in their sample are near $10^5 M_\odot$, we choose an inflow radius $R_{\rm inf} = 100$ pc, which gives a maximum cloud mass ($M_{\rm max}$) of slightly over $10^5\ M_\odot$, thus making it directly comparable to their cloud sample. Figure 3.5 shows the evolution of both the number of massive stars in the model cloud (top panel) and the masses of the dense gas, ionized gas, and stellar components of the cloud (bottom panel). For comparison with the cloud types defined by Kawamura et al. (2009), here we define Type I as the epoch when the model cloud has less than one massive star, Type II as the period when the cloud has less than 20 massive stars, and Type III as the period when the cloud has more than 20 massive stars. We see that the model cloud spends ~ 5 Myr as a Type I, ~ 12 Myr as a Type II, and ~ 10 Myr as a Type III, noting that after such a time the cloud's mass has decreased by more than a factor of two, and may be considered to be on its way to disappearing.

We also note from the bottom panel of Figure 3.5, that the dense gas mass of the model cloud varies only moderately during the time it spends as an either Type I, II or III cloud, although a net increase from Type I to Type II is apparent. Moreover, because the cloud's mass decreases by over a factor of two while it is in the Type III stage, a significant scatter in cloud masses is expected in this class, as is indeed observed in Figure 12 of Kawamura et al. (2009).

From the above discussion, we thus conclude that the evolution of our model GMC, with $R_{\rm inf} = 100$ pc, compares well, both qualitatively and quantitatively, with the evolutionary scheme proposed by Kawamura et al. (2009) for GMCs in the LMC.

3.6.2 Fiducial model versus OMC-1

Next, we compare our model cloud with the physical conditions of real star-forming regions. As an example, we choose the clump known as OMC-1 in the Orion Molecular Cloud, which can be considered a typical massive star-forming region, and has been extensively studied. The total gas mass in OMC-1 is $\sim 2200\, M_\odot$ (Bally et al., 1987), the size is ~ 1.35 pc (which implies a number density $\sim 1.54 \times 10^4\, {\rm cm}^{-3}$), and the mass in stars is $\sim 500\, M_\odot$, which implies that the average SFR is $\langle {\rm SFR} \rangle \gtrsim 2.5 \times 10^{-4}\, M_\odot {\rm yr}^{-1}$, assuming a stellar age spread of $\lesssim 2$ Myr (see Vázquez-Semadeni et al., 2009, and references therein).

To compare with this, we choose a value of $R_{\rm inf} = 10$ pc for our model, which at $t = 27.6$ Myr has the same density as OMC-1, making it directly

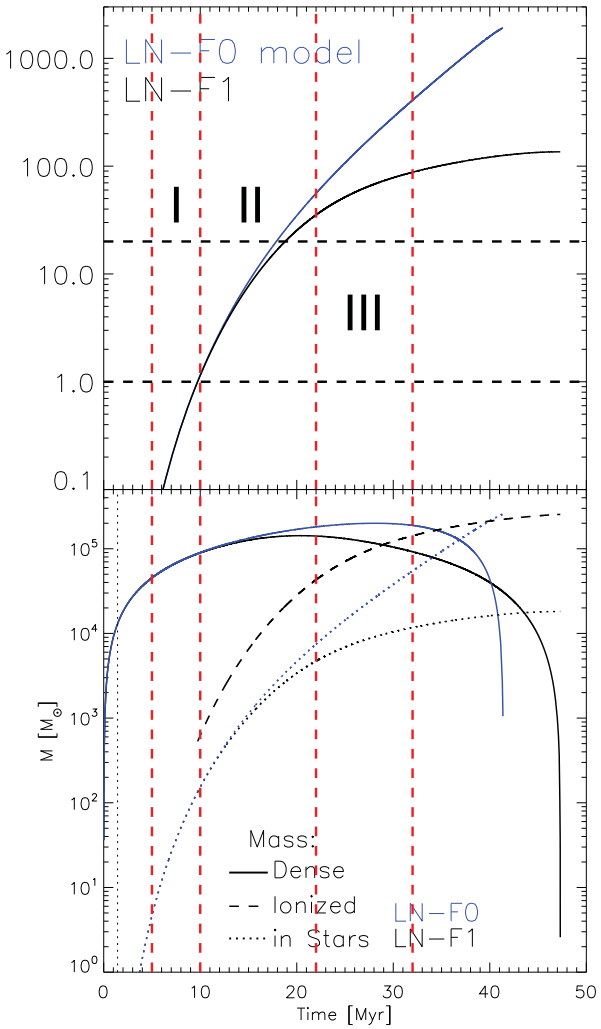

Figure 3.5: Top: evolution of the number of massive stars in the model cloud with $R_{\rm inf} = 100$ pc, showing the periods which roughly correspond to the cloud types defined by Kawamura et al. (2009). Bottom: evolution of the dense gas, ionized and stellar masses for this cloud.

comparable to the latter. At this time, the model cloud has a mass $M \approx 1800\ M_\odot$, a mass in stars $\approx 200\,M_\odot$, and size (diameter) ≈ 1.9 pc. Moreover, the average SFR over the last 2 Myr (the age dispersion used to compute the SFR of OMC-1) is $\langle \mathrm{SFR} \rangle \approx 100\ M_\odot\ \mathrm{Myr}^{-1}$ (see Figure 3.6). These values are in very good agreement with the estimates for OMC-1, suggesting that our

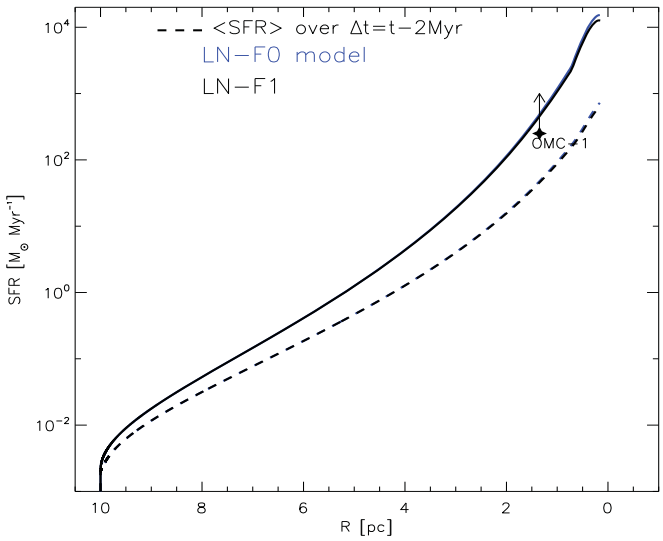

Figure 3.6: Evolution of a model cloud with $R_{\rm inf} = 10$ pc in an SFR vs. size (R) diagram. Note that the size axis is reversed, so that the cloud evolves from left to right as it contracts gravitationally. Also plotted is the locus of the OMC-1 star-forming region in this diagram, showing that the model comes very close to that locus toward the end of its evolution.

evolutionary model correctly describes this cloud.

3.6.3 Kennicutt–Schmidt relation.

Another possible point of comparison of our model with observational data is provided by the so-called Kennicutt–Schmidt relation. Ever since the seminal paper by Schmidt (1959), it has been well known that there exists a relationship between the SFR and the gas density in galaxies. Four decades later, collecting data from various surveys of nearby normal and starburst galaxies, Kennicutt (1998) found a clear correlation between the galaxy-averaged SFR surface density ($\Sigma_{\rm SFR}$) and the galaxy-averaged total gas surface density ($\Sigma_{\rm gas} = \Sigma_{\rm HI} + \Sigma_{\rm H_2}$, where $\Sigma_{\rm HI}$ and $\Sigma_{\rm H_2}$ are the HI and H_2 surface densities, respectively) of the form $\Sigma_{\rm SFR} \propto \Sigma_{\rm gas}^N$, with $N \approx 1.4$.

Recent observations of external galaxies with high spatial resolution (on scales of fractions of kpc) show that $\Sigma_{\rm SFR}$ scales almost linearly with $\Sigma_{\rm H_2}$, while no clear correlation exists with $\Sigma_{\rm HI}$ (see, e.g., Wu et al., 2005; Bigiel et al., 2008). However, observations of individual clouds (e.g., Evans et al., 2009; Heiderman

et al., 2010) systematically show larger values of $\Sigma_{\rm SFR}$ than those implied by the fits by Kennicutt (1998), Bigiel et al. (2008), and Wu et al. (2005). Moreover, the SFRs derived by Heiderman et al. (2010) for their massive clump sample were obtained using extragalactic methods (taken from Wu et al., 2010), and they warn that this could cause the SFRs they report to be underestimated by up to 0.5–1 orders of magnitude, implying an even stronger disagreement with the galaxy-scale measurements.

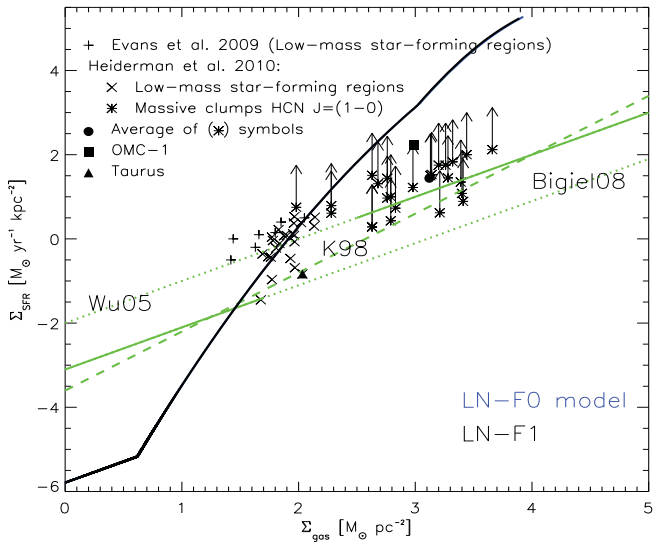

Figure 3.7: SFR surface density $\Sigma_{\rm SFR}$ vs. gas surface density $\Sigma_{\rm gas}$. The dashed line represents the *Kennicutt-Schmidt relation*, while the lower dotted line represents the observational fit by Bigiel et al. (2008) and the top dotted line is the fit by Wu et al. (2005). We also plot the data for individual low- to intermediate-mass star-forming regions by Evans et al. (2009) (+ symbols) and Heiderman et al. (2010) (× symbols) and for massive clumps by Heiderman et al. (2010) (∗ symbols). The filled square represents OMC-1 (see Vázquez-Semadeni et al., 2009) and the filled triangle is Taurus (see, e.g., Heiderman et al., 2010). The arrows in the massive clumps from the latter authors indicate the likely correction to the SFR due to their application of extragalactic methods to Galactic regions. The solid black line shows the evolution of our calibrated model with $R_{\rm inf} = 10$ pc.

These cloud-scale observations occupy a well-defined locus in $\Sigma_{\rm gas} - \Sigma_{\rm SFR}$ space, which can be compared with our model. For this task, we choose an inflow radius $R_{\rm inf} = 10$ pc, for which our model reaches a maximum mass of $M_{\rm max} \approx 2000\ M_\odot$, almost identical to the median mass of the Evans et al. (2009)

sample. In Figure 3.7 we then plot the evolution of this model, as well as the loci of the clouds from the Evans et al. (2009) and Heiderman et al. (2010), adding an upward-pointing arrow to the latter points, of length corresponding to one order of magnitude, to indicate the likely underestimation of the SFR for massive clumps by the latter authors. We also plot the data from OMC-1 (from Vázquez-Semadeni et al., 2009) and Taurus (see, e.g., Heiderman et al., 2010). The model evolves from low to high values of both $\Sigma_{\rm gas}$ and $\Sigma_{\rm SFR}$.

It is interesting to note that the model passes first through the locus of the low-mass star-forming clouds and later near the locus of the clumps forming massive stars. This means that the model predicts that present-day, relatively quiescent, low-mass star-forming clouds may evolve into massive star-forming ones in a few to several Myr. A similar conclusion was reached through numerical simulations by Vázquez-Semadeni et al. (2009). This reinforces the idea that the dispersion of the observational data is due to different evolutionary states of the clouds in a sample (see, e.g., Bigiel et al., 2011).

3.6.4 Stellar age distribution

One important prediction of our model is that the SFR increases over time. This is because, as the cloud contracts and its mean density increases, the fraction of star-forming gas in the cloud increases. An increasing SFR has already been proposed by Palla and Stahler (1999), Palla and Stahler (2000), and Palla and Stahler (2002) on the basis of the age distribution in various low- and high-mass clusters. However, this result has been questioned, since there is evidence suggesting that the older stars are not genuine members of the clusters, but rather belong to a different population (Hartmann, 2003; Ballesteros-Paredes and Hartmann, 2007; Heitsch and Hartmann, 2008). Moreover, Hartmann (2003) has posed the conundrum that, if most clouds form at an accelerated pace only over the last few Myr, and form stars at a very slow rate over the previous 10 Myr or so, most clouds should be found to be in the slow-star-forming period, but this is not what is observed. Our evolutionary scenario for clouds may offer a solution to this debate.

Because in our model we compute the total mass of stars (ΔM) formed at each time step, we can readily obtain the total number of stars formed during that time step as the integral over all masses of the, normalized to ΔM. The left panel of Figure 3.8 shows the stellar age histogram for our calibrated model, with $R_{\rm inf} = 10$ pc ($M_{\rm max} \approx 2000 M_\odot$) at the end of its life —i.e., when it has completely lost its gas. We show the histograms for a case with feedback off (model LN-F0) and one with feedback on (model LN-F1). It is clear from this figure that indeed the age distribution is concentrated toward young ages,

although a few older stars exist.

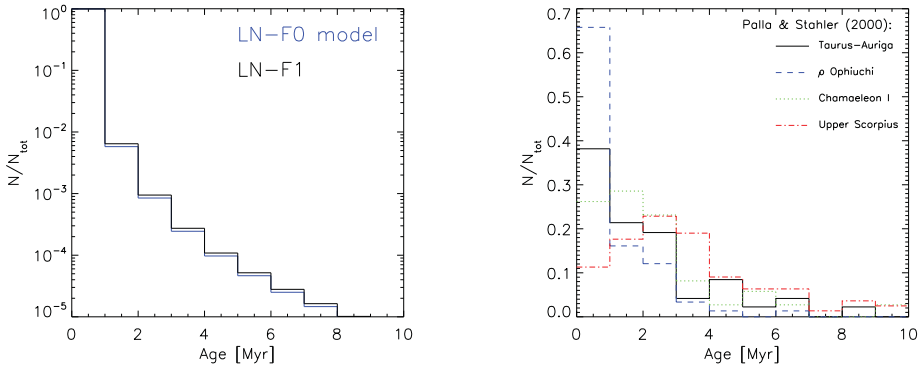

Figure 3.8: Left: stellar age distribution for our calibrated model with $R_{\rm inf} = 10$ pc ($M_{\rm max} \approx 2000 M_\odot$), calculated at the end of the cloud's evolution. Right: compilation of the age histograms for the associations studied by Palla and Stahler (2000).

These results can be compared with the age histograms presented by Palla and Stahler (2000) for the Orion Nebula Cluster (ONC), the Taurus-Auriga region, Lupus, ρ-Oph, Chameleon, Upper Scorpius, and IC348. In these clusters, the fraction of stars with ages up to 1 Myr ranges from $\sim 30\%$ to 66%, while the fraction of stars with ages up to 4 Myr is in the range 80% – 97%. Moreover, only in the case of Upper Scorpius does the age histogram peak at an age larger than 1 Myr, namely at 3 Myr. For this association, the fraction of stars with ages ≤ 1 Myr is only 11%, while the fraction with ages ≤ 4 Myr is 71%. We show a compilation of these in the right panel of Figure 3.8.

We can see that, qualitatively, the stellar age histogram at the end of our model's life resembles those of Palla and Stahler (2000), although, quantitatively, the model's histogram in Figure 3.8 is much more concentrated toward short ages. However, this must be due to the fact that it was calculated at the end of the model's evolution. Clearly this is not the case for the clusters and groups analyzed by Palla and Stahler (2000), because, as those authors themselves point out, in most cases the clusters are still embedded in their parent clouds, with only Upper Scorpius being already exposed. This means that we should consider our model *before* the end of its life.

In Figure 3.9 we show the age histogram for the calibrated model, calculated at 1 and 2 Myr before the end of its evolution, and compare it with one of the histograms from Palla and Stahler (2000) —that for ρ-Oph. We see that the histogram becomes less peaked as earlier times before the cloud's destruction is

taken, becoming more closely resemblant to the histograms of Palla and Stahler (2000). This is because, as the SFR increases toward later times, the fraction of young stars becomes increasingly larger. In particular, the histograms for 1 and 2 Myr before the cloud's dispersal seem to bracket the histogram for ρ-Oph. As seen from the right panel of Figure 3.8, the other regions are less concentrated toward short ages. According to our model, then, ρ Oph is a somewhat more evolved region, well matched by our model at $\lesssim 2$ Myr before its dispersal, while the other regions would correspond to somewhat less evolved stages, at slightly earlier times (3–4 Myr) before destruction.

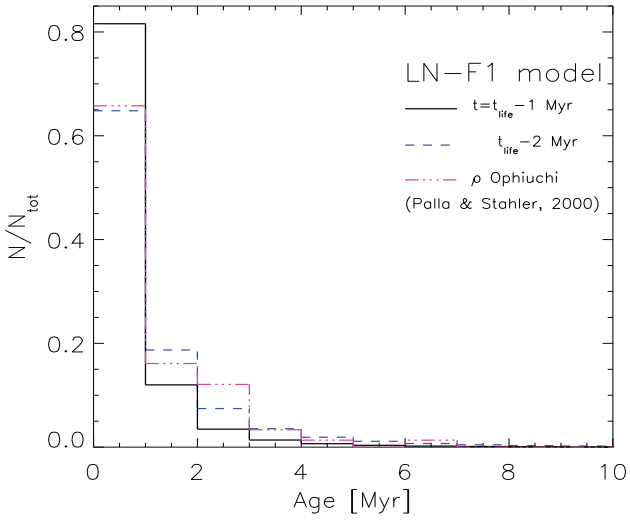

Figure 3.9: Stellar age distribution for our calibrated model with $R_{\rm inf} = 10$ pc ($M_{\rm max} \approx 2000 M_\odot$), calculated at 1 and 2 Myr before the end of the cloud's evolution, compared with the corresponding distribution for the ρ-Oph association (Palla and Stahler, 2000).

These results suggest a possible resolution of the debate between the Palla-Stahler and the Hartmann groups. Specifically, although our model indeed predicts an increase of the SFR in collapsing clouds, this does not conflict with the conundrum posed by Hartmann (2003): no fully formed MCs are observed without significant amounts of star formation *because the clouds themselves are evolving.* Thus, at the time when they had much lower SFRs, they were not fully formed yet, and thus not identifiable as large MCs. Indeed, the clouds' mean density was lower, and thus, in reality, they probably consisted of a few molecular clumps immersed in a still-atomic interclump medium. Only in the

last few Myr of their evolution, the clouds are dense enough on average that most of their bulk is already molecular, and by that time they are forming stars at a much higher rate, as observed. A similar conclusion has been recently reached on the basis of numerical simulations by Hartmann et al. (2012).

3.7 Discussion

3.7.1 The constant-$\mathcal{M}_{\rm rms}$ assumption

A feature of our model that may appear odd at first sight is that we have taken $\mathcal{M}_{\rm rms} = 3$ as the (constant) fiducial value for the rms Mach number of the turbulence within the cloud, as it is contrary, for example, to the famous Larson (1981) velocity-dispersion-size scaling relation. However, it must be recalled that in this paper we are specifically assuming that such a relation, or its more modern rendition by Heyer et al. (2009), is a manifestation of the gravitational contraction of the cloud, rather than a feature of the turbulence (Ballesteros-Paredes et al., 2011a). Thus, the relevant rms Mach number must be the remainder after the collapsing motions have been removed. A competition may be set up between the transfer of kinetic energy from the collapsing motions to the turbulent ones and the dissipation (Vázquez-Semadeni et al., 1998; Klessen and Hennebelle, 2010), and so, in the absence of a reliable model, we consider that the assumption of a constant rms Mach number with the value typical for the CNM (Heiles and Troland, 2003) is reasonable, although a possible alternative recipe for its initial value would be to take it equal to the inflow Mach number (Banerjee et al., 2009). We consider that further work is necessary to better constrain this parameter.

3.7.2 The log-normal PDF assumption

A similar situation arises for the density PDF in the cloud, which we have assumed to have a log-normal shape, even though it is well known that star-forming clouds develop a power-law tail at high densities (Klessen, 2000; Dib and Burkert, 2005; Vázquez-Semadeni et al., 2008; Kainulainen et al., 2009; Ballesteros-Paredes et al., 2011b; Kritsuk et al., 2011). However, Kritsuk et al. (2011) have suggested that such power-law tails are the effect of the development of local collapsing sites with power-law density profiles. In this case, as explained in Section 3.3.5, the power-law tail in the PDF would be the *result* of the collapse, rather than the *seed* for it, and thus the relevant PDF for the seeds for future collapse should be the underlying log-normal one, after removal of the already-collapsing regions. Moreover, there is no complete theory for how the

density PDF should evolve in time from a lognormal to a power law. Unknowns such as the timescale for the transition, the density at which the power-law tail starts, and the final slope of this region are uncertain at present. As above, we consider that further work is necessary to clearly resolve this issue, and in the meantime we settle for the log-normal PDF assumption.

3.7.3 Accelerating star formation

An important precision is in order concerning the acceleration of star formation in our model. Indeed, our model predicts that the SFR increases over time, and therefore, star formation (SF; strictly speaking, the instantaneous stellar mass, $M_{\rm S}(t)$) *accelerates*. However, it is common to find the statement in the literature that it is the SFR that accelerates. This is *not* the case for our model with feedback. The SFR is the time derivative of $M_{\rm S}$. Since the SFR increases in time, the second time derivative of $M_{\rm S}$ is positive, and thus the SF accelerates. However, the second time derivative of the SFR (the third derivative of $M_{\rm S}$) is negative for our model with feedback (see the left panel of Figure 3.4), and thus strictly speaking the SFR decelerates.

3.7.4 Room for improvement

In the present model, we have bypassed the supporting effect of all forms of pressure, and replaced it by the empirical "Larson factor", $f_{\rm L}$, which effectively lengthens the timescale for collapse. In the case of the original work by Larson (1969, Appendix C), this factor represented the support from thermal pressure which, incidentally, should be most important during the earlier stages of the collapse. Calibrating against the SAF1 simulation by Vázquez-Semadeni et al. (2010), we found a value of $f_{\rm L}$ roughly 8% larger than the one found by Larson, suggesting perhaps that turbulent pressure added a certain (small) amount of support (the magnetic field was not included in that simulation). Including physically motivated terms into the collapse prescription that account for thermal, turbulent and magnetic support is an important goal, which we will attempt to pursue in a future contribution.

Nevertheless, it is interesting that our model, calibrated in the non-magnetic case of the SAF1 simulation, gives a good match to a number of observational properties of MCs in a wide range of masses. This suggests that magnetic support is not crucial in these objects. In turn, this is consistent with the recent realization that star-forming clouds tend to be magnetically supercritical in general (Bourke et al., 2001; Crutcher et al., 2003; Troland and Crutcher, 2008), and thus they should be essentially in a free-fall regime.

Finally, in this paper we have not considered the effect of supernova explosions toward the late evolutionary stages of the clouds. This may help in reducing the model's SFR at those stages, probably bringing it to better agreement with the observations (see, e.g. Figure 3.7).

3.8 Summary and Conclusions

In this paper we have developed a semi-empirical analytical model (based on simulations by Vázquez-Semadeni et al., 2010) in which an MC is formed by converging WNM flows. We assumed that the inflow collision produces a CNM cloud, through nonlinear triggering of the thermal instability, and that the cloud becomes turbulent through the combined action of the latter and various other dynamical instabilities, such as the nonlinear thin shell, Kelvin–Helmholtz, and Rayleigh–Taylor ones. We assumed that the rms Mach number of this turbulence remains fixed at the typical values in the CNM ($\mathcal{M}_s \approx 3$), and that over its evolution, the cloud develops further nonthermal motions related to its collapse, not its internal turbulence. We also assumed that the cloud forms stars with a Kroupa (2001)-type IMF, so that massive stars only appear when a sufficiently large number of stars has formed to adequately sample the high-mass tail of the IMF. Finally, we assumed that the density PDF in the cloud has a log-normal shape and a fixed width (corresponding to a constant turbulent Mach number $\mathcal{M}_{\rm rms}$), but whose maximum shifts toward higher densities as the cloud contracts and becomes denser on average.

Using the same WNM inflow parameters as the simulation labeled SAF1 from Vázquez-Semadeni et al. (2010), namely $R_{\rm inf} = 64\,{\rm pc}$, $n_{\rm inf} = 1\ {\rm cm}^{-3}$, and $\mathcal{M}_{\rm rms} = 3$, we calibrated the model by searching the density threshold for star formation, $n_{\rm SF}$, that best matched the simulation's evolution of the SFR and SFE. Our calibrated value was $n_{\rm SF} = 10^6\ {\rm cm}^{-3}$. With the $n_{\rm SF}$, $n_{\rm inf}$, and $\mathcal{M}_{\rm rms}$ parameters fixed, the only remaining free parameter of the model is the WNM inflow radius $R_{\rm inf}$, which essentially controls the maximum mass reached by the model cloud, $M_{\rm max}$. Varying this parameter we then match the model to clouds of various masses, and compare with various properties of such clouds.

The generic behavior of the model cloud, with the parameters of the SAF1 simulation, is as follows: (1) the size of the model cloud decreases faster (by gravitational contraction) in a case *without* stellar feedback (model LN-F0) than in a case *with* it (model LN-F1). This is because feedback partially evaporates the cloud, thus reducing its gravitational potential, and slowing its collapse. (2) The model without feedback approaches a final state of zero size with finite mass (a singularity), while the case with feedback approaches a final state of

zero mass at finite size, i.e., it is completely consumed by SF and ionization before it reaches zero size. (3) Although the SFR increases in both cases, it *accelerates* over time in the LN-F0 model, while it *decelerates* over time in the LN-F1 model.

We then set out to apply the model to explain a number of observed features of MCs of a wide range of masses. First, we compared the predictions of our model with the evolutionary scenario for GMCs recently proposed by Kawamura et al. (2009), in which the GMCs start out having no massive stars, then have reduced numbers of them, so as to only have isolated HII regions, and finally have large numbers of them, so as to clearly contain massive clusters. We find that our model, with a value of $R_{\rm inf}$ that gives $M_{\rm max} \sim 10^5\ M_\odot$, comparable to the mass range reported by those authors, spends similar times in each of the stages reported by them.

We also investigated a model cloud with $R_{\rm inf} = 10$ pc, corresponding to $M_{\rm max} \sim 2000\ M_\odot$. We find that such a model cloud evolves in the $\Sigma_{\rm SFR}$–$\Sigma_{\rm gas}$, or Kennicutt–Schmidt, diagram, in such a way that it passes first through the locus of individual low-mass star-forming clouds and later through the locus of high-mass star-forming clumps, as reported by Evans et al. (2009) and Heiderman et al. (2010). Next, we compared an evolved stage of the calibrated model, also using $R_{\rm inf} = 10$ pc, with the physical conditions in the OMC-1 massive clump, finding that it has similar physical conditions after ~ 26 Myr of evolution since its parent MC first formed, although it spends only about 2 Myr in a state comparable to OMC-1.

Finally, we investigated the stellar age distribution in our isolated-cloud model with $R_{\rm inf} = 10$ pc, showing that, taken a few Myr before the end of the cloud's life, it is consistent with the corresponding distributions presented by Palla and Stahler (2000) for various clusters and associations. Furthermore, the model predicts that the shape of this age distribution depends on the evolutionary stage of the system, being more peaked toward young ages as the system grows older, because of its increasing SFR.

We conclude that our evolutionary and collapsing model of MCs adequately represents actual clouds of a wide range of masses, with no need whatsoever for the consideration of equilibrium states. In this sense, the present model, although idealized, represents a promising first attempt at a non-equilibrium model for MCs and their star-forming properties.

4

An evolutionary model for collapsing Molecular Clouds and their Star Formation activity. II. Mass dependence of the Star Formation Rate

4.1 Abstract

We discuss the evolution, and dependence on cloud mass, of the star formation rate (SFR) and efficiency (SFE) of star-forming molecular clouds (MCs) within the scenario that clouds are undergoing global collapse and that the SFR is controlled by ionization feedback. We find that low-mass clouds ($M_{\rm max} \lesssim 10^4\ M_\odot$) spend most of their evolution at low SFRs, but end their lives with a mini-burst, reaching a peak SFR $\sim 10^4\ M_\odot{\rm Myr}^{-1}$, although their time-averaged SFR is only $\langle{\rm SFR}\rangle \sim 10^2\ M_\odot{\rm Myr}^{-1}$. The corresponding efficiencies are ${\rm SFE}_{\rm final} \lesssim 60\%$ and $\langle{\rm SFE}\rangle \lesssim 1\%$. For more massive clouds ($M_{\rm max} \gtrsim 10^5\ M_\odot$), the SFR first increases and then reaches a plateau, because the clouds are influenced by the stellar feedback since earlier in their evolution. As a function of cloud mass, $\langle{\rm SFR}\rangle$ and $\langle{\rm SFE}\rangle$ are well represented by the fits $\langle{\rm SFR}\rangle \approx 100(1 + M_{\rm max}/1.4 \times 10^5\ M_\odot)^{1.68}\ M_\odot{\rm Myr}^{-1}$ and $\langle{\rm SFE}\rangle \approx 0.03(M_{\rm max}/2.5 \times 10^5\ M_\odot)^{0.33}$, respectively. Moreover, the SFR of our model clouds follows closely the SFR-dense gas mass relation recently found by Lada et al., during the epoch when their instantaneous SFEs are comparable to those of the clouds considered by those authors. Collectively, a Monte Carlo integration of the model-predicted SFR(M) over a Galactic giant molecular cloud mass spectrum yields values for the total Galac-

tic SFR that are within half an order of magnitude from the relation obtained by Gao & Solomon. Our results support the scenario that star-forming MCs may be in global gravitational collapse and that the low observed values of the SFR and SFE are a result of the interruption of each SF episode, caused primarily by the ionizing feedback from massive stars.

4.2 Introduction

The regulation of the star formation rate (SFR) in molecular clouds (MCs) has been a key problem in astrophysics for more than half a century, ever since Schmidt (1959) noticed that the SFR in clouds exhibited a power-law dependence on the gas number density n. A crucial aspect of the SFR was noticed by Zuckerman and Palmer (1974), who pointed out that the observed Galactic SFR is at least one order of magnitude lower than that expected if the clouds were forming stars at the "free-fall rate" given by the ratio of the total molecular gas mass in the Galaxy to the typical free-fall time of this gas. Indeed, current estimates of the total molecular gas mass and density ($M_{\rm mol} \sim 10^9\ M_\odot$, $n \sim 100{\rm cm}^{-3}$; e.g., Ferrière, 2001) imply a free-fall SFR $\sim 200\ M_\odot\ {\rm yr}^{-1}$, while the observed SFR is roughly 100 times smaller (e.g., Chomiuk and Povich, 2011). Thus, it was concluded that MCs could not be in free-fall, contrary to the then-recent suggestion of Goldreich and Kwan (1974), and that the nonthermal linewidths observed in the clouds were produced by small-scale turbulence instead (Zuckerman and Evans, 1974).

Since then, MCs have been assumed to be supported by a number of physical agents, such as magnetic fields (e.g., Shu et al., 1987; Mouschovias, 1991b) or turbulence (e.g., Vazquez-Semadeni et al., 2000; Vázquez-Semadeni et al., 2003; Elmegreen and Scalo, 2004b; Mac Low and Klessen, 2004; Ballesteros-Paredes et al., 2007; McKee and Ostriker, 2007). In both scenarios, the necessary low SFR was attained because a small fraction of the mass managed to escape the support. This fraction was mediated by ambipolar diffusion in the first case and by local turbulent compressions that induced small-scale, low-mass collapses in the second. In the last decade, a number of models for the turbulent regulation of star formation (SF) have been constructed within the scenario of clouds in which both the global support and the local collapses are induced by turbulence (Krumholz and McKee, 2005; Hennebelle and Chabrier, 2011; Padoan and Nordlund, 2011). These models are based on the premise that the high-density tail of the density probability density function (PDF), which takes a log-normal form for supersonic isothermal turbulence (Vazquez-Semadeni, 1994; Padoan et al., 1997; Passot and Vázquez-Semadeni, 1998), is responsible for the instan-

taneous SFR, which is given by this mass divided by a characteristic timescale. The models differ in the threshold density for defining the "high-density" gas and the characteristic timescale. A thorough discussion of these models has been recently provided by Federrath and Klessen (2012).

However, recent evidence from both observations and numerical simulations has suggested that star-forming MCs may be in gravitational collapse after all. Comparing numerical simulations of a variety of turbulent and free-falling regimes to the observed kinematics of the clump NGC 2264-C, Peretto et al. (2007) showed that the best fit was provided by simulations in which infall dominates over turbulence by a large margin (95% of the kinetic energy). Comparing the morphology of the Orion A cloud to that of simulations of gravitational collapse of a nearly elliptical sheet of gas, Hartmann and Burkert (2007) suggested that the entire Orion A cloud may be in gravitational collapse. Also, infall has been observed at multiple scales in the high-mass star-forming region G20.08−0.14 (Galván-Madrid et al., 2009) and from filamentary regions onto clumps, as well as onto the filaments (Schneider et al., 2010; Kirk et al., 2013). On the numerical side, simulations of cold, dense cloud formation including self-gravity (Vázquez-Semadeni et al., 2007; Heitsch and Hartmann, 2008; Vázquez-Semadeni et al., 2009; Vázquez-Semadeni et al., 2010; Vázquez-Semadeni et al., 2011) have shown that the clouds engage in gravitational collapse shortly after they collect enough mass to be Jeans-unstable and long before any star formation begins to occur within them. Moreover, the nonlinear density fluctuations produced by the turbulence in the cloud have shorter free-fall timescales than the cloud at large and therefore complete their collapses before the cloud does. Thus, Vázquez-Semadeni et al. (2009) suggested that MCs are in a state of "hierarchical gravitational collapse", where the *local*, small-scale collapses of dense cores are occurring within the *global*, large-scale collapse of the cloud.

In a previous paper (Zamora-Avilés et al., 2012, hereafter Paper I), we presented an analytical model for the evolution of the SFR in the context of gravitationally collapsing clouds. This model was based on the same prescription for computing the SFR as that used in the models mentioned above, i.e., an integration of the density PDF above a certain threshold density to obtain the mass responsible for the "instantaneous" SFR. The threshold density was obtained by calibrating the evolution of the SFR with the numerical simulations of Vázquez-Semadeni et al. (2010), and the timescale was chosen as the free-fall time at the threshold density. However, the distinctive feature of the model was that the cloud, assumed to have a sheet-like geometry, was considered to be undergoing free-fall gravitational collapse, causing its mean density to increase. Therefore, the density PDF was considered to continuously shift to higher densities and thus the star-forming mass continuously increased in time, implying a system-

atic increase of the SFR. The controlling parameter of the model was found to be the total system mass, and the model successfully described the evolutionary sequence for $\sim 10^5$ $M_\odot$ giant molecular clouds (GMCs) reported by Kawamura et al. (2009), the stellar age histograms for clouds of mass ~ 2000 $M_\odot$ as reported by Palla and Stahler (2000) and Palla and Stahler (2002), and the locus of clouds of this same mass in the Kennicutt−Schmidt diagram, as reported by Evans et al. (2009).

Since the main controlling parameter of the model from Paper I was the cloud's mass, in this paper we now examine the predictions of the model for the dependence of the SFR and the star formation efficiency (SFE) with the mass of the cloud, and from there examine the prediction of the model for the SFR−mass relation first proposed by Gao and Solomon (2004, hereafter, the GS relation). The plan of the paper is as follows. In Section 4.3, we present a brief summary of the model, as well as its application to the present study. In Section 4.4, we present the results for the dependence of the SFR and the SFE with cloud mass and compare the model with the observational GS relation. Then, in Section 4.5, we discuss some implications and limitations of our results. Finally, in Section 4.6, we present a summary.

4.3 The Model

Our model, first presented in Paper I, follows the evolution of the gas mass that initially constitutes a cold atomic cloud, formed by the collision of two streams in the warm neutral medium (WNM). The model is intermediate between a Lagrangian and an Eulerian description, as it follows the collapse of the cold cloud material as soon as it exceeds its Jeans mass, but at the same time allows for the addition of fresh material, coming from the continuing WNM streams ("the inflows"), through the boundaries of the collapsing region. As the cold gas collapses and reduces its size, we only add to it the material entering through its instantaneous, reduced boundaries, while the rest of the inflow material is assumed to be deposited in an envelope whose evolution we ignore. Thus, the model accounts for the fact that a "cloud" is *not* made of the same material throughout its evolution, but rather is constantly accreting fresh material from its environment, as has been proposed by several studies (e.g., Smith et al., 2009; Vázquez-Semadeni et al., 2009; Vázquez-Semadeni et al., 2010; Goldbaum et al., 2011). Within this scenario, we follow the evolution of the material that initially begins to collapse, to which we will, for convenience, refer to as "the cloud", although it must be borne in mind that the entire system consists of this collapsing region plus the material added to the envelope during the evolution.

Thus, the entire system does not contract because of the material continuously added to it.

We assume that the clouds are born with a density of $n = 100$ cm^{-3} and a temperature of ~ 40 K,[1] representative of the cold atomic medium (CNM). In Paper I, the flows were assumed to continue indefinitely, as is done in many numerical simulations (e.g., Audit and Hennebelle, 2005; Hennebelle et al., 2008). Instead, here we assume that the flows subside after 25 Myr, somehow mimicking the duration of the accretion flow that a parcel in the ISM may be subject to when traversing a 1 kpc spiral arm at a speed of ~ 20km s^{-1} (the spiral pattern speed with respect to the gas at the Solar circle). The mass accretion rate onto the cloud is given by $\dot{M}_{\rm inf} = 2\rho_{\rm WNM} v_{\rm inf} (\pi R_{\rm inf}^2)$, where $\rho_{\rm WNM}$ is the WNM density ($= 2.1 \times 10^{-24}$ g cm^{-3}, which corresponds to $n = 1$ cm^{-3} assuming a mean particle mass of 1.27), $v_{\rm inf}$ is the inflow velocity ($= 4.5$ km s^{-1}, obtained from the calibration; see below), and $R_{\rm inf}$ is the radius of the inflow, assumed to have a cylindrical shape. This inflow continues to feed the cloud for 25 Myr, increasing its mass. We assume that the cloud begins to undergo global gravitational collapse as soon as it reaches its Jeans mass, which, for a planar cloud, is given by (Larson, 1985):

$$M_{\rm J} = 4.67 \frac{c_{\rm s}^4}{G^2 \Sigma}, \tag{4.1}$$

where $c_{\rm s}$ is the sound speed in the cloud, assumed constant and uniform ($c_{\rm s}(T = 40\ {\rm K}) = 0.38$ km s^{-1}), and $\Sigma = M_{\rm C}(t)/\pi R_{\rm C}^2(t)$ is the surface density, with $M_{\rm C}(t)$ and $R_{\rm C}(t)$ being the instantaneous mass and radius of the cloud, respectively. Note that we deliberately do not consider turbulent support, as one essential feature of the model is that the large supersonic velocities that develop in molecular clouds are the result of the collapse and thus do not provide support. We also assume that because the initial turbulence is transonic (see below), it does not provide a significant source of additional support. Finally, note also that once the cloud has started to collapse, its radius shrinks, and so we only consider the mass inflow across its instantaneous cross section, assuming that the rest of the material goes into a medium-density (~ 100cm^{-3}) cloud envelope, which is not included in the collapse calculation.

We furthermore assume that the cold dense gas is turbulent, due to the combined action of various instabilities (Vishniac, 1994; Walder and Folini, 2000; Heitsch et al., 2006; Vázquez-Semadeni et al., 2006), with a moderate Mach number $\mathcal{M}_{\rm rms} = 3$. This is consistent with observations of the velocity dispersion in the cold neutral medium (Heiles and Troland, 2003). Note that this

[1] This temperature is obtained considering the heating and cooling processes by Koyama and Inutsuka (2000).

Mach number is significantly lower than the typical Mach numbers, $\mathcal{M}_{\rm rms} \sim 10$–20, usually associated with molecular clouds, which in our model correspond to infall velocities rather than to random turbulence. We stress that numerical simulations in general (Koyama and Inutsuka, 2002; Audit and Hennebelle, 2005; Vázquez-Semadeni et al., 2006; Vázquez-Semadeni et al., 2007; Banerjee et al., 2009) show that the turbulent Mach numbers produced in the atomic precursor of a MC by the flow collision are substantially smaller than those observed in MCs. As discussed in Vázquez-Semadeni et al. (2007), such high Mach numbers are only observed in cloud evolution simulations as a consequence of the gravitational contraction. As a consequence of the turbulence in the dense gas, we assume that the cloud develops a log-normal density PDF of the form

$$P(s) = \frac{1}{\sqrt{2\pi\sigma_s^2}} \exp\left[-\frac{(s-s_{\rm p})^2}{2\sigma_s^2}\right], \tag{4.2}$$

where $s \equiv \ln(\rho/\langle\rho\rangle)$, $s_{\rm p} = \ln(\rho_{\rm p}/\langle\rho\rangle) = -\sigma_s^2/2$, and $\sigma_s^2 = \ln(1+b^2\mathcal{M}_{\rm rms}^2)$, with $\rho_{\rm p}$ being the peak density, $\langle\rho\rangle$ the mean density, and b a proportionality constant related to the compressibility induced by the turbulent forcing (Federrath et al., 2008; Federrath et al., 2010b). For simplicity, we consider only compressible modes, i.e., $b = 1$.

As in other recent SFR models (Krumholz and McKee, 2005; Hennebelle and Chabrier, 2011; Padoan and Nordlund, 2011; Federrath and Klessen, 2012), we assume that the high-density tail of the PDF is responsible for the instantaneous SFR in the cloud, which is calculated as

$$\mathrm{SFR}(t) = \frac{M(n > n_{\rm SF}, t)}{t_{\rm ff}(n_{\rm SF})}, \tag{4.3}$$

where $n_{\rm SF}$ is a threshold number density for defining the mass involved in the instantaneous SFR and $t_{\rm ff}(n_{\rm SF})$ is the free-fall time at number density $n_{\rm SF}$. Note that $n_{\rm SF}$ represents neither the mean density of the cloud nor the typical density of the clumps that form stars. Instead, it is a *free parameter* of the model indicating the density above which the collapse time can be considered to be negligibly small compared to the evolutionary timescale of the system. That is, since the cloud contains a distribution of density fluctuations caused by the turbulence, the densest among these have the shortest collapse timescales. The parameter $n_{\rm SF}$ represents the density fluctuation level whose collapse time can be considered as "instantaneous" in the model. On the other hand, the typical density of a star-forming cloud or clump is represented by the *peak* of the density PDF, and is generally smaller than $n_{\rm SF}$, except at the very last stages of the collapse of a model cloud, when its mean density reaches very high values (see below).

The threshold number density $n_{\rm SF}$ was calibrated in Paper I by matching the evolution of the model to the results of the numerical simulations –specifically, the evolution of the SFR, and the gaseous and stellar masses. The best match was found to occur for $n_{\rm SF} = 10^6 {\rm cm}^{-3}$ (for which the free-fall time is $t_{\rm ff} \approx 0.03$ Myr) and this value was left fixed thereafter. Here we continue to use that value.

In addition, in Equation (4.3), $M(n > n_{\rm SF}, t)$ is the mass of the material at densities above $n_{\rm SF}$, and given by

$$M(n > n_{\rm SF}, t) = f M_{\rm C}(t), \tag{4.4}$$

where f is the mass fraction at densities above $n_{\rm SF}$, given by[1]

$$f = \frac{1}{2}\left[1 - {\rm erf}\left(\frac{s_{\rm SF} - \sigma_s^2/2}{\sqrt{2}\sigma_s}\right)\right] \tag{4.5}$$

and $s_{\rm SF} \equiv \ln(\rho_{\rm SF}/\langle\rho\rangle)$ (see also Elmegreen, 2002; Krumholz and McKee, 2005; Dib et al., 2011).

As mentioned above, in contrast with the models by Krumholz and McKee (2005), Padoan and Nordlund (2011), and Hennebelle and Chabrier (2011), which considered stationary clouds, here we assume that the cloud is collapsing, keeping in mind that it is a sheet-like object and so its collapse proceeds more slowly than that of a three-dimensional object of the same volume density (Burkert and Hartmann, 2004; Pon et al., 2012; Toalá et al., 2012). In the model, we numerically solve the free-fall motion of the sheet-like cloud.

As a consequence of its collapse, the mean density of the cloud increases with time, causing the density PDF to systematically shift towards higher densities. Thus, in our model (based on the notion of hierarchical gravitational collapse; Vázquez-Semadeni et al., 2009), the *global* collapse of the cloud is represented by the fact that the mean density of a cloud or clump increases over time, while the *local* collapses of the densest regions are represented by the calculation of the instantaneous SFR, performed by considering the mass above $n_{\rm SF}$ and dividing it by the free-fall time at this density. This treatment implies that the SFR in the model is an increasing function of time, since the area under the PDF at densities higher than $n_{\rm SF}$ increases as the mean density increases. The total mass in stars at time t in the model is thus given by

$$M_{\rm S}(t) = \int_0^t {\rm SFR}(t')dt'. \tag{4.6}$$

[1]Note that this equation in Paper I contains a typographical error. The form written here is the correct expression.

From this stellar mass, the number of massive stars (with a representative mass of 17 $M_\odot$) is computed using a standard initial mass function (IMF; Kroupa, 2001), with lower and upper mass limits of 0.01 and 60 $M_\odot$, respectively. In turn, this allows us to compute the mass evaporation rate, $\dot{M}_\mathrm{I}(t)$, by these stars using the prescription from Franco et al. (1994) for the evaporation rate induced by a single massive star of age $\hat{t}$ located near the cloud edge, given by

$$\dot{M}_\mathrm{I}(\hat{t}) \simeq 2\pi R_{\mathrm{S},0}^2 m_\mathrm{p} c_{\mathrm{s,I}} \langle n \rangle \left(1 + \frac{5 c_{\mathrm{s,I}} \hat{t}}{2 R_{\mathrm{S},0}}\right)^{1/5} \tag{4.7}$$

where $c_{\mathrm{s,I}}$ is the sound speed in the ionized gas ($= 12.8$ km s^{-1}), $\langle n \rangle$ is the mean number density of the cloud, m_p is the proton mass, and $R_{\mathrm{S},0}$ is the initial Strömgren radius in a medium of density $\langle n \rangle$. To calculate this radius, as in Franco et al. (1994), we additionally assume a recombination coefficient for the ionized gas $\alpha_\mathrm{B} = 2.6 \times 10^{-13}\,\mathrm{cm^{-3}\,s^{-1}}$ and a representative value of the UV Lyman-continuum photon flux $S_* = 2 \times 10^{48}\,\mathrm{s^{-1}}$, corresponding to our generic massive star. Finally, to get the total ionized mass we integrate Equation (4.7) over the lifetime of each massive star formed and add the contributions from all active massive stars.

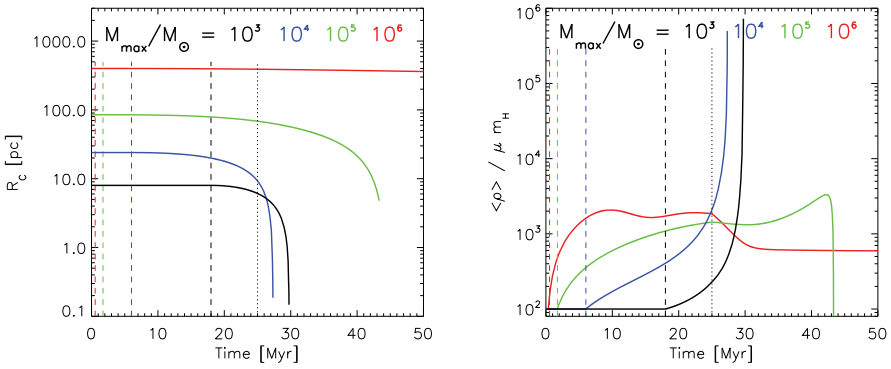

Figure 4.1: Left: time evolution of the radius for clouds with $M_\mathrm{max} = 10^3$, 10^4, 10^5, and $10^6\,M_\odot$ (black, blue, green, and red lines, respectively). The vertical dashed lines represent the time at which the cloud reaches its Jeans mass and begins contracting, whereas the vertical thin dotted black line is the time at which the accretion stops (at $t = 25\,\mathrm{Myr}$). Right: time evolution of the density. The line colors have the same meaning as in the left panel.

With the above ingredients, the instantaneous mass of the cloud is the result of the competition between addition of fresh gas by accretion, the consumption

by star formation, and the evaporation from the massive stars. Thus, the cloud mass evolves according to

$$M_{\rm C}(t) = \int_0^t \dot{M}_{\rm inf}(t')\ {\rm d}t' - M_{\rm S}(t) - M_{\rm I}(t). \tag{4.8}$$

We numerically integrate Equation (4.8), together with Equations (4.6) and (4.7), to obtain the temporal evolution of a specific cloud, until it is finally dispersed.

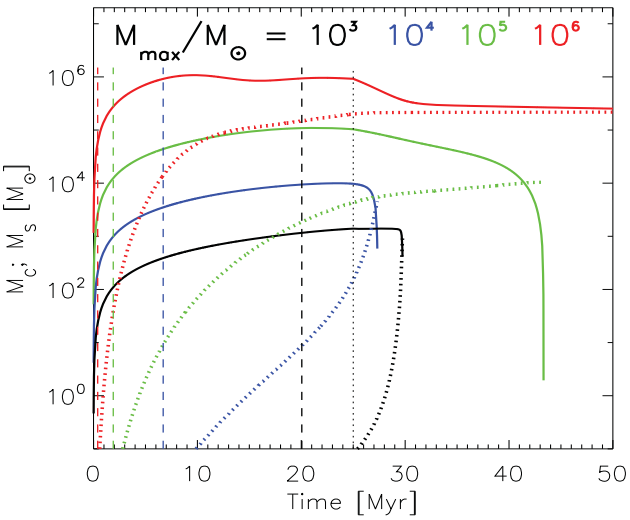

Figure 4.2: Time evolution of the dense gas mas (solid lines; Equation (4.8)), and mass in stars (dotted lines) for clouds with $M_{\rm max} = 10^3$, 10^4, 10^5, and $10^6\,M_\odot$ (black, blue, green, and red lines, respectively). The vertical dashed lines represent the time, $t_{\rm SF}$, at which the cloud starts to form stars, whereas the vertical thin dotted black line is the time at which the accretion stops (at $t = 25\,{\rm Myr}$).

As emphasized in Paper I, the main controlling parameter of this model is the total mass involved in the process, which for fixed values of $\rho_{\rm WNM}$ and $v_{\rm inf}$ is controlled by the cylinder radius $R_{\rm inf}$. In what follows, we thus choose the required value of $R_{\rm inf}$ to obtain the reported maximum cloud mass, which is the maximum mass reached by the cold, dense gas during the model's evolution and labeled $M_{\rm max}$. Since the numerical integration of the model takes only a few seconds on a desktop computer, it allows us to sweep parameter space using

hundreds of models of different masses, a task that cannot be undertaken with full numerical simulations.

Figure 4.1 shows the evolution of the cloud radius and mean density for representative clouds with $M_{\rm max} = 10^3$, 10^4, 10^5, and $10^6\,M_\odot$. A number of features are worth noticing. First, from the left panel of Figure 4.1, it is seen that the radius of a cloud remains essentially constant over more than 10 Myr of evolution, during which the cloud is accreting mass, until it reaches its Jeans mass. Afterward, the cloud's radius begins to decrease at an accelerated pace, with its mean density increasing, as shown by the right panel of Figure 4.1. It is noteworthy that this evolution implies that the material constituting an initially medium-sized cloud of size ~ 10 pc and mass a few thousand $M_\odot$, such as Perseus or Ophiuchus, should evolve into a massive-star-forming clump of density $\sim 10^5$–$10^6 {\rm cm}^{-3}$ and sizes $\lesssim 1$ pc, such as the massive clumps studied by Wu et al. (2010), as shown in Figure 7 of Paper I. It must be borne in mind, however, that by the time the cloud has contracted to a massive clump, it is embedded in the envelope that has been added to the cloud's surroundings by the WNM inflows.

Figure 4.2, in turn, shows the evolution of the dense gas mass and the stellar mass for these models. It is seen that in all but the most massive model (the one with $M_{\rm max} = 10^6\,M_\odot$), the cloud mass increases until the time when the stellar ionizing feedback begins to rapidly erode the dense gas mass, causing it to decrease again. The exception to this behavior is the model with $M_{\rm max} = 10^6\,M_\odot$, for which the dense gas mass stops increasing at $t \sim 10$ Myr. This is due to the fact that its mass is so large that the mass fraction at high density in this cloud allows for the formation of massive stars and the corresponding erosion even before the cloud has had time to contract significantly.[1]

In the next section, we discuss the evolution of the SFR and the SFE for the models as parameterized by their mass.

4.4 Model Predictions

4.4.1 Mass Dependence of the Star Formation Rate

In this and the following sections, we consider a collection of models of various masses, and focus on the variation of the maximum and time-averaged values of the SFR and the SFE (see Section 4.4.2) as a function of $M_{\rm max}$. The time

[1]Recall that in the model, the clouds are assumed to have sheet-like geometry and that their collapse is given by the expression corresponding to such geometry (Burkert and Hartmann, 2004), which is slower than the collapse for a spherical geometry (Pon et al., 2012; Toalá et al., 2012).

averages we consider cover the time span between the formation of $0.01 M_\odot$ (the lower limit in the IMF considered) of stellar products and the destruction of the cloud (see Figure 4.2). To simplify the discussion, we will refer to "low-mass clouds" as those with $M_{\rm max} \lesssim 10^4\,M_\odot$; to "intermediate-mass" clouds as those with maximum masses in the range of $10^4 - 10^5\,M_\odot$; and to "massive clouds" as those with $M_{\rm max} \gtrsim 10^5\,M_\odot$.

It is important to note that, so far, we have referred to our models simply as "clouds". However, in this section, in which we try to predict characteristic values of the SFR and SFE (characterized by their time averages) in *molecular* clouds of different masses, it is important to define the time interval during which the clouds can be considered as "molecular", so that the time averages are computed over this interval. Unfortunately, in our one-zone model without chemistry, there is no direct way to determine this time. Thus, we instead take the beginning of the averaging interval as the time at which the clouds begin to form stars, $t_{\rm SF}$. We have verified that this is a reasonable proxy for determining when the clouds begin to be sufficiently molecular by using the density PDF to compute the mass fraction at densities $n > 10^3 {\rm cm}^{-3}$—which can be reasonably assumed to be already in molecular form—at the time SF starts, finding that this mass fraction is ≥ 0.2 in all models. Thus, hereinafter we will refer to clouds after $t_{\rm SF}$ as "star-forming molecular clouds" (SF-MCs) and to clouds in previous stages as "precursor" clouds.

In the left panel of Figure 4.3, we show the evolution of the SFR for clouds of maximum masses $M_{\rm max} = 10^3,\ 10^4,\ 10^5$, and $10^6\ M_\odot$. We observe that low-mass SF-MCs have a very low SFR over most of their evolution and end their evolution with a short SF burst. This can be understood because due to their low mass, these clouds can only reach large SFRs when a substantial fraction of their mass is involved in SF. This can only occur when their mean density has become comparable to $n_{\rm SF}$, as shown in the right panel of Figure 4.1. At this point, these clouds are quickly destroyed by the first massive stars. This also means that the consumption of the gas in these clouds is mostly due to SF rather than to evaporation by feedback from the massive stars.

On the other hand, intermediate- and high-mass SF-MCs increase their SFR for the first ~ 10 Myr and then reach a plateau, remaining there for roughly 10–20 Myr more. This is because due to their higher masses, they can have larger SFRs since earlier times (even a small fraction of their mass corresponds to a large enough mass involved in active SF). This implies that massive SF starts earlier in these clouds. Nevertheless, due to their larger masses and accretion rates, they are not completely destroyed, although these clouds do lose some of their mass when the first massive stars appear. Moreover, this partial mass dispersal causes a decrease in the SFR and therefore the cloud evolution

reaches an approximately stationary SFR for a significant part of their lifetimes. Thus, in these clouds, a larger fraction of the dense gas consumption is due to evaporation, compared to the low-mass clouds. Note, however, that accretion plays a fundamental role in this behavior since in experiments where we have cut the accretion shortly after the onset of SF, the massive stars quickly destroy the clouds.

In the right panel of Figure 4.3, we show the maximum and the time-averaged values of the SFR as a function of $M_{\rm max}$. Note that each point in this figure corresponds to a full integration of an individual model. We note that for low-mass SF-MCs, the maximum SFR is much larger than its average values because of the short but intense SF burst that characterizes the end of the evolution of these clouds. Instead, for more massive SF-MCs, the peak and the average SFR are similar due to the prolonged epoch of roughly constant SF that occurs in these clouds. As a reasonable approximation, the time-averaged

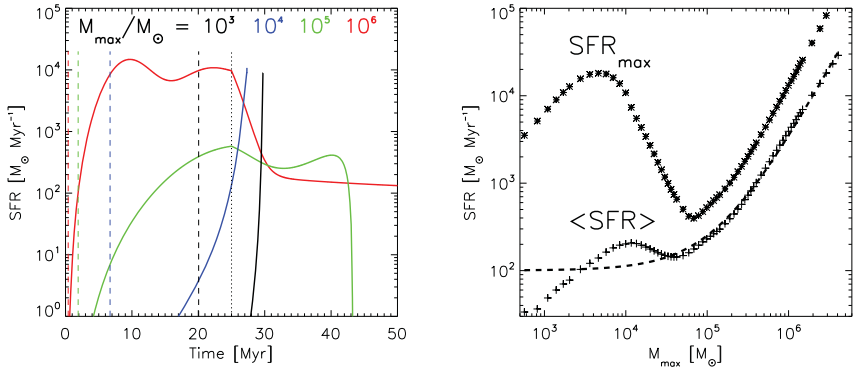

Figure 4.3: Left: time evolution of the SFR for clouds with $M_{\rm max} = 10^3$, 10^4, 10^5, and $10^6\,M_\odot$ (black, blue, green, and red lines, respectively). The vertical dashed lines represent the time, $t_{\rm SF}$, at which the cloud starts to form stars, whereas the vertical thin dotted black line is the time at which the accretion stops (at $t = 25\,{\rm Myr}$). Right: maximum and time-averaged SFR (asterisks and plus symbols, respectively) as a function of the maximum mass achieved by each model cloud. The averaging is performed over the period during which the clouds form stars.

SFR can be fit by a power law of the cloud mass, given by

$$\langle {\rm SFR} \rangle \approx 100 \left(1 + \frac{M_{\rm max}}{1.4 \times 10^5\,M_\odot}\right)^{1.68} M_\odot\,{\rm Myr}^{-1}, \tag{4.9}$$

which is shown as the dashed line in the right panel of Figure 4.3.

4.4.2 Mass Dependence of the Star Formation Efficiency

We now turn to the mass dependence of the SFE. As in Paper I, we define the instantaneous SFE as

$$\mathrm{SFE(t)} = \frac{M_{\mathrm{S}}(t)}{M_{\mathrm{C}}(t) + M_{\mathrm{S}}(t) + M_{\mathrm{I}}(t)}, \tag{4.10}$$

where all the quantities are time-dependent. The left panel of Figure 4.4 shows the time evolution of the SFE for models with $M_{\mathrm{max}} = 10^3$, 10^4, 10^5, and 10^6 $M_\odot$. From this figure, we see that in the low-mass SF-MCs, the final star formation burst (see right panel in Figure 4.3) produces large *final* efficiencies ($\lesssim$60%), although this is not in contradiction with observations, as it is not possible to observationally determine the SFE of a cloud/cluster system after the gas has been dispersed. On the other hand, for the more massive SF-MCs, the SFE reaches a saturated value of $\sim$ 6%. The SFE can saturate due to the interplay between the gas evaporation by the feedback and the accretion of fresh gas, so that the masses of the cloud and of the stellar component increase simultaneously, keeping the instantaneous SFE approximately constant.

The right panel of Figure 4.4 shows the final and time-averaged efficiencies for the SF-MCs as a function of their masses. As in the right panel of Figure 4.3, each point in this plot represents the full temporal integration of one model with a given radius R_{inf}, which reaches the maximum dense gas mass indicated by its horizontal coordinate. From this figure, we see that although the *final* instantaneous SFEs of the low mass clouds are much higher than those of the high-mass ones, the time-averaged values of the SFE increase monotonically with M_{max}. The time-averaged SFE should be representative of the result of observing a MC ensemble of random ages and thus represent the average value of the SFE observed for MCs of the indicated mass. We see that $\langle\mathrm{SFE}\rangle$ is well fit by a power law of the form

$$\langle\mathrm{SFE}\rangle \approx 0.03 \left(\frac{M_{\mathrm{max}}}{2.5\times10^5\,M_\odot}\right)^{0.33}, \tag{4.11}$$

so that we obtain time-averaged SFEs in the range of 0.5−6% for the range of maximum cloud masses shown in Figure 4.4, consistent with observational determinations for GMCs in general (see, e.g., the compilation by Federrath and Klessen, 2013). Thus, our model predicts that the time-averaged SFE should increase with the cloud mass, albeit slowly, with a scatter that might correspond not only to observational errors, but also to the variation of the SFE over the evolution of the clouds.

The exponent in Equation (4.11) is close to the value predicted analytically by Fall et al. (2010) of 0.25 for the case of feedback dominated by ionization

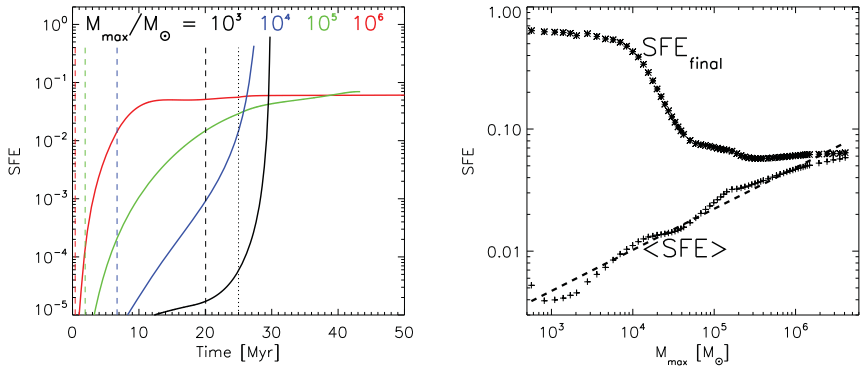

Figure 4.4: Left: time evolution of the SFE for clouds with $M_{\rm max} = 10^3$, 10^4, 10^5, and $10^6\,M_\odot$. The symbolism is the same as in Figure 4.3. Right: maximum and mean SFEs as a function of the maximum cloud mass.

heating. The difference may be due to the fact that those authors considered stationary energy (or momentum, for the case of momentum-dominated feedback) balance, while here we take the additional step of considering the time evolution of the feedback and/or to the different assumed geometries (flat in our case).

4.4.3 Star Formation Rate-Dense Gas Mass Correlation

In Paper I we showed that the evolution of our model clouds with maximum dense gas masses $M_{\rm max} \sim 2000\ M_\odot$, when plotted in the Kennicutt-Schmidt (KS) diagram, took them from the locus of clouds forming low-mass stars such as Perseus, Lupus, Serpens, and Ophiuchus (Evans et al., 2009) to that of clouds forming massive stars, such as the Orion A cloud and the clumps investigated by Heiderman et al. (2010). We now investigate whether, collectively, our clouds conform to observed star formation correlations found for averages over large volumes. This is important because those correlations are often interpreted as the result of a sustained low value of the SFE due to global turbulent support of the clouds (e.g., Krumholz et al., 2009; Krumholz et al., 2012), while our model clouds are in global collapse, and their SFR and SFE are not constant but rather time-dependent. In this case, one can ask whether the *time-averaged* (over their star-forming epoch) SFR and SFE of our model clouds are consistent with the observed SF correlations.

One important such correlation is the one found by Gao and Solomon (2004, hereafter GS04) who, in a sample of luminous and ultraluminous infrared galax-

ies as well as of normal spirals, found a linear relationship between the IR luminosity (a tracer of the SFR) and the HCN luminosity (a tracer of the dense $[n \geq n_{\rm dens} = 3 \times 10^4 \text{ cm}^{-3}]$ gas mass), implying that

$$\text{SFR} \approx 180 \left(\frac{M_{\rm dens}}{10^4 \, M_\odot} \right) M_\odot \, \text{Myr}^{-1}, \tag{4.12}$$

which is a linear relationship between the SFR and $M_{\rm dens}$, the mass at density $\geq n_{\rm dens}$ (Figure 4.5). On MC scales, Lada et al. (2010, hereafter LLA10) found a similar linear relationship (SFR $\propto M_{\rm dens}$) for a sample of nearby MCs (see Figure 4.5), measuring the gas mass at densities above $n \geq n_{\rm dens} = 10^4$ cm^{-3} from extinction maps and estimating the SFR by counting young stellar objects (YSOs) and dividing by a typical age spread, $\Delta t \sim 2$ Myr. These authors also found that the SFEs of their cloud sample fall in the range of 0.1%−-4%.

We wish to compare our model's predictions to these results. To do so, at the individual cloud level, we attempt to replicate the procedure of LLA10. Note that according to our model, both the SFR and the SFE of a cloud increase over time and thus the range of efficiencies observed in LLA10's sample is interpreted as a spread in evolutionary stages. In turn, this implies that the corresponding SFRs should also correspond to a range of evolutionary stages. Thus, for each model cloud, we should consider the range of SFRs that it may have over this range of evolutionary stages for comparison with the observations. However, we have the problem that the evolutionary stage of the clouds considered by LLA10 is not known. To circumvent this problem, we make use of the fact that our model predicts *both* the SFR and the SFE of the clouds as a function of time. These quantities are different from each other, because the SFR is a truly instantaneous quantity, while the SFE involves the integral of both the stellar and gaseous mass accretion rates (see Equation (4.10)). Thus, we can use the instantaneous SFE of a cloud as a proxy for its evolutionary stage and then compute the corresponding SFR predicted by the model at that stage to compare with the observationally inferred SFRs.

Note in addition that the SFR estimates by LLA10 are not strictly instantaneous values but rather averages over the age spread Δt. We thus also estimate the SFR not through the instantaneous SFR predicted by the model, but as the number of stars of age < 2 Myr, divided by this time interval, and compute this estimate at two different times, one labeled t_1, when the clouds' SFE is 0.1% and the other labeled t_2, when the clouds' SFE is 4%, consistent with the range of SFEs exhibited by the LLA10 sample. Thus, for each model cloud we report a range of SFRs. Similarly, the instantaneous mass of the model clouds varies between these two times, and therefore we also report a range of masses for each model cloud. We do this for model clouds with maximum masses in the

same mass range—recall the model clouds are labeled by the maximum mass they reach during their evolution—as the clouds in their sample.

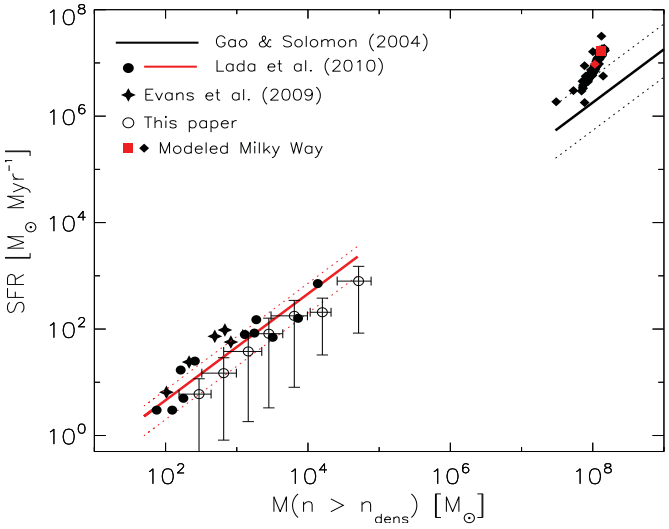

Figure 4.5: SFR as a function of dense gas mass ($M_{\rm dens} = M(n \geq n_{\rm dens})$, with $n_{\rm dens} = 10^4\,{\rm cm}^{-3}$) for low- to intermediate-mass model clouds (open circles with error bars; see the text). In the lower left corner, corresponding to individual cloud masses, the filled stars correspond to data from Evans et al. (2009), while the filled circles correspond to the cloud sample studied by LLA10, with the red solid line denoting the mean fit reported by those authors and its dispersion represented by the red dotted lines. In the upper right corner, corresponding to galactic masses, the solid black line shows the scaling found by GS04 (Equation (4.12), with $n_{\rm dens} = 3 \times 10^4\,{\rm cm}^{-3}$), the black dotted lines showing the scatter of their observational sample. The filled red square shows the position of the modeled Milky Way given by Equation (4.14). Finally, the filled black diamonds represent Monte Carlo realizations of cloud ensembles taken at random evolutionary stages (in the SF-MC stage), with the red filled diamond giving the average value of these experiments.

In Figure 4.5 we show, in the lower left corner, the range of SFRs computed as described above versus the range of dense gas mass (i.e., at densities $n > n_{\rm dens} = 10^4\,{\rm cm}^{-3}$) for our model clouds (open circles with error bars) and for the cloud sample studied by LLA10 (filled black circles) and by Evans et al., 2009 (filled black stars).[1] The ranges of SFR and $M_{\rm dens}$ between t_1 and t_2 for

[1]LLA10 report the dense gas mass, and we take the number directly from them. However,

the model clouds are indicated by the error bars, while the open circles are the mean of these quantities between these two times. It is seen that the slope of the ensemble of models is nearly unity, similarly to the fit by LLA10, and that the locus of the means falls within the scatter reported by those authors.

As a further test of the model, we can estimate the *total* Galactic SFR it predicts by convolving the time-averaged SFR for each cloud mass, $\langle \mathrm{SFR} \rangle (M)$, with a suitable cloud mass spectrum. This can be then compared with the average relation derived by GS04 for external galaxies.

We use the Galactic cloud mass spectrum derived by Williams and McKee (1997), given by

$$d\mathrm{N_C} = N_0 \left(\frac{M_\mathrm{U}}{M} \right)^\alpha d(\ln M), \tag{4.13}$$

where $d\mathrm{N_C}$ is the number of MCs with masses in the range M to $M + \mathrm{d}M$, $N_0 = 63$, $\alpha = 0.6$ and $M_\mathrm{U} = 10^6\ M_\odot$ is the maximum assumed mass of GMCs in the Galaxy (see also McKee and Ostriker, 2007). The total Galactic SFR is then given by

$$\mathrm{SFR_{tot}} = \int_0^{M_\mathrm{U}} \langle \mathrm{SFR} \rangle (M) d\mathrm{N_C} \tag{4.14}$$

This exercise gives a global Galactic SFR of 14 $M_\odot\ \mathrm{yr}^{-1}$, within a factor of five from recent observational estimates (e.g., Chomiuk and Povich, 2011). Also, we can compute the total dense mass above n_dens as

$$M_\mathrm{tot}(n > n_\mathrm{dens}) = \int_0^{M_\mathrm{U}} \langle \mathrm{M}(n > n_\mathrm{dens}) \rangle (M) d\mathrm{N_C}, \tag{4.15}$$

where $M(n > n_\mathrm{dens})$ is given by Equations (4.4) and (4.5), replacing n_SF by n_dens. We find $M_\mathrm{tot}(n > n_\mathrm{dens}) = 1.3 \times 10^8\ M_\odot$. The red filled square near the upper-right corner of Figure 4.5 shows the resulting "model galaxy", based on our model's predicted $\langle \mathrm{SFR} \rangle$, which is seen to be larger than the mean scaling by GS04 by a factor ~ 5. The discrepancy is probably due to the strong SF bursts predicted by our model for low-mass clouds, in which $\sim 40\%$ of the total SFR takes place, according to the mass spectrum.

A perhaps more precise comparison is provided by a Monte Carlo integration, taking the SFR and the corresponding mass at random times for each SF-MC, and integrating again according to the mass spectrum. In the upper right corner

Evans et al., 2009 only report total masses and hence we estimate M_dens for their cloud sample using the same procedure as for our model clouds; that is, we assume a lognormal PDF centered at the mean density of the clouds reported by those authors and with width corresponding to a Mach number of three.

of Figure 4.5 (filled black diamonds), we also show a hundred of these experiments, obtaining average values of 9 $M_\odot$ yr^{-1} and $M_{\rm dens} = 1.1 \times 10^8$ $M_\odot$ for the total SFR and dense mass gas (filled red diamond), respectively. Roughly a third of the points generated in this way are seen to fall within the uncertainties of the GS04 relation. Nevertheless, the set of points always falls above the mean GS04 relation, and so the model does seem to overestimate the Galactic SFR by a factor of three to five. We discuss this further in Section 4.5.2.

4.5 Discussion and limitations

4.5.1 Implications and Insights

One important prediction of our model is that GMCs evolve in such a way that a moderate-size MC eventually becomes a dense, massive-star-forming clump over the course of $\sim$ 10 Myr. We now discuss how this process fits into our established knowledge about MCs.

4.5.1.1 Large- and Small-scale Collapse

The first point to emphasize is that the model is designed to account for both the collapse of small-scale clumps and cores and the collapse of the cloud as a whole. This is in line with the notion advanced by Vázquez-Semadeni et al. (2009) that gravitational collapse in MCs is *hierarchical* so that small-scale, local collapses occur within the environment of a cloud that is also undergoing collapse as a whole (a large-scale collapse). The small-scale collapse is described in the "standard" way (e.g., Krumholz and McKee, 2005; Hennebelle and Chabrier, 2011; Padoan and Nordlund, 2011), by assuming that the cloud contains a distribution of density fluctuations, the densest of which are undergoing instantaneous collapse, and therefore being responsible for the instantaneous SFR of the cloud. This amounts for what is normally referred to as the fragmentation of the cloud.

The large-scale collapse, on the other hand, is accounted for by directly computing the contraction rate of the whole cloud based on its average density and corresponding free-fall time. This contrasts with the models cited above, which assume roughly stationary conditions in the clouds and therefore cannot account for any evolutionary features of the clouds. In our model, the whole evolutionary nature of the process derives from the fact that the cloud is contracting as a whole.

4.5.1.2 Velocity Gradients: Rotation or Infall?

A widespread notion is that MCs rotate and that such rotation would prevent their contraction to clump scales. Indeed, velocity gradients are ubiquitously observed in MCs (e.g., Pound and Goodman, 1997; Brunt, 2003; Rosolowsky et al., 2003; Brunt et al., 2009) as well as in dense cores within them (e.g., Goodman et al., 1993; Kirk et al., 2010, see also the review by Belloche, 2013). However, as stated above, *some* form of contraction must occur in order to form a massive, dense clump.

Although the velocity gradients are almost always interpreted as rotation, it is important to remark that there is no a priori reason to do this, and in fact, Brunt (2003) points out that the Principal Component Analysis of the velocity structure in MCs is inconsistent with the signature of rotation in model clouds. On the other hand, Vázquez-Semadeni et al. (2008) showed that overdense regions in simulations of driven isothermal turbulence exhibit on average a negative velocity divergence (i.e., a velocity convergence) whose magnitude is within the range of velocity gradients reported by Goodman et al. (1993) in cores of similar sizes, suggesting again that a significant component of the observed gradients may actually consist of inflow motions rather than rotation. Similar conclusions were obtained by Csengeri et al. (2011) for massive dense cores in Cygnus-X, where they concluded that infall as well as rotation may be present.

Finally, it should also be noticed that in general, these infalling motions are not expected to be spherically symmetrical, as MCs are observed to consist mostly of filamentary structures (e.g., Myers, 2009; André et al., 2010; Molinari et al., 2010; Kirk et al., 2013), and therefore the classical infall signature (e.g., Evans, 1999, Section 4.7) should not be expected in molecular line observations of objects at these scales, so the failure to detect them does not rule out the possibility that the velocity gradients observed across clouds correspond in fact to collapsing motions.

4.5.1.3 Delayed and Extended Star Formation Activity

Another prediction from the model is that the evolution of the clouds includes a period of time (see left panel of Figure 4.3) with no significant SF (i.e., as *precursor* clouds) and, once star formation starts, they are expected to spend several more Myr at low SFRs. Interestingly, the low-mass clouds spend longer times in these states than the high-mass ones. For example, it can be seen in Figure 4.3 that a cloud with $M_{\rm max} = 10^3 M_\odot$ takes ~ 20 Myr to start forming stars and after that, it spends ~ 8 Myr with very low SFR. This is because the low-mass clouds need to contract by a large factor to reach a large enough mean

density that the mass above the threshold density $n_{\rm SF}$ causes a significant SFR. Instead, the high-mass clouds begin to do so at earlier times, when their mean density is still relatively low, because even a small fraction of their mass above $n_{\rm SF}$ involves sufficient mass for the SFR to already be significant.

However, this prediction might appear contradictory with the notion that MCs form stars rapidly after their formation (Hartmann et al., 2001). What must be borne in mind here is that the model follows the evolution of the clouds from their earliest, cold-atomic stage, which is effectively the precursor of a GMC (Vázquez-Semadeni et al., 2006). Clouds formed by colliding WNM streams are expected to build up their molecular content over relatively long timescales (e.g., Franco and Cox, 1986; Hartmann et al., 2001; Heitsch and Hartmann, 2008; Micic et al., 2013) and should only become mostly molecular by the time when they have become strongly gravitationally bound. In the context of our model, then, the zero- or low-SFR epochs correspond to times when the cloud is still atomic-dominated, consisting of a collection of moderate-mass, slowly star-forming molecular clumps, immersed in an atomic substrate. The high-SFR stages occur when the cloud is already in a mostly molecular state, in agreement with the notion that MCs form stars rapidly, within a few Myr from their formation. The subtle additional consideration is that the clouds have much longer time spans, but they are mostly non-molecula druring most of that time and they are forming stars at very low rates. We estimate the molecular fraction of the clouds' mass as a function of time for the sample clouds of masses 10^3 to $10^6\,M_\odot$, and in all cases, by the time SF starts, 20% or more of the mass is "molecular" (gas with number density greater than $10^3\,{\rm cm}^{-3}$).

We emphasize that this result is consistent with the fact that embedded clusters generally contain a small fraction of older stars, although the majority of their stars is young (Palla and Stahler, 1999; Palla and Stahler, 2000). Indeed, in Paper I, we showed that the model correctly recovers the typical age distributions found in those clusters. Also in this regard, it should be noted that the above discussion implies that the gravitational contraction is likely to start in the mostly atomic stage. This is consistent with numerical simulations of cloud formation that also follow the atomic and molecular fractions, which suggest that molecules actually form *during* the gravitational contraction (Heitsch and Hartmann, 2008) and with the result by Glover and Clark (2012) that molecules are in fact not necessary for producing the cooling needed for gravitational collapse.

Finally, an important point is worth clarifying. The prediction that massive GMCs, with 10^5 – $10^6 M_\odot$, have extended periods of star formation lasting 20 Myr or more may seem to be in conflict with observations of nearby clouds like Orion and "dispersed" regions, such as Sco-Cen, as it is generally accepted

that cloud dispersal by the recently-formed stars occurs rapidly, within a few Myr. However, this quick dispersal refers essentially to the immediate gaseous environs of a newly formed cluster only, as it is also known that SF occurs only over a small fraction of a cloud's volume (e.g., Kirk et al., 2006), while the destruction of a large GMC may easily take over 10 Myr. For example, in the Sco-Cen region, the three main subgroups, Upper Scorpius, Upper Centaurus-Lupus, and Lower centaurus-Crux, have ages that differ by more than 10 Myr, and it has been suggested that the latest events might have been triggered by the earlier ones (e.g., Preibisch and Mamajek, 2008). Thus, SF in the parent GMC might have been going on for at least that amount of time, suggesting that the lifetime predicted by our model for massive clouds is reasonable. In the case of this complex, however, the dispersal has probably been completed already as the clusters there are already devoid of gas. However, the SF episode must have lasted at least the length of time spanned by the age difference between the clusters.

On the other hand, Kawamura et al. (2009) have suggested that GMCs with masses $\sim 10^5$–$10^6 M_\odot$ in the LMC may have lifetimes of ~ 25 Myr, with three well-defined stages in terms of their SF activity. In Paper I, we showed that our model for clouds of those masses matches within a factor of two the duration of the individual stages, while the left panel of Figure 4.3 here shows that indeed this is the time span of the star-forming stages of such clouds.

Thus, we conclude that the cloud evolution predicted by the model is in very good agreement with many known properties and evolutionary features of MCs.

4.5.2 Limitations

Our SFR model is clearly an extreme idealization of the actual process occurring in MCs, as it only considers the effects of self-gravity and photoionization on the evolution of the clouds. In particular, it neglects any support from magnetic fields, which are known to retard the gravitational collapse in comparison with the non-magnetic case (e.g., Ostriker et al., 1999), the momentum injection by the ionizing stellar feedback and by stellar outflows, and the additional feedback from supernovae and radiation pressure from the most massive stars. Since all of these processes tend to either counteract the collapse or to destroy the clouds more rapidly, it is clear that the SFR and SFE predicted by the model are upper limits to those in real clouds.

Nevertheless, it is all the more interesting that within these important limitations, our model in general predicts values of the SFR and the SFE, as well as evolutionary features of the clouds (Paper I), that generally agree well

with the corresponding observational measurements, with the largest deviations occurring when the time-averaged values of the SFR for all cloud masses are added to construct a Galaxy-wide SFR. Better agreement is obtained for the Galaxy-wide SFR when a set of Monte-Carlo realizations is considered, using values of the instantaneous SFR at random times for each cloud mass. This suggests that the final SFR burst predicted by the model for low-mass clouds may be overestimated, and indeed, the time-averaged SFR predicted for these clouds exhibits a bump at low-to-intermediate cloud masses (see Figure 4.3). This suggests that, especially for these clouds, the effects of magnetic fields and outflows may be most important. Nevertheless, the general better-than-order-of-magnitude agreement of the model with the observations suggests that self-gravity and photoionizing radiation, the processes considered by the model, are among the dominant processes controlling the evolution of the clouds and their star formation activity, with the other processes providing second-order corrections only.

On the other hand, possibly the most questionable ingredient of our model is the assumption that the density PDF remains log-normal during the entire evolution of the clouds, an assumption that appears in conflict with the well-known result, from both observations and numerical simulations, that star-forming clouds develop a power-law high-density tail in their column density distributions (e.g., Kainulainen et al., 2009; Ballesteros-Paredes et al., 2011b; Kritsuk et al., 2011; Girichidis et al., 2014). However, in Paper I, we argued that turbulence *alone* produces a log-normal, which is the *seed* of subsequent gravitational collapse, and that the power-law tail is a *result* of this contraction. Thus, the mass in this regime perhaps should not be counted as a seed for subsequent collapse since it is already undergoing collapse. In any case, to minimize the impact of this assumption, in Paper I, we calibrated the value of the $n_{\rm SF}$ by matching the predictions of the model to the output of the self-consistent numerical simulations of Vázquez-Semadeni et al. (2010). The a posteriori confirmation of this procedure is that, using the log-normal, the model was able to match a variety of observations.

Another important point to recall is that the model assumes clouds with a flattened geometry, for which the collapse timescale is significantly longer than for a spherical geometry, typically by factors of half to one order of magnitude, than the standard free-fall time (Pon et al., 2012; Toalá et al., 2012). However, this is probably a reasonable assumption since most clouds are known to consist of flattened or filamentary structures (e.g., Bally et al., 1989). This suggests that another important factor determining the SFR is the non-spherical geometry of MCs.

4.6 Summary and Conclusions

In this paper, we have presented the predictions for the dependence of the time-averaged SFR and SFE on the mass of the parent cloud from our semi-analytical model for the evolution of these quantities in gravitationally collapsing clouds, introduced in Paper I. The model assumes that the cloud forms by the collision of two streams in the WNM, which induces a transition to the cold phase, forming a cold cloud that becomes turbulent due to various instabilities (Heitsch et al., 2005; Heitsch et al., 2006; Vázquez-Semadeni et al., 2006). Soon this turbulent cloud begins to undergo global gravitational collapse. The collapse is *hierarchical* because the turbulence in the cloud produces density fluctuations that have shorter free-fall times than the cloud as a whole, and then form stars before the collapse of the largest scales is completed. The fraction of the cloud's mass involved in instantaneous SF is determined by assuming that the density PDF in the cloud is log-normal and that only the mass above a certain critical density, $n_{\rm SF}$, is instantaneously forming stars. As the cloud collapses, its mean density increases so that the PDF shifts to higher densities, causing the instantaneous SFR to systematically increase in time.

The total amount of gas converted into stars is distributed among stellar masses according to a standard IMF. The most massive stars produce ionizing radiation, which evaporates parts of the cloud through HII regions. While all this is happening, the cloud continues to accrete material from the converging flows. Thus, the evolution of the cloud is regulated by the competition between addition of fresh material by the accretion and the gas consumption by the SF itself as well as by the evaporation by the ionizing radiation from the massive stars. The model neglects the magnetic field and any injection of momentum by the stellar feedback.

In Paper I, we found that the total mass involved in the process is the main free parameter controlling the evolution of the clouds and their SFR. We quantify this parameter by the maximum dense gas mass reached by the clouds, $M_{\rm max}(n \geq 100\,{\rm cm}^{-3})$. In the present contribution, we have considered the evolution, the final values, and the time averages over the star-forming epochs of the model clouds, of the SFR and SFE predicted by the model, as a function of the maximum dense gas mass attained by the model clouds. We have found that low-to-intermediate-mass model clouds ($M \lesssim 10^4\,M_\odot$) spend their early and intermediate evolutionary stages forming stars at low rates while a strong star formation burst is produced during their final, dense stages (when they appear as a massive clump within a larger cloud), at which time massive stars appear and quickly destroy the cloud. Therefore, these clouds have a low time-averaged SFR ($\langle {\rm SFR} \rangle$) but a high final SFR. Instead, in massive clouds

($M \gtrsim 10^5\,M_\odot$), massive stars appear from early in their evolution, and thus the ionizing feedback regulates the SFR almost from the beginning. This leads to a final SFR comparable with the average. We provided fits to the mass dependence of the time-averaged SFR and SFE, given by Equations (4.9) and (4.11).

We then proceeded to investigate the relation between the SFR and the dense cloud mass, $M_{\rm dens}$, for our model clouds, mimicking the procedure followed by LLA10. These authors estimated the SFR as the mass in YSOs (in our case, stars younger than 2 Myr) divided by this time interval. Since the clouds studied by LLA10 span a wide range in SFEs, we considered our model clouds in the time interval during which they span the same SFE range. We found that the mean values of the SFR and the clouds' mass during this time interval fall within the error bars of the mean relation reported by LLA10.

We also estimated the total Galactic SFR predicted by our model, by convolving the SFR (in average or taken it at a random time after the onset of star formation) for each cloud mass with the Galactic cloud mass spectrum by Williams and McKee (1997). The average of a hundred of these random realizations is within half an order of magnitude from the observed Galactic SFR, and from the scaling relation found by GS04 for the global SFR versus galaxy mass of a sample of external galaxies.

With respect to the SFE, we find that for low-mass clouds, in the final star formation burst, the efficiency reaches final values $\sim 60\%$, although these values are not in conflict with observations because they correspond to the stage when no dense gas mass is left around a cluster, at which point it is almost impossible to observationally know the initial amount of gas mass that went into the formation of the cluster. The time-averaged SFE, on the other hand, is $\sim$1%, consistent with observational determinations performed on clusters still embedded in their parent clouds (e.g., Evans et al., 2009). For massive clouds, the SFE reaches values up to 6% (but with averages $\lesssim$5%), consistent with the upper limits of SFE ($\sim 10\%$) determined in Federrath and Klessen (2013).

We next discussed several implications of the model in the context of well established notions about MCs and their SF activity, arguing that although some of the model predictions and implications may seem to be in conflict with those notions, upon closer examination no conflict exists and instead the model offers a new insight about the evolution of MCs.

As pointed out in Section 4.5, the fact that our extremely idealized model, in which only self-gravity and ionizing feedback control the evolution of the SFR in the clouds, fits the observations typically within factors of a few, suggests that these may be the dominant controlling processes, with other processes such as magnetic support and momentum injection from massive-star winds probably

providing mainly second-order adjustments.

5

Numerical simulations: Effect of ionizing feedback in magnetized, collapsing Molecular Clouds

5.1 Abstract

We present radiation-magnetohydrodynamic simulations aimed at studying the effect of ionizing radiation from massive stars on the star formation rate (SFR) and efficiency (SFE) in turbulent, magnetized, and collapsing molecular clouds (MCs) formed by converging flows. We evolve the simulations during the time window before the first supernovae are expected to explode. The modeled MCs are of intermediate mass, with a maximum mass $M_{\rm max} \sim 3 \times 10^4\,M_\odot$. Our main findings are: (1) Dense gas with $n \gtrsim 10^4\,{\rm cm}^{-3}$ only appears once the cloud starts to collapse globally and only $\sim 1.5\,$Myr before the onset of star formation. (2) The SFR increases over time and when massive stars appear, it gradually decreases by about one order of magnitude and remains approximately constant at $\sim 3 \times 10^{-4}\,M_\odot{\rm yr}^{-1}$. The SFE is $\lesssim 10\%$. These values are consistent with observations and previous theoretical works. (3) Comparing the simulation with feedback to the one without, the dense gas mass, $M_{\rm dens} = M(n > 100\,{\rm cm}^{-3})$, does not change significantly and, although the number of sink particles is similar in both simulations, the total sink mass is significantly lower (by a factor of up to 4). (4) We reproduce the morphological characteristics observed in HII regions (champagne flows, elephant trunks, shadows, parsec-scale bow shocks, and isolated globules). (5) Ionizing radiation eventually stops the accretion (through filaments) toward the massive star-forming regions. The new over-pressured HII regions push away the dense gas, thus disrupting the more massive collapse centres. Our results provide additional support to the scenario of MCs

in global collapse, in which the SFR and SFE are regulated mainly by the feedback from massive stars, which interrupts local SF events, rather than by near-equilibrium conditions in the clouds.

5.2 Introduction

Massive stars play a key role in the evolution of galaxies. Through a combination of massive outflows, expanding HII regions, and supernova events, they shape and provide an important input of energy into the interstellar medium (ISM; e.g.˜ Mac Low and Klessen, 2004). In particular, they have a significant effect on their birthplaces through ionizing radiation and expanding HII regions, as well as supernova explosions, eroding and dispersing their parent molecular cloud (MC), directly affecting the star formation activity within the clouds (see, e.g., Vázquez-Semadeni, 2011; Krumholz et al., 2014b, for recent reviews).

It is well known that the negative feedback[1] through blister-type HII regions (or champagne flows) is efficient in eroding and dispersing MCs on timescales of few tens of Myr (Blitz and Shu, 1980; Matzner, 2002). Idealized analytical (e.g., Whitworth, 1979; Franco et al., 1994, see also Section 2.6.4) and numerical (e.g. Bodenheimer et al., 1979; Tenorio-Tagle, 1979) works have shown that blister HII regions are also able to reduce the SFE of GMCs to the low observed values of $\lesssim 10\%$ (e.g., Myers et al., 1986). However, recent radiation-magnetohydrodynamic (RMHD) simulations by Gendelev and Krumholz (2012) suggest that this eroding mechanism is not so efficient as previously thought when magnetic fields are present. Nevertheless, all these simplified models without self-gravity, with plane-parallel geometry and uniform density fields are far from the complex morphology and dynamics observed in MCs (see, e.g.,˜ André et al., 2013, for a recent review). Furthermore, the dynamics (free-fall motions or accretion) and the high-density environment of the birthplaces of massive stars could strongly attenuate the disruptive effect of the massive stars (Yorke et al., 1989; Dale et al., 2005; Peters et al., 2010). In this direction, there is growing evidence that MCs are in global collapse (see, e.g., Hartmann et al., 2001; Burkert and Hartmann, 2004; Hartmann and Burkert, 2007; Peretto et al., 2007; Vázquez-Semadeni et al., 2007; Galván-Madrid et al., 2009; Vázquez-Semadeni et al., 2009; Schneider et al., 2010; Csengeri et al., 2011; Zamora-Avilés et al., 2012; Peretto et al., 2014; Zamora-Avilés and Vázquez-Semadeni, 2014, see

[1] I.e., the suppression of star formation by erosion of the dense regions where massive stars form. We also will refer to *positive feedback* as the promotion of star formation by expanding HII regions, in the classical *collect and collapse* scenario (Elmegreen and Lada, 1977).

also Sections 1.4 and 3.2), so henceforth we will focus in this scenario of MCs without turbulent support and thus prone to a global gravitational collapse.

Simulations by Dale et al. (2005) of cluster formation in highly-structured MCs (spherical, with decaying turbulence, so that they are not supported against gravity) show that accretion of highly anisotropic dense gas onto ionizing sources strongly limits the effect of ionizing feedback. These authors also find evidence of both positive and negative feedback, with SFEs around 10%. In a parameter study with the same setup of Dale et al. (2005), Dale et al. (2012) studied clouds with masses in the range $10^4 - 10^6\,M_\odot$, finding that the effect of the ionizing feedback depends strongly on the cloud escape velocities, i.e., on their masses and sizes. It is very efficient in clouds with escape velocity $\lesssim 10\,\mathrm{km\ s^{-1}}$, but becomes inefficient in extended and massive clouds, for which the escape velocity is greater than this value (see also Dale and Bonnell, 2011).

On the other hand, in a series of papers, Vázquez-Semadeni et al. (2010) and Colín et al. (2013) have presented simulations of clouds formed by colliding flows in the warm neutral medium (WNM). They investigate the competition between the ionizing feedback and the accretion of fresh material onto the clouds, and their effect on both the SFR and SFE within. They find that feedback generally reduces the star formation efficiency to values lower than 10%, although the effect is weaker for more massive clouds, in partial agreement with Dale et al. (2012). However, these authors did not take into account the magnetic field. With the same setup, including magnetic fields but ignoring radiation feedback, Vázquez-Semadeni et al. (2011) found that an increase in the initially uniform magnetic field from 2 to $4\,\mu$G (corresponding to initially magnetically supercritical and subcritical clouds, respectively) causes a delay in the onset of star formation (by several Myr) and a decrease in the SFE (by more than one order of magnitude) (see also Banerjee et al., 2009; Federrath and Klessen, 2012; Federrath and Klessen, 2013). Finally, the geometry of the clouds formed by the collision of WNM streams is far from the spherical setups used by Dale and coworkers, and is closer to being sheet-like.

Zamora-Avilés et al. (2012) presented a semi-analytical model trying to capture the phenomenology of the simulations of MCs formed by converging flows (see also Zamora-Avilés and Vázquez-Semadeni, 2014). These authors find that ionizing feedback is able to reduce the SFE to within half an order of magnitude of the observed values in real MCs (e.g., Myers et al., 1986; Lada and Lada, 2003)

In order to complement the works mentioned in the previous two paragraphs, we present in this contribution RMHD simulations at scale of MCs with realistic properties. We pay special attention on the effect of the ionizing feedback (treated self-consistently; see Rijkhorst et al., 2006; Peters et al., 2010) and

magnetic fields in the evolution of both SFR and SFE. For this, we organize this paper as follows. In Section 5.3, we describe the numerical model. In Section 5.4 we present our results, which are then discussed in Section 5.5. Finally, the summary and conclusions are presented in 5.6.

5.3 The numerical model

We use the Eulerian adaptive mesh refinement (AMR) FLASH2.5 code (Fryxell et al., 2000) to perform three-dimensional, self gravitating, RMHD simulations, including heating and cooling processes. We use an ideal MHD treatment since the diffusive processes such as ambipolar diffusion (AD) at the simulated scales are of the order of numerical noise, and their effect on the results are negligible (Vázquez-Semadeni et al., 2011). The ideal MHD equations, presented in Section 2.8, are solved using the MHD 3-wave Bouchout solver, which preserves positive states for density and internal energy (Bouchut et al., 2007; Waagan, 2009; Bouchut et al., 2010; Waagan et al., 2011). This solver is suitable for highly supersonic astrophysical problems, such as those studied here.

In addition, we use the radiation scheme introduced by Rijkhorst et al. (2006) and improved by Peters et al. (2010). This implementation has successfully passed several tests. It accurately calculates column densities, adequately traces shadows, and is well coupled with hydrodynamics in 3D simulations of photo evaporating clumps (Rijkhorst et al., 2006). Furthermore, it accurately follows the velocity propagation for R-type (in a cosmological context; Iliev et al., 2006) and D-type (corresponding to the analytical Spitzer solution; Peters et al., 2010) ionization fronts.

5.3.1 Sink particles and refinement criterion

The Truelove criterion (Truelove et al., 1997) gives a constraint on the spatial resolution in order to prevent spurious fragmentation in AMR simulations of gravitational collapse. This criterion, which states that artificial fragmentation can be avoided if the Jeans length (Equation (2.17)) is resolved with at least four grid cells (i.e. $\lambda_{\mathbf{J}}(\rho)/\Delta x \gtrsim 4$), is normally used as a for adjusting the resolution and for sink particle formation (see, e.g., Federrath et al., 2010a).Sink particles are used to represent collapsed objects. However, we have found that the sink-particle mass distribution obtained using the Jeans criterion depends on the resolution, thus affecting the stellar population and, through the feedback, the entire evolution of the MCs. Indeed, because the masses of the sink particles

start out as a fixed fraction of the mass of the grid cell in which the sink forms, they become smaller at higher resolutions, implying a weaker feedback.

To avoid this problem, we have implemented a *constant-mass criterion* as follows. We start with a uniform base grid with initial cell size Δx_0 and initial cell density ρ_0, and therefore each cell initially contains a mass given by

$$m_0 = \rho_0 \Delta x_0^3. \tag{5.1}$$

We then refine the cell size by a factor of 2 if the density increases by a factor of 8, so that the density scales with grid cell size as $\rho \propto \Delta x^{-3}$ and so the mass of the new level of refined cells is the same as that of the previous level when it was created.

Once the maximum refinement level is reached in a given cell, no further refinement is performed and a sink particle can be formed when the density in this cell exceeds a threshold density, $\rho_{\rm thr}$. The sink is formed with the excess mass within the cell, that is, $M_{\rm Sink} = (\rho - \rho_{\rm thr})\Delta x^3$. The sink particles can then accrete mass (with $\rho > \rho_{\rm thr}$) from their surroundings (within an accretion radius of $\sim 2.5\Delta x$), increasing their mass (Federrath et al., 2010a).

5.3.2 Subgrid Star Formation prescription

Given the size of our numerical box and the maximum resolution we can achieve, the sink particles rapidly reach hundreds of solar masses via accretion, and therefore we must not treat them as single stars but rather as groups of stars. Thus, we assume a standard initial mass function (IMF) and we estimate the most massive star that the sink can host, which dominates its UV flux. The sink radiates according this flux. We use a Kroupa (2001)-type IMF, which reads

$$\chi(m) \propto m^{-\alpha_i}, \tag{5.2}$$

where α is a piecewise constant, and $dN = \chi(m)dm$ is the number of single stars in the mass interval m to $m + dm$. We normalize this IMF as

$$\int_{0.01 M_\odot}^{M_{\rm up}} m\, \chi(m) dm = M_{\rm Sink}, \tag{5.3}$$

where $M_{\rm sink}$ represents the individual mass of the sink particles. Additionally, $M_{\rm up}$ is the maximum mass that a star could reach, which is the minimum of $60\, M_\odot$ and $M_{\rm Sink}$. The lower limit is $0.01\, M_\odot$ as usual (see Section 3.3.3). We then integrate dN over bins of $1\, M_\odot$ to obtain the number of stars, ΔN, in each

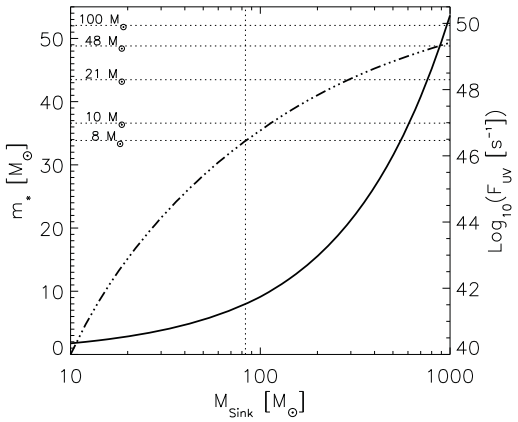

Figure 5.1: Mass of the most massive star (m_*) in a sink particle of mass $M_{\rm Sink}$ (left axis; solid line). The corresponding UV flux is plotted in the right axis (dash-dot-dot line), according to ZAMS models (see the text). The horizontal dot-lines represent the UV flux (right axis) for stars of different masses. According with our prescription, massive stars ($> 8\,M_\odot$) only appear in stellar groups with $M_{\rm Sink} > 83\,M_\odot$ (vertical dot line).

mass bin. The center of the last bin (m_*) satisfying $\Delta N \gtrsim 1$ is taken as the mass of the most massive star that the sink can host (see Figure 5.1).

Finally, from zero-age main sequence (ZAMS) models (Paxton, 2004) we assign an UV flux to the most massive star, m_*, and we assume that this star dominates the emission of ionizing photons from the sink. In Figure 5.1 we plot the mass of the most massive star (m_*) hosted in the sink and its corresponding UV flux ($F_{\rm UV}$) as a function of the sink mass $M_{\rm Sink}$. In order to save computational time, we consider that only sinks containing stars with masses $\gtrsim 8\,M_\odot$[1] (horizontal line in Figure 5.1) emit ionizing radiation, since stars with lower masses do not emit significant amounts of photoionizing photons, as shown in Figure 5.1.

5.3.3 Feedback prescription

We use an adapted version of the hybrid characteristic ray-tracing module in the FLASH code, which was implemented by Rijkhorst et al. (2006) and signifi-

[1]which correspond to $F_{\rm UV} \simeq 10^{46.5}\,{\rm s}^{-1}$ for a cluster of $\simeq 83\,M_\odot$. We allow the massive stars to radiate for 5 Myr.

cantly improved by Peters et al. (2010). The physical bases of this implementation were discussed in Section 2.6 (see also Frank and Mellema, 1994; Mellema and Lundqvist, 2002). The method may be summarized as follows. In order to calculate the flux of ionizing photons arriving at each cell, the column density (Equation A.20) is calculated by interpolation (grid mapping) along rays from the point sources to every cell. Then the ionization fractions (Equations 2.11 and 2.42) and temperature (Equation 2.9) can be computed through an iterative process, taking advantage of the analytical solution to the rate equation for the ionization fractions (Equation 2.42). Furthermore, the heating/cooling can be iterated to convergence (see Section 5.3.4), so that the only restriction on the time-step comes from the MHD module (courant condition). The magnetohydrodynamics and ionization calculations are coupled through operator splitting.

5.3.4 Heating and Cooling

We calculate the heating and cooling rates by breaking them into heating and cooling associated with ionization of hydrogen atoms and all the other sources of cooling and heating (see also Krumholz et al., 2007). For the former, the photoionization rate is (Osterbrock, 1989, see also Equation 2.40)

$$\Gamma_{\rm ph} = n_{\rm HI} \int_{\nu_{\rm T}}^{\infty} \frac{4\pi J_\nu}{h\nu} \sigma_\nu h(\nu - \nu_{\rm T}) d\nu, \tag{5.4}$$

where $n_{\rm HI}$ is the number density of atomic hydrogen, ν is the frequency and $\nu_{\rm T}$ is the ionization threshold frequency (13.6 eV), σ_ν is the absorption cross section of atomic hydrogen, and h is the Planck constant. The specific mean intensity, J_ν, of a point source/star of radius $r_{\rm star}$ and effective temperature $T_{\rm star}$ (assuming a blackbody spectrum) is given by (see also Section 2.6.2 and Equations 2.37 and 2.41; Rijkhorst et al., 2006; Peters et al., 2010)

$$J_\nu(r) = \left(\frac{r_{\rm star}}{r}\right)^2 \frac{1}{2c^2} \frac{h\nu^3}{\exp(h\nu/k_{\rm B}T_{\rm star}) - 1} \exp(-\tau_\nu(r)). \tag{5.5}$$

with $\tau_\nu(r)$ the optical depth at position r computed directly from the column density $N(r)$ (see Equations (A.20), (2.37), and (2.41); Rijkhorst et al., 2006). To counterbalance the photoionization heating rate, $\Gamma_{\rm ph}$, we consider the collisional cooling (ions-electrons), $\Lambda_{\rm col}$, which is the main mechanism for energy loss in partially ionized gas (see, e.g., Dalgarno and McCray, 1972).

On the other hand, for heating and cooling that are not directly due to ionization, we use the analytic fits by Koyama and Inutsuka (2002) for the

heating ($\Gamma_{\rm KI}$) and cooling ($\Lambda_{\rm KI}$) functions (see also Vázquez-Semadeni et al., 2007, for corrections to typographical errors),

$$\Gamma_{\rm KI} = 2.0 \times 10^{-26}\,{\rm erg\,s^{-1}} \tag{5.6}$$

$$\frac{\Lambda_{\rm KI}(T)}{\Gamma_{\rm KI}} = 10^7 \exp\frac{-1.184\times10^5}{T+1000} + 1.4\times10^{-2}\sqrt{T}\exp\frac{-92}{T}\ {\rm cm^3}, \tag{5.7}$$

which are based in the thermal and chemical calculations considered by Wolfire et al. (1995) and Koyama and Inutsuka (2000).

Thus, the net heating and cooling rates are

$$\Gamma = \Gamma_{\rm ph} + \Gamma_{\rm KI}, \qquad \Lambda = n_e n_{\rm HII}\Lambda_{\rm col} + n_{\rm HII}^2\Lambda_{\rm KI} \tag{5.8}$$

where $n_{\rm HI}$, n_e, and $n_{\rm HII}$ refers to the number density of neutral gas, electrons, and ionized gas, respectively.

5.3.5 Initial conditions

We use a setup similar to that of Vázquez-Semadeni et al. (2007, see Figure 3.1 and 5.2). The numerical periodic box, of sizes $L_x = 256\,{\rm pc}$ and $L_y = L_z = 128\,{\rm pc}$, is initially filled with warm neutral gas at uniform density of $2\,{\rm cm^{-3}}$ and constant temperature of 1450 K,[1] which corresponds to the thermal equilibrium (i.e., $\Gamma_{\rm KI} = n\Lambda_{\rm KI}$) temperature at that density. Assuming a composition of atomic hydrogen only (with a mean molecular weight $\mu = 1.27$), the gas mass in the whole box is $\sim 2.6\times10^5\,M_\odot$, whereas the mass contained in the cylinders is $\sim 4.5\times10^4\,M_\odot$.

The initial velocity field contains a random component in magnitude and direction, with a maximum amplitude of $2.1\,{\rm km\ s^{-1}}$. On top of this random field, we add two cylindrical streams, each of radius $R_{\rm inf} = 32\,{\rm pc}$ and length $L_{\rm inf} = 112\,{\rm pc}$, moving in opposite directions at a moderately supersonic velocity of $7.5\,{\rm km\ s^{-1}}$ in the x-direction (implying a Mach number of $\mathcal{M}_{\rm inf} \simeq 1.85$ with respect to the adiabatic sound speed in the WNM), as we show in Figure 5.2.

The numerical box is permeated with a uniform magnetic field of $3\,\mu$G along the x-direction. This magnitude corresponds to the mean value of the uniform component of the Galactic magnetic field (Beck, 2001). The corresponding mass-to-flux ratio is 1.8 times the critical value, so that our clouds are magnetically supercritical.

[1] This temperature implies an isothermal sound speed of $3.1\,{\rm km\ s^{-1}}$.

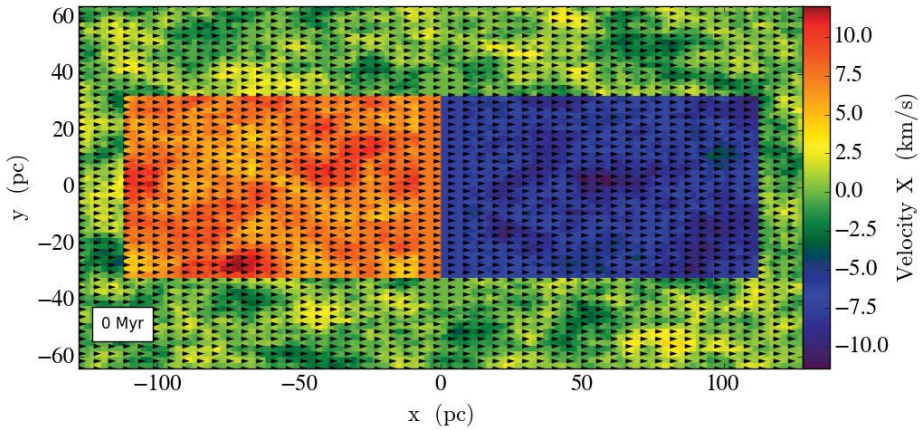

Figure 5.2: Edge-on view of the x-velocity field (in the $x-y$ plane and $z=0$) at $t=0$. Note the velocity perturbations in all the box and the over-imposed cylindrical flows colliding at $\sim 7.5\,\mathrm{km\ s^{-1}}$ in the center of the numerical box. Arrows indicate the direction of the initially uniform magnetic field along the x-axis with magnitude of $3\,\mu$G. The rest of the initial conditions correspond to uniform fields ($n=2\,\mathrm{cm^{-3}}$, $T=1450\,\mathrm{K}$).

We start with a uniform grid[1] with an initial resolution $\Delta x_0 = 2\,\mathrm{pc}$ and a cell mass of $0.5\,M_\odot$. We allow six refinement levels to achieve a maximum resolution of $\Delta x = 0.03\,\mathrm{pc}$.

With this setup and initial conditions we perform two simulations at high resolution, the first without and the second with feedback. We refer to the former as the control simulation.

5.4 Results

In general, the cloud starts as a thin cylindrical sheet that fragments and thickens as time increases, until it becomes gravitationally unstable and begins to contract globally at $t \sim 10\,\mathrm{Myr}$, as shown in Figure 5.3. Shortly after that (at $t_{\mathrm{SF}} \equiv t \sim 11.5\,\mathrm{Myr}$), star formation begins in the densest fragments (clumps), while fragments continue to fall towards the global centre of mass. The first massive star starts to radiate at $t_{\mathrm{F}} \equiv t \sim 12.7\,\mathrm{Myr}$. This behaviour is quantitatively very similar to the magnetically supercritical model (B2-AD) of

[1]Except at the plane where the flows collide, where we add two refinement levels in order to avoid effects due to low initial resolution.

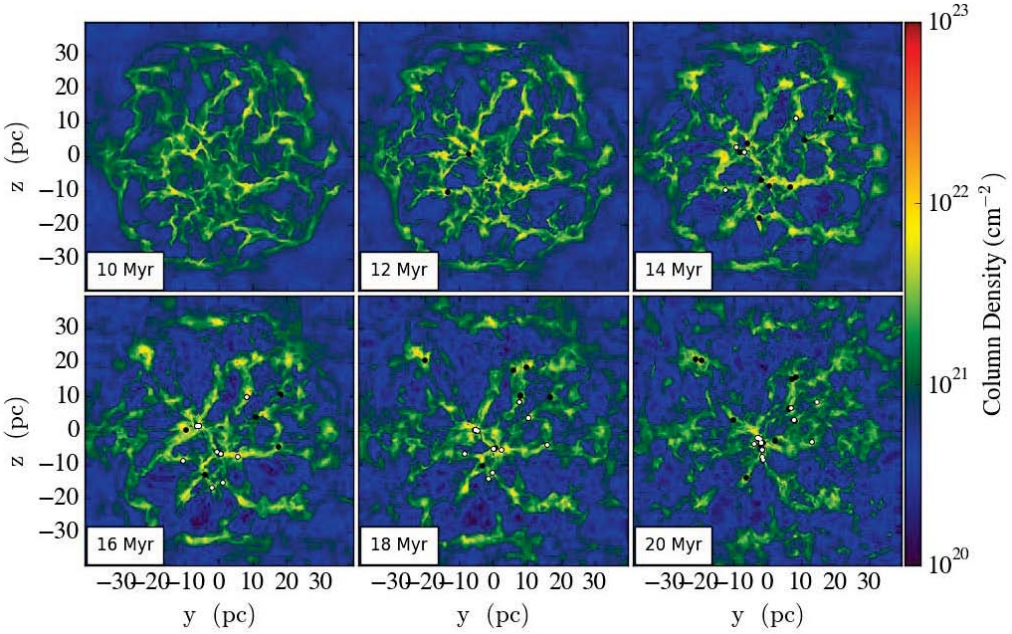

Figure 5.3: Face-on column density view of the "central cloud" in an evolutionary sequence for the simulation without feedback. After 10 Myr, the cloud starts to collapse as a whole. The dots represent the projected position of the sink particles, i.e., collapsed objects. See Figure 5.12 for a similar evolutionary sequence in the simulation with feedback.

Vázquez-Semadeni et al. (2011), and the non-magnetic LAF runs presented in Vázquez-Semadeni et al. (2010) and Colín et al. (2013).

In this section we analyse the simulations until the time when the first supernova is expected to appear, at $t_{\rm SN} \approx 18\,{\rm Myr}$, since after this time the simulation with feedback may no longer be realistic. Also, the simulations are analysed in a central cylindrical region (with a circular cross section of radius 40 pc in the $y-z$ plane and a length of 30 pc in the x-direction) in order to exclude from the statistics the external clumps produced only by turbulence. We will refer to this region as the "central cloud" (see Figures 5.3 and 5.4).

5.4.1 Global evolution

The collision of WNM streams (or *inflows*) in the center of the numerical box (see Figure 5.2) nonlinearly triggers thermal instability, forming a thin cloud of cold atomic gas (see, e.g., Hennebelle and Pérault, 1999; Koyama and Inutsuka,

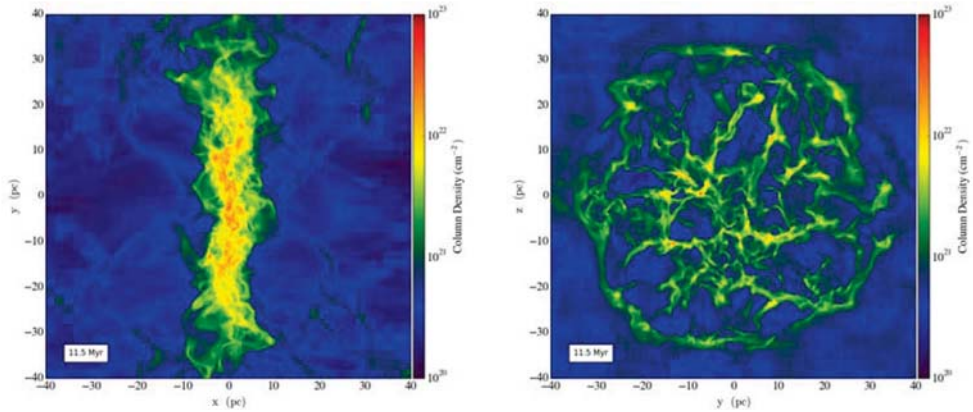

(a) Edge-on view **(b)** Face-on view

Figure 5.4: Column density of the central molecular cloud at $t = 11.5\,\mathrm{Myr}$, when the cloud begins to form stars. Note the complex filamentary structure.

2000; Walder and Folini, 2000; Koyama and Inutsuka, 2002), which at the same time becomes turbulent by the combined action of various dynamical instabilities (see, e.g., Hunter et al., 1986; Vishniac, 1994; Koyama and Inutsuka, 2002; Heitsch et al., 2005; Vázquez-Semadeni et al., 2006). Also, the thermal pressure of the dense gas is in close pressure balance with the total (thermal + ram) pressure of the surrounding WNM, which is significantly larger than the the typical thermal pressure in the ISM. Thus, the dense gas has the physical properties of GMCs[1] (Vázquez-Semadeni et al., 2006; Banerjee et al., 2009).

The cloud soon becomes self-gravitating and begins to contract gravitationally as a whole (at $t \sim 10\,\mathrm{Myr}$; see Figure 5.3). During the large-scale contraction, some local, nonlinear (i.e., large-amplitude) density enhancements produced by the initial turbulence manage to complete a collapse of their own, since their local free-fall time is shorter than the average one for the entire cloud (Vázquez-Semadeni et al., 2007; Heitsch and Hartmann, 2008; Pon et al., 2011). These local collapses involve only a small fraction of the cloud's total mass.

In Figure 5.4 we show the column density structure of the central cloud at 11.5 Myr, when it begins to form stars. Note the highly complex filamentary structure of the dens gas, which is a common feature in observed molecular clouds (see, e.g. André et al., 2013, and references therein) and in simulations (e.g, Gómez and Vázquez-Semadeni, 2014; Smith et al., 2014).

As mentioned in Section 5.3.1, the sinks continue to accrete mass after their

[1]Since we do not follow the chemistry we indistinctly will refer to the dense gas ($n > 100\,\mathrm{cm}^{-3}$) as *molecular*.

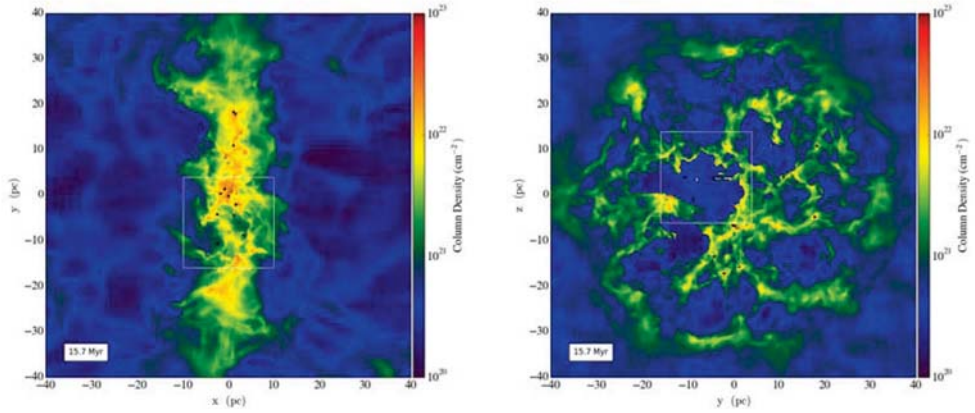

(a) Edge-on **(b)** Face-on

Figure 5.5: Column density of the "central molecular cloud" at $t = 15.7\,\mathrm{Myr}$, for the simulation with feedback. The star formation start at $t \sim 11.5\,\mathrm{Myr}$ (see Figure 5.4) and the first massive star appears roughly one Myr later at $t \sim 12.7\,\mathrm{Myr}$. The dots represent the projected position of the sink particles, being the white (with black borders) the massive enough ones to host massive stars. The sub-region delimited by the white squares is plotted in Figure 5.6.

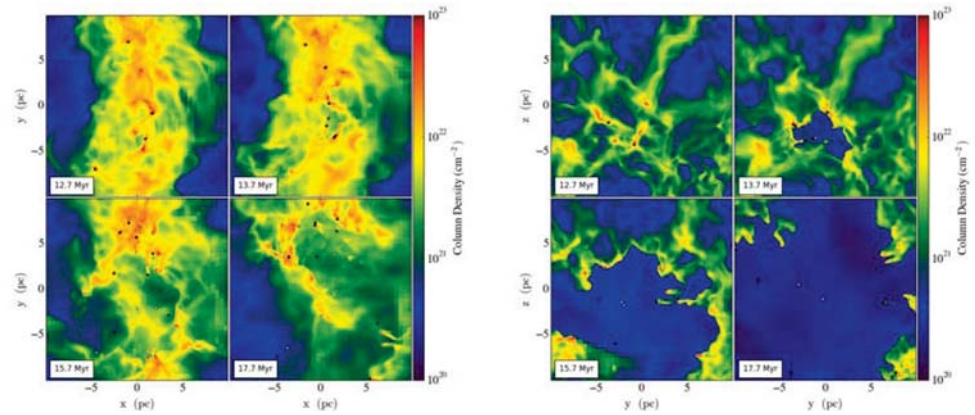

(a) Edge-on **(b)** Face-on

Figure 5.6: Column density of the regions marked with white-squares in Figure 5.5 at $t = 12.7$, 13.7, 15.7, and 17.7 Myr, for the simulation with feedback. The dots represent the projected position of the sink particles, being the white (with black borders) those containing massive stars.

formation, and eventually reach a high enough mass ($M_{\rm Sink} \gtrsim 83\,M_\odot$) that they can host a massive star. The sinks then begin to feed energy back radiate into the cloud, ionizing and dispersing it before a significant fraction of gas can fall onto new or existing sinks (see Figure 5.5).

5.4.2 The Star Formation Rate and Efficiency

The star formation process in the simulations exhibits strong intermittence in both space and time. Because the cloud is gravitationally contracting, it is globally becoming denser. Therefore, quantities such as the SFE and SFR are naturally time dependent. As usual, the instantaneous SFE is computed as

$$\mathrm{SFE}(t) = \frac{M_{\rm S}(t)}{M_{\rm C}(t) + M_{\rm S}(t)}, \tag{5.9}$$

where $M_{\rm C}$ is the dense gas mass ($n > 100\,\mathrm{cm}^{-3}$), and $M_{\rm S}$ is the total mass in stars, which we assume equal to the total mass in sinks, $M_{\rm sink,tot}$. In systems with massive stars, we should include the mass of ionized gas in the total cloud mass. However, this quantity is difficult to determine in the simulations, since it is not possible to distinguish which part of the total amount of ionized gas in the simulation was processed through an HII region. Therefore, the values of the SFE reported here are upper limits.

We take the time derivative of the total sink mass, $dM_{\rm sink,tot}(t)/dt$ (which is calculated by dividing the difference in the total sink mass in a time step by the duration of the step), as a proxy for the SFR, which accounts for both the mass collapsed onto new sinks and the mass accreted onto the existing ones. Figure 5.8 shows the time evolution of the SFR and SFE for the simulations with (dotted line) and without (solid line) feedback. In general, both the SFE and the SFR grow monotonically, although, in the simulation with feedback, the SFR decreases after the first massive star appears (at $t_{\rm F} \sim 12.7\,\mathrm{Myr}$). At $t_{\rm SN}$ ($\sim 18\,\mathrm{Myr}$), the SFE is $\sim 30\%$ in the control simulation without feedback (consistent with the supercritical model by Vázquez-Semadeni et al., 2011) while it is $\sim 10\%$ in the simulation where the feedback is included (in agreement with the LAF models by Vázquez-Semadeni et al., 2010; Colín et al., 2013).

This behavior of the SFE and SFR can be understood by looking at Figure 5.7, which shows the time evolution of the dense gas mass ($M_{\rm dens} = M(n > 100\,\mathrm{cm}^{-3})$), the total sink mass ($M_{\rm sink,tot}$), and the total cloud mass ($M_{\rm dens} + M_{\rm sink,tot}$). Interestingly, comparing the simulation with feedback to the one without, the dense gas mass (Figure 5.7a) does not change significantly and, although the number of sink particles is similar in both simulations, the total sink mass is significantly lower (by a factor of up to 4) because the ionization

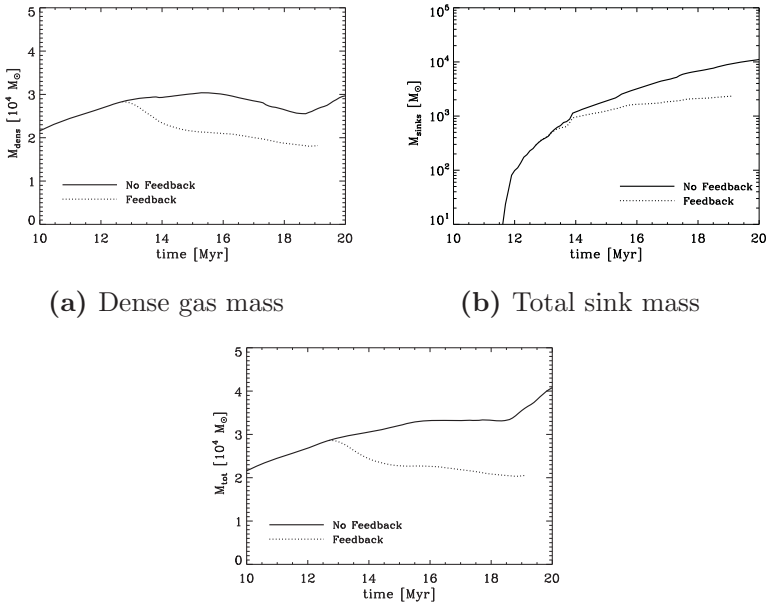

(a) Dense gas mass **(b)** Total sink mass

(c) Total cloud mass

Figure 5.7: Evolution of (a) the dense gas mass ($M_{\rm dens}$; $n > 100\,{\rm cm}^{-3}$), (b) total sink mass ($M_{\rm sink,tot}$), and (c) total mass, $M_{\rm dens} + M_{\rm sink,tot}$, for the simulations with (dotted lines) and without (solid lines) feedback. Note that the vertical axis is logarithmic in panel (b).

suppresses mass accretion onto the massive sinks ($M_{\rm Sink} \gtrsim 100\,M_\odot$) that host massive stars (see Figure 5.7b). Thus, for instance, at $t = 18.3\,{\rm Myr}$, the sink masses fall in the ranges $0.7 < M_{\rm Sink} < 194\,M_\odot$, and $0.4 < M_{\rm Sink} < 2026\,M_\odot$ for the simulations with and without feedback, respectively. This is in agreement with the results by Vázquez-Semadeni et al. (2010), where a similar effect was reported in simulations not including the magnetic field and using a crude prescription for the radiative transfer. Those authors interpreted the result as implying that the stellar feedback energy is injected mostly in the gas that is on its final stages of collapse, and directed towards the newly-formed stellar objects, diverting a large fraction of it back to the warm ionized phase.

5.4.3 Evolution of the Dense Gas

An important clue for understanding the effect of ionizing feedback on the star formation process is provided by the evolution of the dense gas. The dense phase

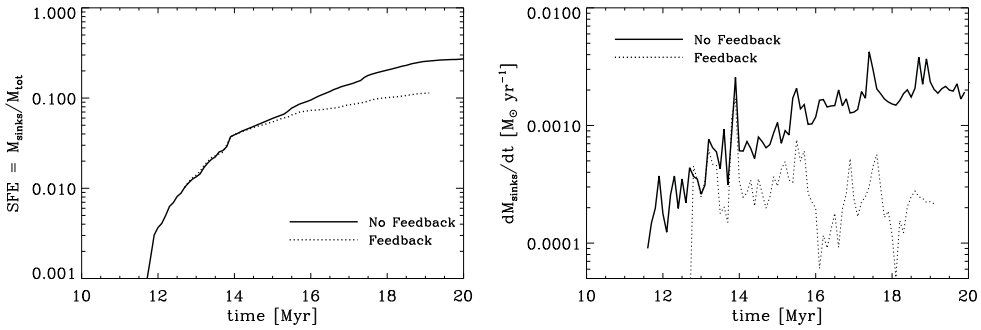

(a) Star Formation Efficiency **(b)** Star Formation Rate

Figure 5.8: Evolution of the Star Formation Rate and Efficiency for the simulations with (dotted lines) and without (solid lines) feedback. The SFE reduces to 10% in the simulation with feedback. The irregular lines tracing the SFR (b) reflect the temporal intermittency of the star formation process.

appears at $t \sim 1.5\,\mathrm{Myr}$, but with physical conditions corresponding to those of the CNM. Gas with densities (in the range $100 - 10^6\,\mathrm{cm}^{-3}$) representative of MCs only appears at $t \approx 11\,\mathrm{Myr}$, as a consequence of gravitational contraction.

5.4.3.1 Density PDF

In Figure 5.9a we show the density probability density function (PDF) at $t =$ 12.7, 13.7, 15.7, and 17.7 Myr. At all these times, gravity dominates and star formation has already begun. The density distribution exhibits power laws, in agreement with what is observed in evolved star-forming regions (see, e.g., Kainulainen et al., 2009). Interestingly, we have found that these distributions (specially at $n > 100\,\mathrm{cm}^{-3}$) are insensitive to the presence of radiation fields, and therefore can only be the result of self-gravity, as suggested by Schneider et al., 2014. Furthermore, in some cases we have a double power law in the high density part (see the panels at $t = 13.7$ and 15.7 Myr in Figure 5.9a), as observed for instance in Cep OB3, W43, RoseSe, Mon R2.[1]

To study the effect of the feedback on the dense gas, in Figure 5.9b we show mass histograms as a function of density at $t = 12.7$, 13.7, 15.7, and 17.7 Myr for both the simulations with and without feedback. It is noteworthy that the feedback affects mainly the low density gas ($n < 100\,\mathrm{cm}^{-3}$, from the envelopes of denser gas) and the very dense gas ($n > 10^4\,\mathrm{cm}^{-3}$, from the sites of massive star formation), leaving the distribution of the gas around $10^3\,\mathrm{cm}^{-3}$ unaltered.

[1] Schneider, et al., in prep., private communication.

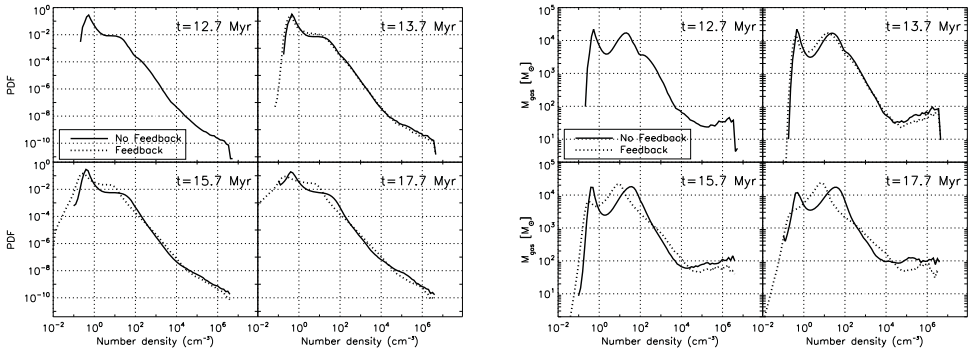

(a) Density PDFs **(b)** Mass histograms

Figure 5.9: Density PDFs and mass histograms for the central cloud at t = 12.7, 13.7, 15.7, and 17.7 Myr. The solid and dotted lines refer to the simulation without and without feedback, respectively.

5.4.3.2 Mass

In figure 5.10 we show the evolution of the gas mass at various densities. From this figure, we can see that gas at density $n \gtrsim 100\,\mathrm{cm}^{-3}$ (black lines), appears early at $t \sim 1.5\,\mathrm{Myr}$, whereas gas with density $\gtrsim 10^3\,\mathrm{cm}^{-3}$ is formed at $t \sim 3\,\mathrm{Myr}$ (purple lines). However, gas with density $\gtrsim 10^4\,\mathrm{cm}^{-3}$ only appears several Myr later (at $t \sim 10\,\mathrm{Myr}$), when the self-gravity of the dense gas is already important. At this stage, the gas is rapidly compressed to reach higher densities and eventually begins forming stars at $t \sim 11.5\,\mathrm{Myr}$. This suggests that the very dense gas is predominantly a product of gravitational contraction, and explains why the SFR is strongly related to the content of gas with density $\gtrsim 10^4\,\mathrm{cm}^{-3}$ (see, e.g., Gao and Solomon, 2004; Evans et al., 2009; Zamora-Avilés and Vázquez-Semadeni, 2014).

5.5 Discussion

5.5.1 Comparison with the analytical model

Here we compare our results with the non-magnetic semi-analytic model presented in Chapters 3 and 4 (see Zamora-Avilés et al., 2012; Zamora-Avilés and Vázquez-Semadeni, 2014). Figure 5.11 shows the evolution of the SFR and SFE in the simulations discussed in this work (black lines) and in the semi-analytical model (blue lines) for a cloud with the same radius (32 pc), initial

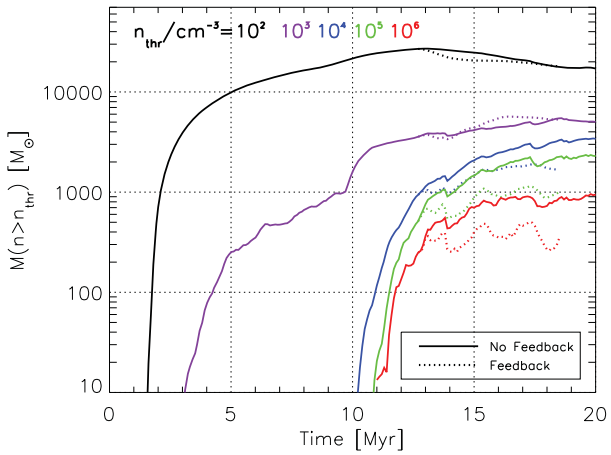

Figure 5.10: Evolution of the dense gas mass ($n > n_{\rm thr}$) for the central cloud, with $n_{\rm thr} = 10^2$ (black lines), 10^3 (purple lines), 10^4 (blue lines), 10^5 (green lines, and $10^6\,{\rm cm}^{-3}$ (red lines). The solid and dotted lines refer to the simulation without and without feedback, respectively.

density ($2\,{\rm cm}^{-3}$), and ending time for the inflow. Therefore the model and simulations also have the same maximum mass ($M_{\rm max} \sim 3 \times 10^4\,M_\odot$). We added to this figure curves from a simulation at lower resolution (red lines; with maximum resolution of $\Delta x = 0.25\,{\rm pc}$).

Although the two sets of simulations at the two resolutions show some moderate systematic differences between each other, they differ only by factors of a few in both the SFR and SFE. Comparing the high-resolution simulation with the semi-analytical model we observe differences of up to one order of magnitude in both the SFE and SFR throughout the time evolution. In particular, it is intriguing that the SFR in the simulations is nearly stationary in time, not showing a significant systematic increase, contrary to the behavior of the model and of the non-magnetic simulations of Vázquez-Semadeni et al. (2010) (see Figure 3.4). This suggest that the presence of the magnetic field reduces the acceleration of the SF process. However, control simulations without the magnetic field, to be presented elsewhere, are necessary to confirm this result, in order to perform the comparison with a consistent set of simulations. However, there are points of agreement; for instance, the lifetime and the terminal SFE are consistent in both the model and the simulations (comparing with the low resolution simulation; see Figure 5.11). This study will be continued in future work.

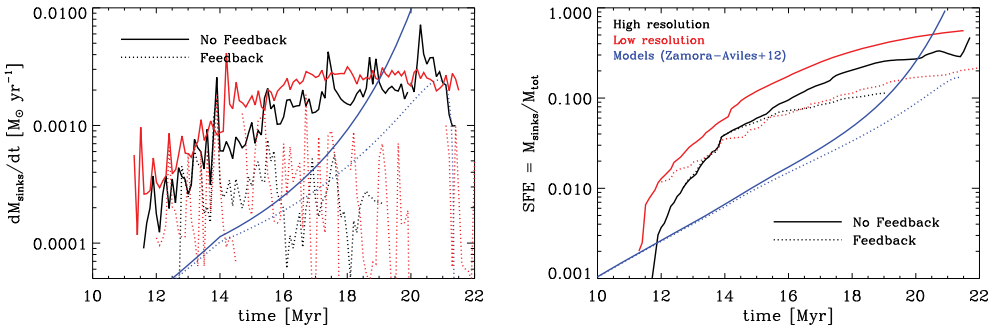

(a) Star Formation Rate **(b)** Star Formation Efficiency

Figure 5.11: Evolution of the SFR and SFE for simulations at high (black lines; see Figure 5.8) and low (red lines) resolution, and the prediction of the model (blue lines) presented in Chapter 3 (see Zamora-Avilés et al., 2012).

5.5.2 Cloud disruption

The low resolution simulation indicates that the molecular cloud ends its evolution at $t \approx 22\,\mathrm{Myr}$ (in the sense that itsstar formation terminates, since, although not all of its gas is ionized, the cloud is ultimately dispersed in small low-mass cloudlets). Note that this lifetime is similar to that predicted by the semi-analytical model (Chapters 3 and 4; see Figure 5.11) for a cloud of the same mass. However, the first supernova is expected to explode at $t \sim 18\,\mathrm{Myr}$, which could accelerate the destruction or dispersion of the cloud (see Figure 5.12).

5.5.3 Limitations

Our *constant-mass* refinement criterion does not fulfill the Truelove criterion (Truelove et al., 1997) for preventing spurious fragmentation, since the resolution does not scale linearly with the Jeans length. We thus expect some artificial fragmentation (sink formation). However, this should not significantly affect our results, as we are not measuring the core mass function nor the stellar IMF, but rather only the SFR and SFE, which do not depend on the details of the fragmentation. Another important caveat is that, although our constant-mass refinement criterion guarantees robustness of the sink mass spectrum at variable resolution, the effect of the feedback on the gas does still depend on resolution, since, at higher resolutions, the sinks form in higher-density environments that are more difficult to disperse. Further investigation on the dependence of the

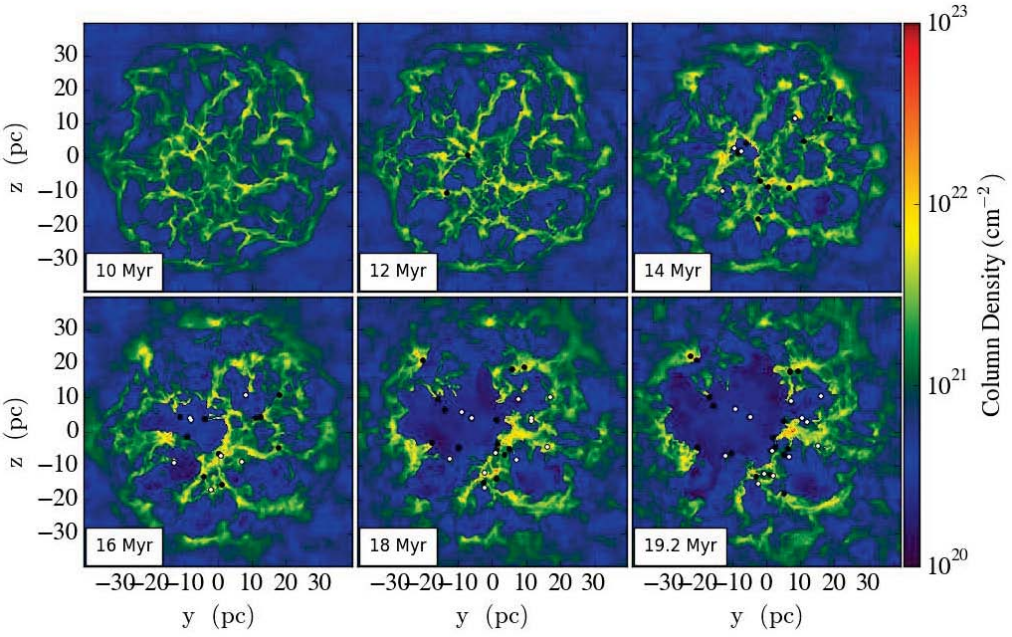

Figure 5.12: Face-on column density view of the "central cloud" in an evolutionary sequence for the simulation with feedback. After $\sim 18\,\mathrm{Myr}$, the first supernova event is expected to appear. The dots represent the projected position of the sink particles. See also Figure 5.3.

global evolution, including the SFR and SFE, on resolution needs to be performed.

Regarding physical processes, one of the most notable caveats is the omission of supernova explosions, which can help in dispersing the cloud and reducing both the SFR and the SFE. We expect the first supernova event at $t \sim 18\,\mathrm{Myr}$, so the simulation may become unrealistic at this time.

5.6 Summary and Conclusions

In this paper, we have presented radiation-MHD simulations to study the evolution of MCs formed by diffuse converging flows in the presence of magnetic fields and massive-star ionization feedback. In particular we quantitatively studied the effect of ionizing feedback on the SFR and SFE, as well as its interplay with the magnetic field.

Analyzing two simulations, with and without feedback, during a time window of 5 Myr since the time when the first massive star appears (i.e., before

the first expected supernova event), we first study the evolution of the SFR and SFE, noting that, in the simulation with feedback we obtain a maximum SFE of $\sim 10\%$, in agreement with previous numerical work, semi-analytical models and observations toward massive star forming regions. The SFR first increases and then decreases, as predicted by the theoretical model of Zamora-Avilés et al. (2012).

We next studied the density PDF of both simulations, and found that dense gas with $n \gtrsim 10^4\,\mathrm{cm}^{-3}$ appears only until $t \sim 10\,\mathrm{Myr}$, once the cloud starts to collapse globally implying that it is formed by gravitational contraction, not turbulence (in which case it should be present from the start as soon as the turbulence becomes stationary). After the onset of massive star formation (at $t \sim 12.7\,\mathrm{Myr}$), we found no significant difference in the high-density part of the PDFs, which sometimes exhibit a double power law. Comparing the simulation with feedback to the one without, the dense gas mass, $M_{\mathrm{dens}} = M(n > 100\,\mathrm{cm}^{-3})$, does not change significantly and, although the number of sink particles is similar in both simulations, the total sink mass is significantly lower (by a factor of up to 4) because the ionization suppresses mass accretion onto the massive sinks that host massive stars.

We then compared the predictions from the numerical simulations with the analytic model from Chapters 3 and 4, and we found that the SFR and SFE are more stationary in the simulations than in the model and in non-magnetic simulations. The origin of this distinction will be investigated in future work.

6

Summary and outlook

Throughout this thesis, we have studied the star formation rate (SFR) and efficiency (SFE) in *evolving* molecular clouds (MCs), from an analytical and a numerical point of view. Our models account for the evolution of MCs in the solar neighbourhood, from their formation to their eventual destruction by ionizing feedback from massive stars. In this scenario, MCs are formed by two colliding warm neutral medium (WNM) flows, which nonlinearly trigger thermal instability, producing a cold, dense atomic cloud. The inflow increases the cloud's mass and drives turbulence within it, until it eventually begins to undergo gravitational collapse. The overdensities generated by the turbulence collapse faster than whole cloud, starting to form stars through local collapses while the cloud undergoes global collapse. Thus, the SFR is instantaneously controlled by evaporation of the cloud material by massive-star ionization feedback.

6.1 The semi-analytical model

Within this general scenario, we presented in Chapter 3 an idealized semi-analytical model, in which we assume that the instantaneous SFR is given by the ratio of the mass above a certain density threshold to the free-fall time corresponding to this density. The entire density PDF evolves by shifting towards higher densities as the cloud collapses. The instantaneous number of massive stars is computed assuming a Kroupa initial mass function. These stars feed back on the cloud through ionizing radiation, eroding it. *It is important to note that our model is currently the only model for the SFR of an evolutionary nature in the literature.* We found:

- The main controlling parameter of the clouds evolution turns out to be

the maximum cloud mass, $M_{\rm max}$ (assuming they all start from cold neutral medium conditions and with a flattened geometry).

- The star formation rate (SFR) and the star formation efficiency (SFR) are time-dependent, and in general, these should be addressed as evolving quantities, together with the quantities defining them (such as cloud mass and mass in stars).

- The SFR (and cloud density) increase in time, until the cloud is destroyed by stellar feedback. Thus, the SFR (and SFE) is correlated with the density in agreement with observations (e.g., Louvet et al., 2014).

In addition, by analyzing two models, of low- ($M_{\rm max} \sim 2000\,M_{\odot}$) and high-mass ($M_{\rm max} \sim 10^5\,M_{\odot}$), and comparing them with observations, we found that:

- The low-mass cloud compares well with the physical conditions of massive star-forming regions, such as the typical OMC-1 in the Orion Molecular Cloud.

- Our low-mass model evolves in the KennicuttSchmidt diagram, first passing through the locus of typical low- to intermediate-mass star-forming clouds, and then moving towards the locus of high-mass star-forming ones over the course of ~ 10 Myr. Like observed individual clouds, our modelled cloud lies higher in the diagram than spatially-averaged (galaxy-scale or kpc-scale) regions, implying that large-scale averages include much non-star-forming gas. The scatter in this diagram should be understood as different evolutionary states.

- The stellar age histograms for the low-mass cloud a few Myr before its destruction agree very well with those observed in the ρ-Oph stellar association (e.g., Palla and Stahler, 2000), whose parent cloud has a similar mass. This is a consequence of the fact that the SFR of the clouds increases with time.

- The evolution of the high-mass cloud adheres very well to the evolutionary scenario recently inferred by Kawamura et al. (2009) for GMCs in the Large Magellanic Cloud.

In Chapter 4 we extended this semi-analytical model by performing a parameter study, varying the cloud mass. We found that:

- Low-mass clouds ($M_{\rm max} \lesssim 10^4\ M_\odot$) spend most of their evolution at low SFRs, but end their lives with a mini-burst. This is consistent with the notion that the formation of massive stars is most likely the result of a violent process like this star-forming mini-bursts (Hans Zinnecker, private communication). The clouds reach a peak SFR $\sim 10^4\ M_\odot{\rm Myr}^{-1}$, although their time-averaged SFR is only $\langle{\rm SFR}\rangle \sim 10^2\ M_\odot{\rm Myr}^{-1}$. The corresponding efficiencies are ${\rm SFE}_{\rm final} \lesssim 60\%$ and $\langle{\rm SFE}\rangle \lesssim 1\%$.

- For more massive clouds ($M_{\rm max} \gtrsim 10^5\ M_\odot$), the SFR first increases and then reaches a plateau, because the clouds are influenced by the stellar feedback since earlier in their evolution, regulating their SFR.

- As a function of cloud mass, the $\langle{\rm SFR}\rangle$ and $\langle{\rm SFE}\rangle$ are well represented by the fits

$$\langle{\rm SFR}\rangle \approx 100 \left(1 + \frac{M_{\rm max}}{1.4 \times 10^5\ M_\odot}\right)^{1.68} M_\odot\,{\rm Myr}^{-1}, \tag{6.1}$$

  and

$$\langle{\rm SFE}\rangle \approx 0.03 \left(\frac{M_{\rm max}}{2.5 \times 10^5\ M_\odot}\right)^{0.33}. \tag{6.2}$$

  These fits are potentially usable in cosmological simulations to provide a sub-grid prescriptions of star formation.

- The SFR of our model clouds follows closely the SFR-dense gas mass relation recently found by Lada et al. (2010), during the epoch when their instantaneous SFEs are comparable to those of the clouds considered by those authors.

- Collectively, a Monte Carlo integration of the model-predicted SFR(M) over a Galactic giant molecular cloud mass spectrum yields values for the total Galactic SFR that are consistent with the relation obtained by Gao and Solomon (2004).

In general, this semi-analytical model fits several observational features within a precision of half an order of magnitude. In future work, we will extend the model to include the effect of magnetic fields, other feedback mechanisms (such as winds, supernova explosions, and radiation pressure), and a self-consistent modeling of the evolution of the density PDF. We expect that these improvements will allow us to obtain second-order corrections and thus an even more precise account of the observations.

6.2 The numerical simulations

In Chapter 5 we performed numerical simulations with a similar setup and physical process content as those of the semi-analytical model, but also including magnetic fields and a detailed treatment of radiative transport. We use *sink particles* representing collapsed objects (stars or groups of stars). Assuming a standard *initial mass function* in each sink (Kroupa, 2001), we calculate the most massive star that the sink can host. When this mass exceeds $8\,M_{\odot}$, the corresponding sink begins to ionize the surrounding medium.

Using the FLASH code we performed two simulations, with and without feedback, finding that:

- The simulation with feedback qualitatively reproduces the morphological characteristics observed in HII regions.
- Dense gas with $n \gtrsim 10^4\,\mathrm{cm}^{-3}$ is formed by gravitational contraction, not turbulence. Shortly after ($\sim 1.5\,\mathrm{Myr}$) this dense gas appears, star formation begins.
- Early collapses produce enough massive stars to eventually disperse the cloud long before all of its mass is consumed.
- Ionizing radiation eventually stops both the gas accretion toward the massive star-forming regions and the star formation in these regions.
- The SFR increases over time until when massive stars appears, at which point it gradually decreases by about one order of magnitude and remains approximately constant at $\sim 3 \times 10^{-4}\,M_{\odot}\mathrm{yr}^{-1}$. This implies that the ionizing feedback regulates the SFR.
- The final SFE is $\lesssim 10\%$. These values are consistent with observations (e.g., Lada and Lada, 2003) and previous theoretical works (e.g., Vázquez-Semadeni et al., 2010; Colín et al., 2013).

The star formation is an intermittent process in space and time and only a small fraction of the gas ($\lesssim 10\%$) is involved in it. This ssolves the Zuckerman & Palmer conundrum (see Section 1.4).

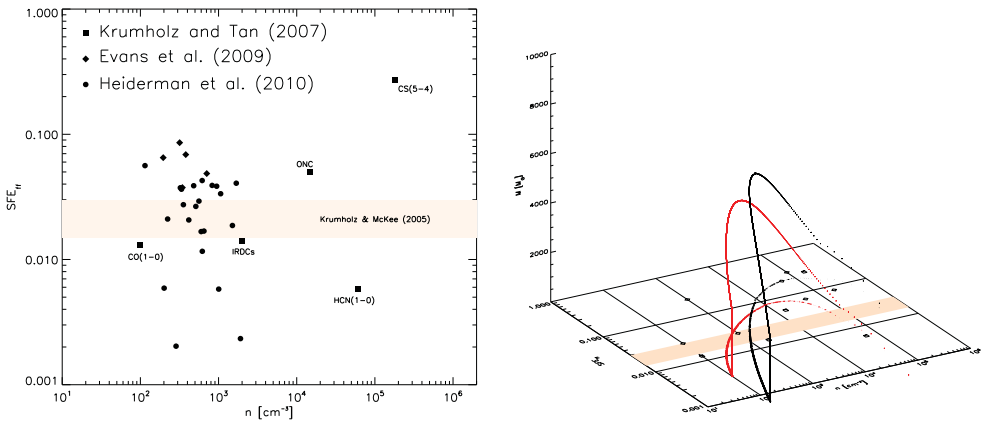

(a) $\mathrm{SFE_{ff}}$ from observations **(b)** $\mathrm{SFE_{ff}}$ from our models

Figure 6.1: (a) Star formation efficiency per free-fall time ($\mathrm{SFE_{ff}}$) for objects with number density n. We plot the theoretical prediction by Krumholz and McKee (2005, horizontal band), observational data by Krumholz and Tan (2007, filled squares, which are based on Galactic averages), and observational data of individual clouds by Evans et al. (2009, filled diamonds) and Heiderman et al. (2010, filled circles). (b) Same $\mathrm{SFE_{ff}} - n$ diagram, but including the cloud mass in a third dimension. We overplot the evolutionary tracks for two of our models with arbitrary maximum masses (red and black lines), which are also projected in the $\mathrm{SFE_{ff}} - n$ plane.

6.3 Conclusion: A revised star formation paradigm

Going back to the title of this thesis, *Reformulation of the concept of Star Formation Efficiency in evolving Molecular Clouds*, we claim that the results presented throughout this thesis imply a change in the paradigm of the star formation theory.

In the traditional turbulent *cloud-support* models[1] (represented by Krumholz and McKee, 2005; Hennebelle and Chabrier, 2011; Padoan and Nordlund, 2011; Federrath and Klessen, 2012; Federrath and Klessen, 2013), clouds are assumed to be in a quasi-equilibrium state, with support against self-gravity being provided by turbulence and possibly magnetic fields, thus preventing global collapse and maintaining a low global SFRs and SFEs. In this scenario the clouds are

[1]This classification comes from Molinari et al. (2014), who also refer to models of clouds in global gravitational collapse as *cloud-collapse* models.

time-stationary, since global cloud evolution is not considered. These models predict a *star formation efficiency per free-fall time*,[1] $\mathrm{SFE_{ff}}$, of $\sim 1-10\%$ (see Figure 6.1), in claimed qualitative agreement with observations (e.g., Krumholz and Tan, 2007), although the claim has been disputed (e.g., Elmegreen, 2007). In addition, this scenario is unable to explain many features observed in MCs (see, e.g., Hartmann and Burkert, 2007; Galván-Madrid et al., 2009; Schneider et al., 2010; Csengeri et al., 2011; Louvet et al., 2014; Peretto et al., 2014).

According to the picture presented here (a *cloud-collapse* model), since our model continuosly evolves, the $\mathrm{SFE_{ff}}$ only makes sense as an average at galactic scale (cloud ensemble) or over the cloud lifetime. This is evident when we plot observations of individual clouds in the $\mathrm{SFE_{ff}} - n$ diagram as shown in Figure 6.1a. We note a significant dispersion, which can be explained because clouds may be in different evolutionary stages, as our semi-analytical model suggests (see Figure 6.1b).

Finally, from the results of both the semi-analytic model and numerical simulations, we conclude that the scenario of MCs in global collapse, with the SFR and SFE regulated by massive-star feedback, is not only entirely feasible and in agreement with observations of MCs, but also necessary to explain key observational features that *cloud-support* models are unable to reproduce.

[1] I.e., the SFE achieved on the free-fall time scale

Appendix **A**

A.1 Radiation Fields

The *specific intensity* (or *brightness*) $I_\nu(\mathbf{x}, \hat{\mathbf{k}}, \nu, t)$ of radiation or set of rays at position $\mathbf{x}$, traveling in direction $\hat{\mathbf{k}}$, with frequency ν, at time t is defined such that the amount of energy, dE_ν, transported by radiation of frequencies $(\nu, \nu + d\nu)$ across an element of area dA with unit normal $\hat{\mathbf{n}}$ into a solid angle $d\Omega$ around $\hat{\mathbf{k}}$ in a time interval dt is given by

$$dE_\nu = I_\nu(\mathbf{x}, \hat{\mathbf{k}}, \nu, t) \cos\theta \, dA \, d\Omega \, d\nu \, dt, \tag{A.1}$$

where θ is the angle between the direction of the beam and the normal to the surface (i.e. $\cos\theta = \hat{\mathbf{k}} \cdot \hat{\mathbf{n}}$). Thus defined, the specific intensity provides a complete description of the radiation field from a macroscopic point of view.

We define the total intensity,

$$I = \int_0^\infty I_\nu \, d\nu, \tag{A.2}$$

where $I_\nu \equiv I_\nu(\mathbf{x}, \hat{\mathbf{k}}, \nu, t)$. Also, the *specific radiative flux*, F_ν, is the amount of energy passing through a small element of area within an interval frequency interval per unit time in all directions, i.e.,

$$F_\nu = \oint I_\nu \cos\theta \, d\Omega. \tag{A.3}$$

Now, to determine how much energy is contained within the radiation field, we consider the *specific energy density*, u_ν, defined as the energy per unit volume per unit frequency range. To determine this quantity it is convenient to consider first the energy density per unit solid angle $u_\nu(\Omega)$, given by $dE_\nu = u_\nu(\Omega) \, dV \, d\Omega \, d\nu$, where dV is a volume element. We consider a cylinder around a ray of length cdt and circular area dA. Since the volume of the cylinder is $cdtdA$, then

$$dE_\nu = u_\nu(\Omega)\, dA\, c\, dt\, d\Omega\, d\nu, \tag{A.4}$$

The radiation travels at velocity c, so that in time dt all the radiation in the cylinder will pass out of it, and then

$$dE_\nu = I_\nu\, dA\, d\Omega\, dt\, d\nu. \tag{A.5}$$

Equating the above two expressions yields

$$u_\nu(\Omega) = \frac{I_\nu}{c}. \tag{A.6}$$

And integrating over all solid angles we have

$$u_\nu = \oint u_\nu(\Omega)\, d\Omega = \frac{1}{c} \oint I_\nu d\Omega, \tag{A.7}$$

or

$$u_\nu = \frac{4\pi}{c} J_\nu, \tag{A.8}$$

where we have defined the *mean specific intensity*, J_ν, as the average of the specific intensity over all solid angle, that is

$$J_\nu = \frac{1}{4\pi} \oint I_\nu\, d\Omega. \tag{A.9}$$

We obtain the total energy density, whose units are $[u] = \mathrm{erg\,cm^{-3}}$, simply integrating u_ν over all frequencies

$$u = \frac{4\pi}{c} J, \tag{A.10}$$

J being the *mean total intensity*,

$$J = \frac{1}{4\pi} \oint I\, d\Omega. \tag{A.11}$$

For further discussion see, e.g., Rybicki and Lightman (1979), Osterbrock (1989), and Shu (1991)

A.2 Radiative Transport

We now describe the effect of a radiation field that propagates through some matter. We consider a medium containing absorbers with number density$n$ and an effective cross section σ_ν. The energy absorbed out of a ray crossing this medium is

$$dI_\nu \, dA \, d\Omega \, dt \, d\nu \;=\; -\, I_\nu \, (n \, \sigma_\nu \, dA \, dr) \, d\Omega \, dt \, d\nu, \tag{A.12}$$

where dr is a path length element. Thus,

$$dI_\nu \;=\; -\, n \, \sigma_\nu \, I_\nu \, dr, \tag{A.13}$$

which is the *transfer equation* (without emissivity and time independent). Following Osterbrock (1989), the absorption cross section of atomic hydrogen is

$$\sigma_\nu \;=\; \sigma_\mathrm{T} \Big[\beta \Big(\frac{\nu}{\nu_\mathrm{T}} \Big)^{-s} + (1-\beta) \Big(\frac{\nu}{\nu_\mathrm{T}} \Big)^{-s-1} \Big] \tag{A.14}$$

for $\nu > \nu_\mathrm{T} = 13.6$ eV (the ionization threshold frequency), with the remaining parameters $\beta = 1.34$, $\sigma_\mathrm{T} = 6.3 \times 10^{-18}$ cm^2, and $s = 2.99$.

The absorption coefficient is defined as

$$\alpha_\nu \;=\; n \, \sigma_\nu = \rho \, \kappa_\nu, \tag{A.15}$$

where κ_ν (in cm^2 g^{-1}) is called the mass absorption coefficient or the opacity coefficient. Thus, we can directly integrate Equation (A.13) to obtain

$$I_\nu(r) \;=\; I_\nu(0) \, \exp(-\tau_\nu(r)), \tag{A.16}$$

where we have defined the optical depth as

$$\tau_\nu \;=\; \int_0^r \alpha_\nu(r') \, dr'. \tag{A.17}$$

Material with $\tau_\nu < 1$ is called *optically thin*, and material with $\tau_\nu > 1$ is called *optically thick*. If α_ν is spatially constant, using Equation (A.15) we can rewrite the optical depth as

$$\tau_\nu \;=\; \sigma_\nu \, N(r), \tag{A.18}$$

where the column density along some ray is given by

$$N(r) \;=\; \int_0^r n(r') \, dr'. \tag{A.19}$$

Since σ_ν is independent of temperature (see, e.g., Osterbrock, 1989), we can use Equations (2.11) and (A.18) to calculate the optical depth for a gas containing atomic hydrogen as

$$N(r) \;=\; \int_0^r n_{\rm H}(r')\, x_{\rm HI}(r')\, dr', \tag{A.20}$$

with $n_{\rm H}$ the total number density and $x_{\rm HI}$ the fraction of atomic hydrogen. Once the optical depth is calculated, we can use it to find the ionization, heating and cooling rates, and calculate the ionization state and temperature of the gas caused by radiation sources within the gas, as we will see next.

References

Allen, A. and F. H. Shu (2000). "A Toy Model of Giant Molecular Clouds". In: *ApJ* 536, pp. 368–379. DOI: 10.1086/308912 (cit. on p. 8).

Andersson, B.-G. and P. G. Wannier (1993). "Warm neutral halos around molecular clouds. VI - Physical and chemical modeling". In: *ApJ* 402, pp. 585–592. DOI: 10.1086/172161 (cit. on p. 6).

André, P., J. Di Francesco, D. Ward-Thompson, S.-i. Inutsuka, R. E. Pudritz, and J. Pineda (2013). "From Filamentary Networks to Dense Cores in Molecular Clouds: Toward a New Paradigm for Star Formation". In: *ArXiv e-prints* (cit. on pp. 86, 95).

André, P. et al. (2010). "From filamentary clouds to prestellar cores to the stellar IMF: Initial highlights from the Herschel Gould Belt Survey". In: *A&A* 518, L102, p. L102. DOI: 10.1051/0004-6361/201014666 (cit. on p. 78).

Audit, E. and P. Hennebelle (2005). "Thermal condensation in a turbulent atomic hydrogen flow". In: *A&A* 433, pp. 1–13. DOI: 10.1051/0004-6361:20041474 (cit. on pp. 10, 64, 65).

Ballesteros-Paredes, J., P. D'Alessio, and L. Hartmann (2012). "On the structure of molecular clouds". In: *MNRAS* 427, pp. 2562–2571. DOI: 10.1111/j.1365-2966.2012.22130.x (cit. on p. 4).

Ballesteros-Paredes, J. and L. Hartmann (2007). "Remarks on Rapid vs. Slow Star Formation". In: *RevMexAA* 43, pp. 123–136 (cit. on p. 53).

Ballesteros-Paredes, J., L. W. Hartmann, E. Vázquez-Semadeni, F. Heitsch, and M. A. Zamora-Avilés (2011a). "Gravity or turbulence? Velocity dispersion-size relation". In: *MNRAS* 411, pp. 65–70. DOI: 10.1111/j.1365-2966.2010.17657.x (cit. on pp. 4, 43, 56).

Ballesteros-Paredes, J., L. Hartmann, and E. Vázquez-Semadeni (1999a). "Turbulent Flow-driven Molecular Cloud Formation: A Solution to the Post-T Tauri Problem?" In: *ApJ* 527, pp. 285–297. DOI: 10.1086/308076 (cit. on pp. 6, 7, 10).

Ballesteros-Paredes, J., R. S. Klessen, M.-M. Mac Low, and E. Vazquez-Semadeni (2007). "Molecular Cloud Turbulence and Star Formation". In: *Protostars and Planets V*, pp. 63–80 (cit. on p. 61).

Ballesteros-Paredes, J., E. Vázquez-Semadeni, A. Gazol, L. W. Hartmann, F. Heitsch, and P. Colín (2011b). "Gravity or turbulence? - II. Evolving column density probability distribution functions in molecular clouds". In: *MNRAS* 416, pp. 1436–1442. DOI: 10.1111/j.1365-2966.2011.19141.x (cit. on pp. 42, 56, 81).

Ballesteros-Paredes, J., E. Vázquez-Semadeni, and J. Scalo (1999b). "Clouds as Turbulent Density Fluctuations: Implications for Pressure Confinement and Spectral Line Data Interpretation". In: *ApJ* 515, pp. 286–303. DOI: 10.1086/307007 (cit. on p. 9).

Bally, J., W. D. Langer, A. A. Stark, and R. W. Wilson (1987). "Filamentary structure in the Orion molecular cloud". In: *ApJL* 312, pp. L45–L49. DOI: 10.1086/184817 (cit. on p. 49).

Bally, J., A. A. Stark, R. W. Wilson, and W. D. Langer (1989). "The structure and kinematics of molecular clouds from large scale mapping of millimeter lines". In: *The Physics and Chemistry of Interstellar Molecular Clouds - mm and Sub-mm Observations in Astrophysics*. Ed. by G. Winnewisser and J. T. Armstrong. Vol. 331. Lecture Notes in Physics, Berlin Springer Verlag, pp. 81–86. DOI: 10.1007/BFb0119451 (cit. on p. 81).

Banerjee, R., E. Vázquez-Semadeni, P. Hennebelle, and R. S. Klessen (2009). "Clump morphology and evolution in MHD simulations of molecular cloud formation". In: *MNRAS* 398, pp. 1082–1092. DOI: 10.1111/j.1365-2966.2009.15115.x (cit. on pp. 56, 65, 87, 95).

Bate, M. R., I. A. Bonnell, and N. M. Price (1995). "Modelling accretion in protobinary systems". In: *MNRAS* 277, pp. 362–376 (cit. on p. 44).

Beck, R. (2001). "Galactic and Extragalactic Magnetic Fields". In: 99, pp. 243–260 (cit. on p. 92).

Bigiel, F., A. Leroy, and F. Walter (2011). "Scaling Relations between Gas and Star Formation in Nearby Galaxies". In: *Computational Star Formation*. Ed. by J. Alves, B. G. Elmegreen, J. M. Girart, and V. Trimble. Vol. 270. IAU Symposium, pp. 327–334. DOI: 10.1017/S1743921311000597 (cit. on p. 53).

Bigiel, F., A. Leroy, F. Walter, E. Brinks, W. J. G. de Blok, B. Madore, and M. D. Thornley (2008). "The Star Formation Law in Nearby Galaxies on Sub-Kpc Scales". In: *AJ* 136, pp. 2846–2871. DOI: 10.1088/0004-6256/136/6/2846 (cit. on pp. 51, 52).

Biskamp, D. (2003). *Magnetohydrodynamic Turbulence* (cit. on p. 29).

Blitz, L. (1993). "Giant molecular clouds". In: *Protostars and Planets III*. Ed. by E. H. Levy and J. I. Lunine, pp. 125–161 (cit. on p. 6).

Blitz, L., Y. Fukui, A. Kawamura, A. Leroy, N. Mizuno, and E. Rosolowsky (2007). "Giant Molecular Clouds in Local Group Galaxies". In: *Protostars and Planets V*, pp. 81–96 (cit. on p. 6).

Blitz, L. and F. H. Shu (1980). "The origin and lifetime of giant molecular cloud complexes". In: *ApJ* 238, pp. 148–157. DOI: 10.1086/157968 (cit. on p. 86).

Blitz, L. and P. Thaddeus (1980). "Giant molecular complexes and OB associations. I - The Rosette molecular complex". In: *ApJ* 241, pp. 676–696. DOI: 10.1086/158379 (cit. on p. 6).

Bodenheimer, P., G. Tenorio-Tagle, and H. W. Yorke (1979). "The gas dynamics of H II regions. II - Two-dimensional axisymmetric calculations". In: *ApJ* 233, pp. 85–96. DOI: 10.1086/157368 (cit. on pp. 12, 86).

Bouchut, F., C. Klingenberg, and K. Waagan (2007). "A multiwave approximate Riemann solver for ideal MHD based on relaxation. I: theoretical framework". In: *Numerische Mathematik* 108, pp. 7–42. DOI: 10.1007/s00211-007-0108-8 (cit. on p. 88).

— (2010). "A multiwave approximate Riemann solver for ideal MHD based on relaxation II: numerical implementation with 3 and 5 waves". In: *Numerische Mathematik* 115, pp. 647–679. DOI: 10.1007/s00211-010-0289-4 (cit. on p. 88).

Bourke, T. L., P. C. Myers, G. Robinson, and A. R. Hyland (2001). "New OH Zeeman Measurements of Magnetic Field Strengths in Molecular Clouds". In: *ApJ* 554, pp. 916–932. DOI: 10.1086/321405 (cit. on p. 57).

Bronfman, L., R. S. Cohen, H. Alvarez, J. May, and P. Thaddeus (1988). "A CO survey of the southern Milky Way - The mean radial distribution of molecular clouds within the solar circle". In: *ApJ* 324, pp. 248–266. DOI: 10.1086/165892 (cit. on p. 3).

Brunt, C. M. (2003). "Large-Scale Turbulence in Molecular Clouds". In: *ApJ* 583, pp. 280–295. DOI: 10.1086/345294 (cit. on pp. 6, 78).

Brunt, C. M., M. H. Heyer, and M.-M. Mac Low (2009). "Turbulent driving scales in molecular clouds". In: *A&A* 504, pp. 883–890. DOI: 10.1051/0004-6361/200911797 (cit. on p. 78).

Burkert, A. and L. Hartmann (2004). "Collapse and Fragmentation in Finite Sheets". In: *ApJ* 616, pp. 288–300. DOI: 10.1086/424895 (cit. on pp. 7, 36, 66, 69, 86).

Chomiuk, L. and M. S. Povich (2011). "Toward a Unification of Star Formation Rate Determinations in the Milky Way and Other Galaxies". In: *AJ* 142, 197, p. 197. DOI: 10.1088/0004-6256/142/6/197 (cit. on pp. 61, 76).

Ciolek, G. E. and S. Basu (2001). "On the Timescale for the Formation of Protostellar Cores in Magnetic Interstellar Clouds". In: *ApJ* 547, pp. 272–279. DOI: 10.1086/318348 (cit. on p. 10).

Clark, P. C. and I. A. Bonnell (2004). "Star formation in transient molecular clouds". In: *MNRAS* 347, pp. L36–L40. DOI: 10.1111/j.1365-2966.2004.07377.x (cit. on p. 8).

— (2005). "The onset of collapse in turbulently supported molecular clouds". In: *MNRAS* 361, pp. 2–16. DOI: 10.1111/j.1365-2966.2005.09105.x (cit. on p. 36).

Clemens, D. P., D. B. Sanders, and N. Z. Scoville (1988). "The large-scale distribution of molecular gas in the first Galactic quadrant". In: *ApJ* 327, pp. 139–155. DOI: 10.1086/166177 (cit. on p. 3).

Colín, P., E. Vázquez-Semadeni, and G. C. Gómez (2013). "Molecular cloud evolution - V. Cloud destruction by stellar feedback". In: *MNRAS* 435, pp. 1701–1714. DOI: 10.1093/mnras/stt1409 (cit. on pp. 11, 13, 87, 94, 97, 108).

Cox, D. P. (1983). "Self-regulating star formation - The rate limit set by ionizing photons". In: *ApJL* 265, p. L61. DOI: 10.1086/183958 (cit. on p. 7).

Cox, D. P. and W. H. Tucker (1969). "Ionization Equilibrium and Radiative Cooling of a Low-Density Plasma". In: *ApJ* 157, p. 1157. DOI: 10.1086/150144 (cit. on p. 27).

Crutcher, R. M. (1999). "Magnetic Fields in Molecular Clouds: Observations Confront Theory". In: *ApJ* 520, pp. 706–713. DOI: 10.1086/307483 (cit. on pp. 5, 10).

Crutcher, R. M., B. Wandelt, C. Heiles, E. Falgarone, and T. H. Troland (2010). "Magnetic Fields in Interstellar Clouds from Zeeman Observations: Inference of Total Field Strengths by Bayesian Analysis". In: *ApJ* 725, pp. 466–479. DOI: 10.1088/0004-637X/725/1/466 (cit. on p. 5).

Crutcher, R., C. Heiles, and T. Troland (2003). "Observations of Interstellar Magnetic Fields". In: *Turbulence and Magnetic Fields in Astrophysics*. Ed. by E. Falgarone and T. Passot. Vol. 614. Lecture Notes in Physics, Berlin Springer Verlag, pp. 155–181 (cit. on p. 57).

Csengeri, T., S. Bontemps, N. Schneider, F. Motte, and S. Dib (2011). "Gas dynamics in massive dense cores in Cygnus-X". In: *A&A* 527, A135, A135. DOI: 10.1051/0004-6361/201014984 (cit. on pp. 7, 36, 78, 86, 110).

Dale, J. E. and I. Bonnell (2011). "Ionizing feedback from massive stars in massive clusters: fake bubbles and untriggered star formation". In: *MNRAS* 414, pp. 321–328. DOI: 10.1111/j.1365-2966.2011.18392.x (cit. on pp. 12, 87).

Dale, J. E., I. A. Bonnell, C. J. Clarke, and M. R. Bate (2005). "Photoionizing feedback in star cluster formation". In: *MNRAS* 358, pp. 291–304. DOI: 10.1111/j.1365-2966.2005.08806.x (cit. on pp. 13, 86, 87).

Dale, J. E., B. Ercolano, and I. A. Bonnell (2012). "Ionizing feedback from massive stars in massive clusters - II. Disruption of bound clusters by photoionization". In: *MNRAS* 424, pp. 377–392. DOI: 10.1111/j.1365-2966.2012.21205.x (cit. on pp. 11, 87).

— (2013). "Ionizing feedback from massive stars in massive clusters - III. Disruption of partially unbound clouds". In: *MNRAS* 430, pp. 234–246. DOI: 10.1093/mnras/sts592 (cit. on p. 11).

Dalgarno, A. and R. A. McCray (1972). "Heating and Ionization of HI Regions". In: *ARA&A* 10, p. 375. DOI: 10.1146/annurev.aa.10.090172.002111 (cit. on pp. 18, 20, 91).

Dib, S. and A. Burkert (2005). "On the Origin of the H I Holes in the Interstellar Medium of Dwarf Irregular Galaxies". In: *ApJ* 630, pp. 238–249. DOI: 10.1086/431785 (cit. on pp. 42, 56).

Dib, S., L. Piau, S. Mohanty, and J. Braine (2011). "Star formation efficiency as a function of metallicity: from star clusters to galaxies". In: *MNRAS* 415, pp. 3439–3454. DOI: 10.1111/j.1365-2966.2011.18966.x (cit. on pp. 36, 44, 66).

Draine, B. T. (1990). "Evolution of interstellar dust". In: *The Evolution of the Interstellar Medium*. Ed. by L. Blitz. Vol. 12. Astronomical Society of the Pacific Conference Series, pp. 193–205 (cit. on p. 4).

Duley, W. W. and D. A. Williams (1981). "The infrared spectrum of interstellar dust - Surface functional groups on carbon". In: *MNRAS* 196, pp. 269–274 (cit. on p. 4).

Dyson, J. E. and D. A. Williams (1980). *Physics of the interstellar medium* (cit. on p. 15).

Elmegreen, B. G. (1983). "Quiescent formation of bound galactic clusters". In: *MNRAS* 203, pp. 1011–1020 (cit. on p. 7).

— (1993). "Star Formation at Compressed Interfaces in Turbulent Self-gravitating Clouds". In: *ApJL* 419, p. L29. DOI: 10.1086/187129 (cit. on p. 9).

— (2002). "Star Formation from Galaxies to Globules". In: *ApJ* 577, pp. 206–220. DOI: 10.1086/342177 (cit. on pp. 44, 66).

— (2007). "On the Rapid Collapse and Evolution of Molecular Clouds". In: *ApJ* 668, pp. 1064–1082. DOI: 10.1086/521327 (cit. on p. 110).

Elmegreen, B. G. and C. J. Lada (1977). "Sequential formation of subgroups in OB associations". In: *ApJ* 214, pp. 725–741. DOI: 10.1086/155302 (cit. on p. 86).

Elmegreen, B. G. and J. Scalo (2004a). "Interstellar Turbulence I: Observations and Processes". In: *ARA&A* 42, pp. 211–273. DOI: 10.1146/annurev.astro.41.011802.094859 (cit. on pp. 1, 29).

— (2004b). "Interstellar Turbulence I: Observations and Processes". In: *ARA&A* 42, pp. 211–273. DOI: 10.1146/annurev.astro.41.011802.094859 (cit. on p. 61).

Evans II, N. J. (1999). "Physical Conditions in Regions of Star Formation". In: *ARA&A* 37, pp. 311–362. DOI: 10.1146/annurev.astro.37.1.311 (cit. on p. 78).

Evans II, N. J. et al. (2009). "The Spitzer c2d Legacy Results: Star-Formation Rates and Efficiencies; Evolution and Lifetimes". In: *ApJS* 181, 321, pp. 321–350. DOI: 10.1088/0067-0049/181/2/321 (cit. on pp. 51–53, 59, 63, 73, 75, 76, 83, 100, 109).

Fall, S. M., M. R. Krumholz, and C. D. Matzner (2010). "Stellar Feedback in Molecular Clouds and its Influence on the Mass Function of Young Star Clusters". In: *ApJL* 710, pp. L142–L146. DOI: 10.1088/2041-8205/710/2/L142 (cit. on p. 72).

Fatuzzo, M. and F. C. Adams (2002). "Enhancement of Ambipolar Diffusion Rates through Field Fluctuations". In: *ApJ* 570, pp. 210–221. DOI: 10.1086/339502 (cit. on p. 10).

Federrath, C., R. Banerjee, P. C. Clark, and R. S. Klessen (2010a). "Modeling Collapse and Accretion in Turbulent Gas Clouds: Implementation and Comparison of Sink Particles in AMR and SPH". In: *ApJ* 713, pp. 269–290. DOI: 10.1088/0004-637X/713/1/269 (cit. on pp. 44, 88, 89).

Federrath, C. and R. S. Klessen (2012). "The Star Formation Rate of Turbulent Magnetized Clouds: Comparing Theory, Simulations, and Observations". In: *ApJ* 761, 156, p. 156. DOI: 10.1088/0004-637X/761/2/156 (cit. on pp. 9, 62, 65, 87, 109).

— (2013). "On the Star Formation Efficiency of Turbulent Magnetized Clouds". In: *ApJ* 763, 51, p. 51. DOI: 10.1088/0004-637X/763/1/51 (cit. on pp. 9, 72, 83, 87, 109).

Federrath, C., R. S. Klessen, and W. Schmidt (2008). "The Density Probability Distribution in Compressible Isothermal Turbulence: Solenoidal versus Compressive Forcing". In: *ApJL* 688, pp. L79–L82. DOI: 10.1086/595280 (cit. on pp. 42, 65).

Federrath, C., J. Roman-Duval, R. S. Klessen, W. Schmidt, and M.-M. Mac Low (2010b). "Comparing the statistics of interstellar turbulence in simulations and observations. Solenoidal versus compressive turbulence forcing". In: *A&A* 512, A81, A81. DOI: 10.1051/0004-6361/200912437 (cit. on p. 65).

Ferrière, K. M. (2001). "The interstellar environment of our galaxy". In: *Reviews of Modern Physics* 73, pp. 1031–1066. DOI: 10.1103/RevModPhys.73.1031 (cit. on pp. 2, 3, 61).

Field, G. B. (1970). "Theory of Star Formation, Introductory Report". In: *Memoires of the Societe Royale des Sciences de Liege* 19, p. 29 (cit. on p. 7).

Field, G. B. and W. C. Saslaw (1965). "A Statistical Model of the Formation of Stars and Interstellar Clouds." In: *ApJ* 142, p. 568. DOI: 10.1086/148318 (cit. on p. 12).

Folini, D. and R. Walder (2006). "Supersonic turbulence in shock-bound interaction zones. I. Symmetric settings". In: *A& A* 459, pp. 1–19. DOI: 10.1051/0004-6361:20053898 (cit. on p. 40).

Franco, J. and D. P. Cox (1986). "Molecular clouds in galaxies with different Z - Fragmentation of diffuse clouds driven by opacity". In: *PASP* 98, pp. 1076–1079. DOI: 10.1086/131876 (cit. on p. 79).

Franco, J., S. N. Shore, and G. Tenorio-Tagle (1994). "On the massive star-forming capacity of molecular clouds". In: *ApJ* 436, pp. 795–799. DOI: 10.1086/174955 (cit. on pp. 7, 12, 13, 39, 67, 86).

Frank, A. and G. Mellema (1994). "A radiation-gasdynamical method for numerical simulations of ionized nebulae: Radiation-gasdynamics of PNe I". In: *A& A* 289, pp. 937–945 (cit. on pp. 25, 91).

Frisch, U. (1995). *Turbulence. The legacy of A. N. Kolmogorov.* (Cit. on p. 29).

Fryxell, B. et al. (2000). "FLASH: An Adaptive Mesh Hydrodynamics Code for Modeling Astrophysical Thermonuclear Flashes". In: *ApJS* 131, pp. 273–334. DOI: 10.1086/317361 (cit. on p. 88).

Galván-Madrid, R., E. Keto, Q. Zhang, S. Kurtz, L. F. Rodríguez, and P. T. P. Ho (2009). "Formation of an O-Star Cluster by Hierarchical Accretion in G20.08-0.14 N". In: *ApJ* 706, pp. 1036–1053. DOI: 10.1088/0004-637X/706/2/1036 (cit. on pp. 7, 36, 62, 86, 110).

Galván-Madrid, R., E. Vázquez-Semadeni, J. Kim, and J. Ballesteros-Paredes (2007). "Statistics of Core Lifetimes in Numerical Simulations of Turbulent, Magnetically Supercritical Molecular Clouds". In: *ApJ* 670, pp. 480–488. DOI: 10.1086/522081 (cit. on p. 46).

Gammie, C. F. and E. C. Ostriker (1996). "Can Nonlinear Hydromagnetic Waves Support a Self-gravitating Cloud?" In: *ApJ* 466, p. 814. DOI: 10.1086/177556 (cit. on p. 9).

Gao, Y. and P. M. Solomon (2004). "The Star Formation Rate and Dense Molecular Gas in Galaxies". In: *ApJ* 606, pp. 271–290. DOI: 10.1086/382999 (cit. on pp. 63, 73, 100, 107).

Gendelev, L. and M. R. Krumholz (2012). "Evolution of Blister-type H II Regions in a Magnetized Medium". In: *ApJ* 745, 158, p. 158. DOI: 10.1088/0004-637X/745/2/158 (cit. on p. 86).

Girichidis, P., L. Konstandin, A. P. Whitworth, and R. S. Klessen (2014). "On the Evolution of the Density Probability Density Function in Strongly Self-gravitating Systems". In: *ApJ* 781, 91, p. 91. DOI: 10.1088/0004-637X/781/2/91 (cit. on p. 81).

Glover, S. C. O. and P. C. Clark (2012). "Is molecular gas necessary for star formation?" In: *MNRAS* 421, pp. 9–19. DOI: 10.1111/j.1365-2966.2011.19648.x (cit. on p. 79).

Goldbaum, N. J., M. R. Krumholz, C. D. Matzner, and C. F. McKee (2011). "The Global Evolution of Giant Molecular Clouds. II. The Role of Accretion". In: *ApJ* 738, 101, p. 101. DOI: 10.1088/0004-637X/738/1/101 (cit. on pp. 35, 63).

Goldreich, P. and J. Kwan (1974). "Molecular Clouds". In: *ApJ* 189, pp. 441–454. DOI: 10.1086/152821 (cit. on pp. 7, 11, 61).

Goldsmith, P. F. (1987). "Molecular clouds - an overview". In: *Interstellar Processes*. Ed. by D. J. Hollenbach and H. A. Thronson Jr. Vol. 134. Astrophysics and Space Science Library, pp. 51–70 (cit. on p. 4).

— (2001). "Molecular Depletion and Thermal Balance in Dark Cloud Cores". In: *ApJ* 557, pp. 736–746. DOI: 10.1086/322255 (cit. on p. 20).

Gómez, G. C. and E. Vázquez-Semadeni (2014). "Filaments in Simulations of Molecular Cloud Formation". In: *ApJ* 791, 124, p. 124. DOI: 10.1088/0004-637X/791/2/124 (cit. on p. 95).

Goodman, A. A., P. J. Benson, G. A. Fuller, and P. C. Myers (1993). "Dense cores in dark clouds. VIII - Velocity gradients". In: *ApJ* 406, pp. 528–547. DOI: 10.1086/172465 (cit. on p. 78).

Hartmann, L. (2003). "Comments on Inferences of Star Formation Histories and Birth Lines". In: *ApJ* 585, pp. 398–405. DOI: 10.1086/345933 (cit. on pp. 53, 55).

Hartmann, L., J. Ballesteros-Paredes, and E. A. Bergin (2001). "Rapid Formation of Molecular Clouds and Stars in the Solar Neighborhood". In: *ApJ* 562, pp. 852–868. DOI: 10.1086/323863 (cit. on pp. 7, 36, 79, 86).

Hartmann, L., J. Ballesteros-Paredes, and F. Heitsch (2012). "Rapid star formation and global gravitational collapse". In: *MNRAS* 420, pp. 1457–1461. DOI: 10.1111/j.1365-2966.2011.20131.x (cit. on p. 56).

Hartmann, L. and A. Burkert (2007). "On the Structure of the Orion A Cloud and the Formation of the Orion Nebula Cluster". In: *ApJ* 654, pp. 988–997. DOI: 10.1086/509321 (cit. on pp. 7, 10, 36, 62, 86, 110).

Heiderman, A., N. J. Evans II, L. E. Allen, T. Huard, and M. Heyer (2010). "The Star Formation Rate and Gas Surface Density Relation in the Milky Way: Implications for Extragalactic Studies". In: *ApJ* 723, 1019, pp. 1019–1037. DOI: 10.1088/0004-637X/723/2/1019 (cit. on pp. 51–53, 59, 73, 109).

Heiles, C. (2001). "The McKee/Ostriker Model: Paradigm?" In: *Tetons 4: Galactic Structure, Stars and the Interstellar Medium*. Ed. by C. E. Woodward, M. D. Bicay, and J. M. Shull. Vol. 231. Astronomical Society of the Pacific Conference Series, p. 294 (cit. on p. 3).

Heiles, C. and T. H. Troland (2003). "The Millennium Arecibo 21 Centimeter Absorption-Line Survey. II. Properties of the Warm and Cold Neutral Media". In: *ApJ* 586, pp. 1067–1093. DOI: 10.1086/367828 (cit. on pp. 44, 56, 64).

Heitsch, F., A. Burkert, L. W. Hartmann, A. D. Slyz, and J. E. G. Devriendt (2005). "Formation of Structure in Molecular Clouds: A Case Study". In: *ApJL* 633, pp. L113–L116. DOI: 10.1086/498413 (cit. on pp. 10, 11, 37, 42, 82, 95).

Heitsch, F. and L. Hartmann (2008). "Rapid Molecular Cloud and Star Formation: Mechanisms and Movies". In: *ApJ* 689, pp. 290–301. DOI: 10.1086/592491 (cit. on pp. 10, 36, 37, 41, 46, 53, 62, 79, 95).

Heitsch, F., M.-M. Mac Low, and R. S. Klessen (2001). "Gravitational Collapse in Turbulent Molecular Clouds. II. Magnetohydrodynamical Turbulence". In: *ApJ* 547, pp. 280–291. DOI: 10.1086/318335 (cit. on p. 9).

Heitsch, F., A. D. Slyz, J. E. G. Devriendt, L. W. Hartmann, and A. Burkert (2006). "The Birth of Molecular Clouds: Formation of Atomic Precursors in Colliding Flows". In: *ApJ* 648, pp. 1052–1065. DOI: 10.1086/505931 (cit. on pp. 42, 64, 82).

Heitsch, F., E. G. Zweibel, A. D. Slyz, and J. E. G. Devriendt (2004). "Turbulent Ambipolar Diffusion: Numerical Studies in Two Dimensions". In: *ApJ* 603, pp. 165–179. DOI: 10.1086/381428 (cit. on p. 10).

Hennebelle, P., R. Banerjee, E. Vázquez-Semadeni, R. S. Klessen, and E. Audit (2008). "From the warm magnetized atomic medium to molecular clouds". In: *A& A* 486, pp. L43–L46. DOI: 10.1051/0004-6361:200810165 (cit. on p. 64).

Hennebelle, P. and G. Chabrier (2011). "Analytical Star Formation Rate from Gravoturbulent Fragmentation". In: *ApJL* 743, L29, p. L29. DOI: 10.1088/2041-8205/743/2/L29 (cit. on pp. 9, 61, 65, 66, 77, 109).

Hennebelle, P. and M. Pérault (1999). "Dynamical condensation in a thermally bistable flow. Application to interstellar cirrus". In: *A& A* 351, pp. 309–322 (cit. on pp. 7, 36, 94).

Heyer, M. H. and C. Brunt (2007). "Turbulence in the molecular interstellar medium". In: *IAU Symposium*. Ed. by B. G. Elmegreen and J. Palous. Vol. 237. IAU Symposium, pp. 9–16. DOI: 10.1017/S1743921307001159 (cit. on p. 10).

Heyer, M., C. Krawczyk, J. Duval, and J. M. Jackson (2009). "Re-Examining Larson's Scaling Relationships in Galactic Molecular Clouds". In: *ApJ* 699, pp. 1092–1103. DOI: 10.1088/0004-637X/699/2/1092 (cit. on pp. 4, 56).

Hollenbach, D. and E. E. Salpeter (1971). "Surface Recombination of Hydrogen Molecules". In: *ApJ* 163, p. 155. DOI: 10.1086/150754 (cit. on p. 5).

Hunter Jr., J. H., M. T. Sandford II, R. W. Whitaker, and R. I. Klein (1986). "Star formation in colliding gas flows". In: *ApJ* 305, pp. 309–332. DOI: 10.1086/164249 (cit. on pp. 37, 95).

Iliev, I. T. et al. (2006). "Cosmological radiative transfer codes comparison project - I. The static density field tests". In: *MNRAS* 371, pp. 1057–1086. DOI: 10.1111/j.1365-2966.2006.10775.x (cit. on p. 88).

Kainulainen, J., H. Beuther, T. Henning, and R. Plume (2009). "Probing the evolution of molecular cloud structure. From quiescence to birth". In: *A&A* 508, pp. L35–L38. DOI: 10.1051/0004-6361/200913605 (cit. on pp. 42, 56, 81, 99).

Katz, N., I. Furman, O. Biham, V. Pirronello, and G. Vidali (1999). "Molecular Hydrogen Formation on Astrophysically Relevant Surfaces". In: *ApJ* 522, pp. 305–312. DOI: 10.1086/307642 (cit. on p. 5).

Kawamura, A. et al. (2009). "The Second Survey of the Molecular Clouds in the Large Magellanic Cloud by NANTEN. II. Star Formation". In: *ApJS* 184, pp. 1–17. DOI: 10.1088/0067-0049/184/1/1 (cit. on pp. 6, 48–50, 59, 63, 80, 106).

Kegel, W. H. (1989). "The interpretation of correlations between observed parameters of molecular clouds". In: *A&A* 225, pp. 517–520 (cit. on p. 4).

Kennicutt Jr., R. C. (1998). "The Global Schmidt Law in Star-forming Galaxies". In: *ApJ* 498, pp. 541–552. DOI: 10.1086/305588 (cit. on pp. 51, 52).

Kirk, H., D. Johnstone, and J. Di Francesco (2006). "The Large- and Small-Scale Structures of Dust in the Star-forming Perseus Molecular Cloud". In: *ApJ* 646, pp. 1009–1023. DOI: 10.1086/503193 (cit. on p. 80).

Kirk, H., P. C. Myers, T. L. Bourke, R. A. Gutermuth, A. Hedden, and G. W. Wilson (2013). "Filamentary Accretion Flows in the Embedded Serpens South Protocluster". In: *ApJ* 766, 115, p. 115. DOI: 10.1088/0004-637X/766/2/115 (cit. on pp. 62, 78).

Kirk, H., J. E. Pineda, D. Johnstone, and A. Goodman (2010). "The Dynamics of Dense Cores in the Perseus Molecular Cloud. II. The Relationship Between

Dense Cores and the Cloud". In: *ApJ* 723, pp. 457–475. DOI: 10.1088/0004-637X/723/1/457 (cit. on p. 78).

Klessen, R. S. (2000). "One-Point Probability Distribution Functions of Supersonic Turbulent Flows in Self-gravitating Media". In: *ApJ* 535, pp. 869–886. DOI: 10.1086/308854 (cit. on pp. 42, 56).

Klessen, R. S. and A. Burkert (2000). "The Formation of Stellar Clusters: Gaussian Cloud Conditions. I." In: *ApJS* 128, pp. 287–319. DOI: 10.1086/313371 (cit. on p. 9).

Klessen, R. S., F. Heitsch, and M.-M. Mac Low (2000). "Gravitational Collapse in Turbulent Molecular Clouds. I. Gasdynamical Turbulence". In: *ApJ* 535, pp. 887–906. DOI: 10.1086/308891 (cit. on p. 9).

Klessen, R. S. and P. Hennebelle (2010). "Accretion-driven turbulence as universal process: galaxies, molecular clouds, and protostellar disks". In: *A&A* 520, A17, A17. DOI: 10.1051/0004-6361/200913780 (cit. on pp. 43, 56).

Koyama, H. and S. I. Inutsuka (2000). "Molecular Cloud Formation in Shock-compressed Layers". In: *ApJ* 532, pp. 980–993. DOI: 10.1086/308594 (cit. on pp. 7, 18, 19, 37, 40, 64, 92, 94).

— (2002). "An Origin of Supersonic Motions in Interstellar Clouds". In: *ApJL* 564, pp. L97–L100. DOI: 10.1086/338978 (cit. on pp. 7, 10, 37, 65, 91, 95).

Kritsuk, A. G., M. L. Norman, P. Padoan, and R. Wagner (2007). "The Statistics of Supersonic Isothermal Turbulence". In: *ApJ* 665, pp. 416–431. DOI: 10.1086/519443 (cit. on p. 33).

Kritsuk, A. G., M. L. Norman, and R. Wagner (2011). "On the Density Distribution in Star-forming Interstellar Clouds". In: *ApJL* 727, L20, p. L20. DOI: 10.1088/2041-8205/727/1/L20 (cit. on pp. 42, 56, 81).

Kroupa, P. (2001). "On the variation of the initial mass function". In: *MNRAS* 322, pp. 231–246. DOI: 10.1046/j.1365-8711.2001.04022.x (cit. on pp. 39, 58, 67, 89, 108).

Krumholz, M. R., M. R. Bate, H. G. Arce, J. E. Dale, R. Gutermuth, R. I. Klein, Z.-Y. Li, F. Nakamura, and Q. Zhang (2014a). "Star Cluster Formation and Feedback". In: *ArXiv e-prints* (cit. on p. 12).

— (2014b). "Star Cluster Formation and Feedback". In: *ArXiv e-prints* (cit. on p. 86).

Krumholz, M. R., A. Dekel, and C. F. McKee (2012). "A Universal, Local Star Formation Law in Galactic Clouds, nearby Galaxies, High-redshift Disks, and Starbursts". In: *ApJ* 745, 69, p. 69. DOI: 10.1088/0004-637X/745/1/69 (cit. on p. 73).

Krumholz, M. R., C. D. Matzner, and C. F. McKee (2006). "The Global Evolution of Giant Molecular Clouds. I. Model Formulation and Quasi-Equilibrium Behavior". In: *ApJ* 653, pp. 361–382. DOI: 10.1086/508679 (cit. on p. 35).

Krumholz, M. R. and C. F. McKee (2005). "A General Theory of Turbulence-regulated Star Formation, from Spirals to Ultraluminous Infrared Galaxies". In: *ApJ* 630, pp. 250–268. DOI: 10.1086/431734 (cit. on pp. 7, 9, 35, 44, 61, 65, 66, 77, 109).

Krumholz, M. R., C. F. McKee, and J. Tumlinson (2009). "The Star Formation Law in Atomic and Molecular Gas". In: *ApJ* 699, pp. 850–856. DOI: 10.1088/0004-637X/699/1/850 (cit. on pp. 12, 73).

Krumholz, M. R., J. M. Stone, and T. A. Gardiner (2007). "Magnetohydrodynamic Evolution of H II Regions in Molecular Clouds: Simulation Methodology, Tests, and Uniform Media". In: *ApJ* 671, pp. 518–535. DOI: 10.1086/522665 (cit. on p. 91).

Krumholz, M. R. and J. C. Tan (2007). "Slow Star Formation in Dense Gas: Evidence and Implications". In: *ApJ* 654, pp. 304–315. DOI: 10.1086/509101 (cit. on pp. 109, 110).

Lada, C. J. and E. A. Lada (2003). "Embedded Clusters in Molecular Clouds". In: *ARA&A* 41, pp. 57–115. DOI: 10.1146/annurev.astro.41.011802.094844 (cit. on pp. 87, 108).

Lada, C. J., M. Lombardi, and J. F. Alves (2010). "On the Star Formation Rates in Molecular Clouds". In: *ApJ* 724, pp. 687–693. DOI: 10.1088/0004-637X/724/1/687 (cit. on pp. 74, 107).

Larson, R. B. (1969). "Numerical calculations of the dynamics of collapsing proto-star". In: *MNRAS* 145, p. 271 (cit. on pp. 41, 42, 45, 57).

— (1981). "Turbulence and star formation in molecular clouds". In: *MNRAS* 194, pp. 809–826 (cit. on pp. 4, 56).

— (1985). "Cloud fragmentation and stellar masses". In: *MNRAS* 214, pp. 379–398 (cit. on pp. 40, 64).

Leger, A. and J. L. Puget (1984). "Identification of the 'unidentified' IR emission features of interstellar dust?" In: *A& A* 137, pp. L5–L8 (cit. on p. 4).

Leisawitz, D., F. N. Bash, and P. Thaddeus (1989). "A CO survey of regions around 34 open clusters". In: *ApJS* 70, pp. 731–812. DOI: 10.1086/191357 (cit. on p. 47).

Leorat, J., T. Passot, and A. Pouquet (1990). "Influence of supersonic turbulence on self-gravitating flows". In: *MNRAS* 243, pp. 293–311 (cit. on p. 9).

Lesieur, M. (2008). *Turbulence in Fluids* (cit. on p. 29).

Li, Z.-Y. and F. Nakamura (2006). "Cluster Formation in Protostellar Outflow-driven Turbulence". In: *ApJL* 640, pp. L187–L190. DOI: 10.1086/503419 (cit. on pp. 7, 35).

Louvet, F. et al. (2014). "The W43-MM1 mini-starburst ridge, a test for star formation efficiency models". In: *A& A* 570, A15, A15. DOI: 10.1051/0004-6361/201423603 (cit. on pp. 106, 110).

Mac Low, M.-M. and R. S. Klessen (2004). "Control of star formation by supersonic turbulence". In: *Reviews of Modern Physics* 76, pp. 125–194. DOI: 10.1103/RevModPhys.76.125 (cit. on pp. 1, 7, 9, 29, 35, 61, 86).

Mac Low, M.-M., J. Toraskar, J. S. Oishi, and T. Abel (2007). "Dynamical Expansion of H II Regions from Ultracompact to Compact Sizes in Turbulent, Self-gravitating Molecular Clouds". In: *ApJ* 668, pp. 980–992. DOI: 10.1086/521292 (cit. on p. 13).

Matzner, C. D. (2002). "On the Role of Massive Stars in the Support and Destruction of Giant Molecular Clouds". In: *ApJ* 566, pp. 302–314. DOI: 10.1086/338030 (cit. on pp. 7, 12, 25, 35, 37, 86).

Mazurek, T. J. (1980). "H II bubbles and disruption of molecular clouds". In: *A& A* 90, pp. 65–69 (cit. on p. 12).

McCray, R. and T. P. Snow Jr. (1979). "The violent interstellar medium". In: *ARA&A* 17, pp. 213–240. DOI: 10.1146/annurev.aa.17.090179.001241 (cit. on p. 1).

McKee, C. F. (1989). "Photoionization-regulated star formation and the structure of molecular clouds". In: *ApJ* 345, pp. 782–801. DOI: 10.1086/167950 (cit. on pp. 7, 13, 35).

McKee, C. F. and E. C. Ostriker (2007). "Theory of Star Formation". In: *ARA&A* 45, pp. 565–687. DOI: 10.1146/annurev.astro.45.051806.110602 (cit. on pp. 35, 61, 76).

Mellema, G. and P. Lundqvist (2002). "Stellar wind bubbles around WR and [WR] stars". In: *A& A* 394, pp. 901–909. DOI: 10.1051/0004-6361:20021164 (cit. on p. 91).

Mestel, L. (1966). "The magnetic field of a contracting gas cloud. I,Strict flux-freezing". In: *MNRAS* 133, p. 265 (cit. on p. 5).

Micic, M., S. C. O. Glover, R. Banerjee, and R. S. Klessen (2013). "Cloud formation in colliding flows: influence of the choice of cooling function". In: *MNRAS* 432, pp. 626–636. DOI: 10.1093/mnras/stt489 (cit. on p. 79).

Molinari, S. et al. (2010). "Clouds, filaments, and protostars: The Herschel Hi-GAL Milky Way". In: *A& A* 518, L100, p. L100. DOI: 10.1051/0004-6361/201014659 (cit. on p. 78).

Molinari, S. et al. (2014). "The Milky Way as a Star Formation Engine". In: *ArXiv e-prints* (cit. on pp. 6, 109).

Mouschovias, T. C. (1991a). "Magnetic braking, ambipolar diffusion, cloud cores, and star formation - Natural length scales and protostellar masses". In: *ApJ* 373, pp. 169–186. DOI: 10.1086/170035 (cit. on p. 8).

— (1991b). "Single-Stage Fragmentation and a Modern Theory of Star Formation". In: *NATO ASIC Proc. 342: The Physics of Star Formation and Early Stellar Evolution*. Ed. by C. J. Lada and N. D. Kylafis, p. 449 (cit. on p. 61).

Myers, P. C. (2009). "Filamentary Structure of Star-forming Complexes". In: *ApJ* 700, pp. 1609–1625. DOI: 10.1088/0004-637X/700/2/1609 (cit. on p. 78).

Myers, P. C., T. M. Dame, P. Thaddeus, R. S. Cohen, R. F. Silverberg, E. Dwek, and M. G. Hauser (1986). "Molecular clouds and star formation in the inner galaxy - A comparison of CO, H II, and far-infrared surveys". In: *ApJ* 301, pp. 398–422. DOI: 10.1086/163909 (cit. on pp. 9, 86, 87).

Myers, P. C., A. A. Goodman, R. Gusten, and C. Heiles (1995). "Observations of magnetic fields in diffuse clouds". In: *ApJ* 442, pp. 177–185. DOI: 10.1086/175433 (cit. on p. 5).

Nakamura, F. and Z.-Y. Li (2005). "Quiescent Cores and the Efficiency of Turbulence-accelerated, Magnetically Regulated Star Formation". In: *ApJ* 631, pp. 411–428. DOI: 10.1086/432606 (cit. on p. 9).

— (2007). "Protostellar Turbulence Driven by Collimated Outflows". In: *ApJ* 662, pp. 395–412. DOI: 10.1086/517515 (cit. on pp. 7, 35).

Norman, C. and J. Silk (1980). "Clumpy molecular clouds - A dynamic model self-consistently regulated by T Tauri star formation". In: *ApJ* 238, pp. 158–174. DOI: 10.1086/157969 (cit. on pp. 7, 35).

Oort, J. H. (1954). "Outline of a theory on the origin and acceleration of interstellar clouds and O associations". In: 12, p. 177 (cit. on p. 12).

Osterbrock, D. E. (1989). *Astrophysics of gaseous nebulae and active galactic nuclei* (cit. on pp. 25–27, 91, 112–114).

Ostriker, E. C., C. F. Gammie, and J. M. Stone (1999). "Kinetic and Structural Evolution of Self-gravitating, Magnetized Clouds: 2.5-dimensional Simulations of Decaying Turbulence". In: *ApJ* 513, pp. 259–274. DOI: 10.1086/306842 (cit. on pp. 9, 80).

Ostriker, E. C., J. M. Stone, and C. F. Gammie (2001). "Density, Velocity, and Magnetic Field Structure in Turbulent Molecular Cloud Models". In: *ApJ* 546, pp. 980–1005. DOI: 10.1086/318290 (cit. on p. 9).

Padoan, P. and Å. Nordlund (1999). "A Super-Alfvénic Model of Dark Clouds". In: *ApJ* 526, pp. 279–294. DOI: 10.1086/307956 (cit. on p. 9).

— (2011). "The Star Formation Rate of Supersonic Magnetohydrodynamic Turbulence". In: *ApJ* 730, 40, p. 40. DOI: 10.1088/0004-637X/730/1/40 (cit. on pp. 9, 61, 65, 66, 77, 109).

Padoan, P., A. Nordlund, and B. J. T. Jones (1997). "The universality of the stellar initial mass function". In: *MNRAS* 288, pp. 145–152 (cit. on pp. 42, 61).

Palla, F. and S. W. Stahler (1999). "Star Formation in the Orion Nebula Cluster". In: *ApJ* 525, pp. 772–783. DOI: 10.1086/307928 (cit. on pp. 53, 79).

Palla, F. and S. W. Stahler (2000). "Accelerating Star Formation in Clusters and Associations". In: *ApJ* 540, pp. 255–270. DOI: 10.1086/309312 (cit. on pp. 53–55, 59, 63, 79, 106).

— (2002). "Star Formation in Space and Time: Taurus-Auriga". In: *ApJ* 581, pp. 1194–1203. DOI: 10.1086/344293 (cit. on pp. 53, 63).

Passot, T. and E. Vázquez-Semadeni (1998). "Density probability distribution in one-dimensional polytropic gas dynamics". In: 58, pp. 4501–4510. DOI: 10.1103/PhysRevE.58.4501 (cit. on pp. 9, 42, 61).

Paxton, B. (2004). "EZ to Evolve ZAMS Stars: A Program Derived from Eggleton's Stellar Evolution Code". In: *PASP* 116, pp. 699–701. DOI: 10.1086/422345 (cit. on p. 90).

Penston, M. V. (1969). "Dynamics of self-gravitating gaseous spheres-III. Analytical results in the free-fall of isothermal cases". In: *MNRAS* 144, p. 425 (cit. on p. 42).

Peretto, N., P. Hennebelle, and P. André (2007). "Probing the formation of intermediate- to high-mass stars in protoclusters. II. Comparison between millimeter interferometric observations of NGC 2264-C and SPH simulations of a collapsing clump". In: *A& A* 464, pp. 983–994. DOI: 10.1051/0004-6361:20065653 (cit. on pp. 7, 10, 36, 62, 86).

Peretto, N. et al. (2013). "Global collapse of molecular clouds as a formation mechanism for the most massive stars". In: *A& A* 555, A112, A112. DOI: 10.1051/0004-6361/201321318 (cit. on p. 10).

Peretto, N. et al. (2014). "SDC13 infrared dark clouds: Longitudinally collapsing filaments?" In: *A& A* 561, A83, A83. DOI: 10.1051/0004-6361/201322172 (cit. on pp. 7, 86, 110).

Peters, T., R. Banerjee, R. S. Klessen, M.-M. Mac Low, R. Galván-Madrid, and E. R. Keto (2010). "H II Regions: Witnesses to Massive Star Formation". In: *ApJ* 711, pp. 1017–1028. DOI: 10.1088/0004-637X/711/2/1017 (cit. on pp. 25, 86–88, 91).

Pon, A., D. Johnstone, and F. Heitsch (2011). "Modes of Star Formation in Finite Molecular Clouds". In: *ApJ* 740, 88, p. 88. DOI: 10.1088/0004-637X/740/2/88 (cit. on pp. 37, 95).

Pon, A., J. A. Toalá, D. Johnstone, E. Vázquez-Semadeni, F. Heitsch, and G. C. Gómez (2012). "Aspect Ratio Dependence of the Free-fall Time for Non-spherical Symmetries". In: *ApJ* 756, 145, p. 145. DOI: 10.1088/0004-637X/756/2/145 (cit. on pp. 66, 69, 81).

Pound, M. W. and A. A. Goodman (1997). "Kinematics of the Ursa Major Molecular Clouds". In: *ApJ* 482, pp. 334–354 (cit. on p. 78).

Preibisch, T. and E. Mamajek (2008). "The Nearest OB Association: Scorpius-Centaurus (Sco OB2)". In: *Handbook of Star Forming Regions, Volume II*. Ed. by B. Reipurth, p. 235 (cit. on p. 80).

Rand, R. J. and S. R. Kulkarni (1989). "The local Galactic magnetic field". In: *ApJ* 343, pp. 760–772. DOI: 10.1086/167747 (cit. on p. 5).

Rand, R. J. and A. G. Lyne (1994). "New Rotation Measures of Distant Pulsars in the Inner Galaxy and Magnetic Field Reversals". In: *MNRAS* 268, p. 497 (cit. on p. 5).

Rijkhorst, E.-J., T. Plewa, A. Dubey, and G. Mellema (2006). "Hybrid characteristics: 3D radiative transfer for parallel adaptive mesh refinement hydrodynamics". In: *A& A* 452, pp. 907–920. DOI: 10.1051/0004-6361:20053401 (cit. on pp. 25, 26, 87, 88, 90, 91).

Rosas-Guevara, Y., E. Vázquez-Semadeni, G. C. Gómez, and A. K. Jappsen (2010). "Dependence of the star formation efficiency on global parameters of molecular clouds". In: *MNRAS* 406, pp. 1875–1884. DOI: 10.1111/j.1365-2966.2010.16782.x (cit. on p. 36).

Rosolowsky, E., G. Engargiola, R. Plambeck, and L. Blitz (2003). "Giant Molecular Clouds in M33. II. High-Resolution Observations". In: *ApJ* 599, pp. 258–274. DOI: 10.1086/379166 (cit. on p. 78).

Rybicki, G. B. and A. P. Lightman (1979). *Radiative processes in astrophysics* (cit. on pp. 25, 112).

Sasao, T. (1973). "On the Generation of Density Fluctuations Due to Turbulence in Self-Gravitating Media". In: *PASJ* 25, p. 1 (cit. on p. 9).

Scalo, J. (1990). "Perception of interstellar structure - Facing complexity". In: *Physical Processes in Fragmentation and Star Formation*. Ed. by R. Capuzzo-Dolcetta, C. Chiosi, and A. di Fazio. Vol. 162. Astrophysics and Space Science Library, pp. 151–176 (cit. on p. 4).

Scalo, J. M. (1987). "Theoretical approaches to interstellar turbulence". In: *Interstellar Processes*. Ed. by D. J. Hollenbach and H. A. Thronson Jr. Vol. 134. Astrophysics and Space Science Library, pp. 349–392 (cit. on p. 29).

Schmidt, M. (1959). "The Rate of Star Formation." In: *ApJ* 129, p. 243. DOI: 10.1086/146614 (cit. on pp. 51, 61).

Schneider, N., T. Csengeri, S. Bontemps, F. Motte, R. Simon, P. Hennebelle, C. Federrath, and R. Klessen (2010). "Dynamic star formation in the massive DR21 filament". In: *A& A* 520, A49, A49. DOI: 10.1051/0004-6361/201014481 (cit. on pp. 7, 36, 62, 86, 110).

Schneider, N., T. Csengeri, R. S. Klessen, P. Tremblin, V. Ossenkopf, and N. Peretto (2014). "On the similarity of IR-bright and IR-dark molecular clouds". In: *ArXiv e-prints* (cit. on p. 99).

Shu, F. H. (1977). "Self-similar collapse of isothermal spheres and star formation". In: *ApJ* 214, pp. 488–497. DOI: 10.1086/155274 (cit. on p. 42).
— (1991). *The physics of astrophysics. Volume 1: Radiation.* (Cit. on pp. 25, 112).
— (1992). *The physics of astrophysics. Volume II: Gas dynamics.* (Cit. on pp. 5, 15, 21, 24).
Shu, F. H., F. C. Adams, and S. Lizano (1987). "Star formation in molecular clouds - Observation and theory". In: *ARA&A* 25, pp. 23–81. DOI: 10.1146/annurev.aa.25.090187.000323 (cit. on pp. 6, 8, 61).
Smith, R. J., S. C. O. Glover, and R. S. Klessen (2014). "On the nature of star-forming filaments - I. Filament morphologies". In: *MNRAS* 445, pp. 2900–2917. DOI: 10.1093/mnras/stu1915 (cit. on p. 95).
Smith, R. J., S. Longmore, and I. Bonnell (2009). "The simultaneous formation of massive stars and stellar clusters". In: *MNRAS* 400, pp. 1775–1784. DOI: 10.1111/j.1365-2966.2009.15621.x (cit. on p. 63).
Tenorio-Tagle, G. (1979). "The gas dynamics of H II regions. I - The champagne model". In: *A& A* 71, pp. 59–65 (cit. on p. 86).
Toalá, J. A., E. Vázquez-Semadeni, and G. C. Gómez (2012). "The Free-fall Time of Finite Sheets and Filaments". In: *ApJ* 744, 190, p. 190. DOI: 10.1088/0004-637X/744/2/190 (cit. on pp. 66, 69, 81).
Troland, T. H. and R. M. Crutcher (2008). "Magnetic Fields in Dark Cloud Cores: Arecibo OH Zeeman Observations". In: *ApJ* 680, pp. 457–465. DOI: 10.1086/587546 (cit. on p. 57).
Troland, T. H. and C. Heiles (1986). "Interstellar magnetic field strengths and gas densities Observational and theoretical perspectives". In: *ApJ* 301, pp. 339–345. DOI: 10.1086/163904 (cit. on p. 5).
Truelove, J. K., R. I. Klein, C. F. McKee, J. H. Holliman II, L. H. Howell, and J. A. Greenough (1997). "The Jeans Condition: A New Constraint on Spatial Resolution in Simulations of Isothermal Self-gravitational Hydrodynamics". In: *ApJL* 489, pp. L179–L183. DOI: 10.1086/310975 (cit. on pp. 88, 102).
Vazquez-Semadeni, E. (1994). "Hierarchical Structure in Nearly Pressureless Flows as a Consequence of Self-similar Statistics". In: *ApJ* 423, p. 681. DOI: 10.1086/173847 (cit. on pp. 9, 42, 61).
Vázquez-Semadeni, E. (1999). "Turbulence in Molecular Clouds". In: *Millimeter-Wave Astronomy: Molecular Chemistry Physics in Space*. Ed. by W. F. Wall, A. Carramiñana, and L. Carrasco. Vol. 241. Astrophysics and Space Science Library, p. 161. DOI: 10.1007/978-94-011-4714-9_9 (cit. on p. 29).
— (2010). "Molecular Cloud Evolution". In: *Astronomical Society of the Pacific Conference Series*. Ed. by R. Kothes, T. L. Landecker, and A. G. Willis.

Vol. 438. Astronomical Society of the Pacific Conference Series, p. 83 (cit. on pp. 6, 7).

Vázquez-Semadeni, E. (2011). "Theory of Feedback in Clusters and Molecular Cloud Turbulence". In: *Computational Star Formation*. Ed. by J. Alves, B. G. Elmegreen, J. M. Girart, and V. Trimble. Vol. 270. IAU Symposium, pp. 275–282. DOI: 10.1017/S1743921311000500 (cit. on p. 86).

— (2012). "Interstellar MHD Turbulence and Star Formation". In: *ArXiv e-prints* (cit. on p. 6).

Vázquez-Semadeni, E., J. Ballesteros-Paredes, and R. S. Klessen (2003). "A Holistic Scenario of Turbulent Molecular Cloud Evolution and Control of the Star Formation Efficiency: First Tests". In: *ApJL* 585, pp. L131–L134. DOI: 10.1086/374325 (cit. on pp. 9, 61).

Vázquez-Semadeni, E., R. Banerjee, G. C. Gómez, P. Hennebelle, D. Duffin, and R. S. Klessen (2011). "Molecular cloud evolution - IV. Magnetic fields, ambipolar diffusion and the star formation efficiency". In: *MNRAS* 414, pp. 2511–2527. DOI: 10.1111/j.1365-2966.2011.18569.x (cit. on pp. 10, 13, 36, 41, 62, 87, 88, 94, 97).

Vázquez-Semadeni, E., J. Cantó, and S. Lizano (1998). "Does Turbulent Pressure Behave as a Logatrope?" In: *ApJ* 492, pp. 596–602. DOI: 10.1086/305064 (cit. on pp. 43, 56).

Vázquez-Semadeni, E., P. Colín, G. C. Gómez, J. Ballesteros-Paredes, and A. W. Watson (2010). "Molecular Cloud Evolution. III. Accretion Versus Stellar Feedback". In: *ApJ* 715, pp. 1302–1317. DOI: 10.1088/0004-637X/715/2/1302 (cit. on pp. 10, 11, 36, 41, 44–47, 57, 58, 62, 63, 81, 87, 94, 97, 98, 101, 108).

Vazquez-Semadeni, E. and A. Gazol (1995). "Gravitational instability in turbulent, non-uniform media." In: *A& A* 303, p. 204 (cit. on p. 4).

Vázquez-Semadeni, E., G. C. Gómez, A. K. Jappsen, J. Ballesteros-Paredes, R. F. González, and R. S. Klessen (2007). "Molecular Cloud Evolution. II. From Cloud Formation to the Early Stages of Star Formation in Decaying Conditions". In: *ApJ* 657, pp. 870–883. DOI: 10.1086/510771 (cit. on pp. 7, 10, 11, 13, 36, 40, 41, 46, 62, 65, 86, 92, 95).

Vázquez-Semadeni, E., G. C. Gómez, A. K. Jappsen, J. Ballesteros-Paredes, and R. S. Klessen (2009). "High- and Low-Mass Star-Forming Regions from Hierarchical Gravitational Fragmentation. High Local Star Formation Rates with Low Global Efficiencies". In: *ApJ* 707, pp. 1023–1033. DOI: 10.1088/0004-637X/707/2/1023 (cit. on pp. 7, 10, 36, 49, 52, 53, 62, 63, 66, 77, 86).

Vázquez-Semadeni, E., R. F. González, J. Ballesteros-Paredes, A. Gazol, and J. Kim (2008). "The nature of the velocity field in molecular clouds - I. The

non-magnetic case". In: *MNRAS* 390, pp. 769–780. DOI: 10.1111/j.1365-2966.2008.13778.x (cit. on pp. 11, 42, 56, 78).

Vázquez-Semadeni, E., J. Kim, and J. Ballesteros-Paredes (2005a). "Star Formation Efficiency in Driven, Supercritical, Turbulent Clouds". In: *ApJL* 630, pp. L49–L52. DOI: 10.1086/491650 (cit. on p. 9).

Vázquez-Semadeni, E., J. Kim, M. Shadmehri, and J. Ballesteros-Paredes (2005b). "The Lifetimes and Evolution of Molecular Cloud Cores". In: *ApJ* 618, pp. 344–359. DOI: 10.1086/425951 (cit. on p. 9).

Vazquez-Semadeni, E., E. C. Ostriker, T. Passot, C. F. Gammie, and J. M. Stone (2000). "Compressible MHD Turbulence: Implications for Molecular Cloud and Star Formation". In: *Protostars and Planets IV*, p. 3 (cit. on pp. 9, 61).

Vazquez-Semadeni, E., T. Passot, and A. Pouquet (1996). "Influence of Cooling-induced Compressibility on the Structure of Turbulent Flows and Gravitational Collapse". In: *ApJ* 473, p. 881. DOI: 10.1086/178200 (cit. on p. 32).

Vázquez-Semadeni, E., D. Ryu, T. Passot, R. F. González, and A. Gazol (2006). "Molecular Cloud Evolution. I. Molecular Cloud and Thin Cold Neutral Medium Sheet Formation". In: *ApJ* 643, pp. 245–259. DOI: 10.1086/502710 (cit. on pp. 10, 37, 38, 40, 42, 64, 65, 79, 82, 95).

Vishniac, E. T. (1994). "Nonlinear instabilities in shock-bounded slabs". In: *ApJ* 428, pp. 186–208. DOI: 10.1086/174231 (cit. on pp. 37, 42, 64, 95).

von Weizsäcker, C. F. (1951). "The Evolution of Galaxies and Stars." In: *ApJ* 114, p. 165. DOI: 10.1086/145462 (cit. on p. 9).

Waagan, K. (2009). "A positive MUSCL-Hancock scheme for ideal magnetohydrodynamics". In: *Journal of Computational Physics* 228.23, pp. 8609–8626. DOI: http://dx.doi.org/10.1016/j.jcp.2009.08.020 (cit. on p. 88).

Waagan, K., C. Federrath, and C. Klingenberg (2011). "A robust numerical scheme for highly compressible magnetohydrodynamics: Nonlinear stability, implementation and tests". In: *Journal of Computational Physics* 230, pp. 3331–3351. DOI: 10.1016/j.jcp.2011.01.026 (cit. on p. 88).

Wada, K. and C. A. Norman (1999). "The Global Structure and Evolution of a Self-Gravitating Multiphase Interstellar Medium in a Galactic Disk". In: *ApJL* 516, pp. L13–L16. DOI: 10.1086/311987 (cit. on p. 9).

Walder, R. and D. Folini (2000). "On the Stability of Colliding Flows: Radiative Shocks, Thin Shells, and Supersonic Turbulence". In: *Ap& SS* 274, pp. 343–352. DOI: 10.1023/A:1026597318472 (cit. on pp. 37, 42, 64, 95).

Wang, P., Z.-Y. Li, T. Abel, and F. Nakamura (2010). "Outflow Feedback Regulated Massive Star Formation in Parsec-Scale Cluster-Forming Clumps". In: *ApJ* 709, pp. 27–41. DOI: 10.1088/0004-637X/709/1/27 (cit. on pp. 7, 35).

Wannier, P. G., S. M. Lichten, and M. Morris (1983). "Warm H I halos around molecular clouds". In: *ApJ* 268, pp. 727–738. DOI: 10.1086/160995 (cit. on p. 6).

Whitworth, A. (1979). "The erosion and dispersal of massive molecular clouds by young stars". In: *MNRAS* 186, pp. 59–67 (cit. on pp. 7, 12, 13, 86).

Williams, J. P., L. Blitz, and C. F. McKee (2000). "The Structure and Evolution of Molecular Clouds: from Clumps to Cores to the IMF". In: *Protostars and Planets IV*, p. 97 (cit. on p. 6).

Williams, J. P. and C. F. McKee (1997). "The Galactic Distribution of OB Associations in Molecular Clouds". In: *ApJ* 476, pp. 166–183 (cit. on pp. 76, 83).

Wolfire, M. G., D. Hollenbach, C. F. McKee, A. G. G. M. Tielens, and E. L. O. Bakes (1995). "The neutral atomic phases of the interstellar medium". In: *ApJ* 443, pp. 152–168. DOI: 10.1086/175510 (cit. on pp. 18, 19, 92).

Woolf, N. J. and E. P. Ney (1969). "Circumstellar Infrared Emission from Cool Stars". In: *ApJL* 155, p. L181. DOI: 10.1086/180331 (cit. on p. 4).

Wu, J., N. J. Evans II, Y. Gao, P. M. Solomon, Y. L. Shirley, and P. A. Vanden Bout (2005). "Connecting Dense Gas Tracers of Star Formation in our Galaxy to High-z Star Formation". In: *ApJL* 635, pp. L173–L176. DOI: 10.1086/499623 (cit. on pp. 51, 52).

Wu, J., N. J. Evans II, Y. L. Shirley, and C. Knez (2010). "The Properties of Massive, Dense Clumps: Mapping Surveys of HCN and CS". In: *ApJS* 188, 313, pp. 313–357. DOI: 10.1088/0067-0049/188/2/313 (cit. on pp. 52, 69).

Yorke, H. W., G. Tenorio-Tagle, P. Bodenheimer, and M. Rozyczka (1989). "The combined role of ionization and supernova explosions in the destruction of molecular clouds". In: *A& A* 216, pp. 207–214 (cit. on pp. 12, 86).

Zamora-Avilés, M. and E. Vázquez-Semadeni (2014). "An Evolutionary Model for Collapsing Molecular Clouds and their Star Formation Activity. II. Mass Dependence of the Star Formation Rate". In: *ApJ* 793, 84, p. 84. DOI: 10.1088/0004-637X/793/2/84 (cit. on pp. 86, 87, 100).

Zamora-Avilés, M., E. Vázquez-Semadeni, and P. Colín (2012). "An Evolutionary Model for Collapsing Molecular Clouds and Their Star Formation Activity". In: *ApJ* 751, 77, p. 77. DOI: 10.1088/0004-637X/751/1/77 (cit. on pp. 62, 86, 87, 100, 102, 104).

Zuckerman, B. and N. J. Evans II (1974). "Models of massive molecular clouds". In: *ApJL* 192, pp. L149–L152. DOI: 10.1086/181613 (cit. on pp. 2, 7, 61).

Zuckerman, B. and P. Palmer (1974). "Radio radiation from interstellar molecules". In: *ARA&A* 12, pp. 279–313. DOI: 10.1146/annurev.aa.12.090174.001431 (cit. on pp. 2, 7, 61).